

Dissertation
submitted to the
Combined Faculty of Natural Sciences and Mathematics
of Heidelberg University, Germany
for the degree of
Doctor of Natural Sciences

Put forward by
Piotr, Korbeń
born in: Radziejów, Poland
Oral examination: 20.07.2021

Estimation of methane emissions and investigation
of isotopic composition of methane from selected
sources in Germany, Poland and Romania

Referees:

Prof. Dr. Norbert Frank

Prof. Dr. André Butz

Zusammenfassung

Diese Studie quantifiziert die Methanemissionsraten aus anthropogenen Quellen in Europa. Regelmäßige mobile Messkampagnen wurden an lokalen Quellen wie Milchviehbetrieben, Biogasanlagen, Deponien und Gaskompressorstationen durchgeführt um die Methanemissionsraten und ihre isotopische Quellensignatur zu quantifizieren. Während zweier Kampagnen wurden Messungen an Kohlebergwerke in Polen und Öl- und Gasbohrungen in Rumänien durchgeführt, die zu einem großen Anteil zu den fossilen Methanemissionen in Europa beitragen. Zur Abschätzung der Methanemissionsraten wurden zwei Methoden verwendet: Ein Gaußsches Modell und die OTM 33A Methode, die auch bei Experimenten zur kontrollierten CH_4 -Freisetzung getestet wurden. Beide Methoden liefern zuverlässige Schätzungen der Emissionsraten und können zur Quantifizierung lokaler und regionaler Methanquellen verwendet werden. Die Ergebnisse der geschätzten Methanemissionsraten und Isotopensignaturen zeigen die saisonalen Variationen für Mülldeponien und den signifikanten Beitrag von Methanemissionen aus Biogasanlagen. Die Emissionen der rumänischen Öl und Gasproduktion zeigen ähnliche Werte wie die in den USA gemessenen Emissionen. Die Ergebnisse dieser Studie wurden im Rahmen des europäischen ITN-Projekts *MEMO*² verglichen, und in diese Datenbank berichtet und kann so für politischen Entscheidungsträger dienen wird.

Abstract

This study quantifies methane emission rates from anthropogenic sources in Europe. Regular mobile measurement campaigns were conducted at local sources like dairy farms, biogas plants, landfill and gas compressor station with the aim to quantify methane emission rates and its isotopic source signature. During two measurement campaigns, coal mines in Poland and oil and gas wells in Romania were visited, which are sources of large methane emissions in Europe. Two methods were used to estimate methane emission rates: Gaussian Plume Model and Other Test Method 33A, which were also tested during controlled CH_4 release experiments. Both methods give reliable estimates of emissions rates and can be used to quantify local and regional methane sources. The results of the estimated methane emission rates and isotopic signatures show the seasonal emissions for landfill and the significant contribution of methane emissions from biogas plants facilities at dairy farms. Emissions estimated for oil and gas production in Romania show similar values to emissions measured in the US. This study was compared with similar ones in the frame of the European ITN project *MEMO*² allowed for the creation of a database which will serve as a report for the policymakers.

Contents

List of symbols	11
1 Introduction	13
I Theoretical background	15
2 Fundamentals	15
2.1 Methane and its characteristics	15
2.2 The sources and sinks of methane and global methane budget	16
2.3 CH_4 Isotopes	20
2.4 Emission estimation	25
2.4.1 Gaussian Plume Model	25
2.4.2 Other Test Method 33A	30
II Methodology and research sites	39
3 Measurement techniques	39
3.1 Cavity Ring Down Spectroscopy	39
3.2 Optical Feedback - Cavity Enhanced Absorption Spectroscopy	42
3.3 AirCore	44
3.4 2D and 3D weather station	47
4 Research sites	50
4.1 Release experiments	50
4.2 Field campaigns - Heidelberg	51
4.2.1 Dairy farm in Weinheim	51
4.2.2 Dairy farm in Ladenburg	53
4.2.3 Biogas plant in Pfaffengrund	55
4.2.4 Gas compressor station in Gernsheim	56
4.2.5 Landfill in Sinsheim	57
4.3 Field campaigns in Poland and Romania	59
4.3.1 CoMet campaign in Poland	59
4.3.2 ROMEO campaign in Romania	61
III Results and discussions	63

5	Controlled Release Experiments	63
5.1	Gaussian Plume Model release tests	63
5.1.1	Analysis of Mannheim 1 and Mannheim 2 release test	64
5.1.2	Analysis of Mannheim 4 release experiment	66
5.1.3	Analysis of Mannheim 5 release experiment	69
5.2	Other Test Method 33A release tests	73
5.2.1	DuREX campaign	74
5.2.2	Validation of stability class averaging	77
5.2.3	Calculation of the uncertainty	78
5.2.4	Test of the measurement duration	79
5.2.5	Mannheim release tests	80
5.2.6	Conclusions	82
6	Quantification of CH_4 emitters in Heidelberg region	83
6.1	Dairy Farm in Weinheim	85
6.2	Dairy Farm in Ladenburg	88
6.3	Biogas plant in Pfaffengrund	89
6.4	Discussion of results for farms and biogas plant	92
6.5	Gas Compressor Station in Gernsheim - results and discussion	96
6.6	Landfill in Sinsheim - results and discussion	99
7	Romanian oil and gas wells	104
7.1	Methodology	105
7.1.1	CH_4 calibration scale	105
7.1.2	Instrumentation and measurement vehicles	105
7.2	Site selection	108
7.3	GPM results	111
7.4	OTM-33A results	112
7.5	Revisited sites	113
7.6	Emission rates below the detection limit	114
7.7	Comparison of estimated methane emission rates for regions and type of visited sites	115
7.8	Comparison to other studies	117
8	Isotopic results	119
8.1	Heidelberg sources	119
8.1.1	Isotopic analysis for farms in Weinheim and Ladenburg	121

8.1.2	Isotopic analysis for biogas plant in Pfaffengrund and landfill in Sinsheim	122
8.1.3	Isotopic analysis for gas sources	124
8.2	Polish coal mines	126
8.3	Isotopic database of <i>MEMO</i> ²	129
9	Conclusions and Outlook	131
10	List of publications of the author	134
	Appendices	135
A	List of figures	135
B	List of tables	141
C	Calibration gases for ROMEO campaign	142
D	Coal mines in Poland - description	143
	References	145

List of Symbols

$\delta^{13}CH_4$	methane isotopic signature $\delta(13C, CH_4)$ in VPDB scale
<i>AGH</i>	Faculty of Physics and Applied Computer Science, AGH University of Science and Technology in Cracow, Poland
<i>BTU</i>	British thermal unit
<i>CH₄</i>	Methane
<i>CO₂</i>	Carbon dioxide
<i>CoMet</i>	Carbon Dioxide and Methane Mission for HALO
<i>CRDS</i>	Cavity Ring Down Spectroscopy
<i>DF</i>	Dairy farm
<i>DLR</i>	Deutsches Zentrum für Luft- und Raumfahrt, German Aerospace Center
<i>DuREX</i>	Dübendorf Release EXperiment
<i>DQI</i>	Data Quality Indicator
<i>EMPA</i>	Swiss Federal Laboratories for Material Science and Technology, Dübendorf, Switzerland
<i>FTiR</i>	Fourier-transform infrared spectroscopy
<i>GCS</i>	Gas Compressor Station
<i>GHG</i>	Greenhouse Gas
<i>GPM</i>	Gaussian Plume Model
<i>GMAP</i>	Geospatial Measurement of Air Pollution
<i>GWP</i>	Global Warming Potential
<i>UU</i>	Institute for Marine and Atmospheric research Utrecht, Utrecht University, Netherlands
<i>IPCC</i>	Intergovernmental Panel on Climate Change
<i>MEMO²</i>	<i>MEMO²</i> project, MEthane goes MObile – MEasurements and MOdelling
<i>NOAA</i>	National Oceanic Atmospheric Administration

OFCEAS Optical Feedback - Cavity-Enhanced Absorption

OTM – 33A Other Test Method 33A

REQ Remote Emissions Quantification

ROMEIO Romanian Methane Emissions from Oil and Gas

UBA Umwelt Bundesamt

UBB Faculty of Environmental Science and Engineering, Babeş-Bolyai University,
Cluj-Napoca, Romania

UG University of Groningen, Groningen, Netherlands

UHEI Heidelberg University, Heidelberg, Germany

UNFCCC United Nations Framework Convention on Climate Change

USCB Upper Silesian Coal Basin

UU Institute for Marine and Atmospheric research Utrecht, Utrecht University,
the Netherlands

WWTP Wastewater Treatment Plant

1 Introduction

Nowadays, one of the most important topics of public debate is climate change. The latest IPCC report (the Intergovernmental Panel on Climate Change, 2018) states that human-induced warming reached about 1°C above pre-industrial levels in 2017, increasing at a rate of about 0.2°C per decade. Global warming is one of the causes of climate change in the world. It is mainly caused by anthropogenic greenhouse gases emissions (GHGs). Methane is the second most important greenhouse gas impacted by human activity after carbon dioxide (Saunois et al., 2020), but comparing them to each other methane has a much higher (30 times) global warming potential than CO_2 in a 100 year horizon. To assess realistic mitigation pathways, it is important to understand and quantify the global and regional methane budget (Saunois et al., 2020). Although both CO_2 and methane occur naturally, they also occur as a result of human activity, which increases their concentration in the atmosphere and introduces a local to regional emission dynamic to the GHG cycles. Recent abdications show that by scaling up existing technology and industry best practices and policy options, methane emission reductions of up to 110 Tg per year are possible. This would reduce the overall methane burden even within a decade and would bring great benefits at relatively low cost (Nisbet et al., 2020). Currently, methane accounts for 15% of global greenhouse gas emissions, including all sectors. The main anthropogenic methane emissions are related to two sectors, electricity and heat production, and agriculture, forestry and other land use, together account for nearly 50% of methane emissions (IPCC report, 2018).

However not all methane emissions are well quantified and the uncertainties of methane emissions in the global budget range from 30 to 300 Tg of CH_4 (Frank ,2018; Saunois et al., 2020; Kirschke et al., 2013). Methane emissions from cows are relatively well defined because with well determined emission factor and precise number of cows in countries or regions, whereas it is more difficult to determine methane emission from gas leaks. Emission from production of coal, gas or oil in countries like Romania and Poland are not well quantified. Especially in sectors with large mitigation potential more studies are needed to identify and quantify large emitters. These measurements may be supported by isotopic measurements of methane which can help to separate emissions from two nearby emitters (Frank, 2018; Nisbet et al., 2016).

The European Training Network developed *MEMO*² (MEthane goes MObile - MEasurements and MOdelling), a project where more than 20 collaborators from 7 countries worked together to identify and evaluate methane (CH_4) emissions and support mitigation measures (*MEMO*² web). The project is designed to train a new generation of scientists who will be able to effectively implement new measurement and modelling tools. As part of the *MEMO*² project, various anthropogenic sources of methane emissions were vis-

ited and monitored creating a database of information for policy makers. In this project I have contributed to the understanding of emission balancing models through conducting release experiments followed by the studies of methane emission rates from European sources as well as isotope fingerprinting of sources. This has allowed me to deepen my knowledge and improve my own research skills and interpretation of the results obtained.

The dissertation is structured in three main parts: (I) Theoretical background, (II) Methodology and Research Sites , (III) Results and discussion. The first part contains fundamental information about methane and its global budget. It also describes the methods used to estimate methane emission rates. The next part contains a description of the equipment used in the conducted research and also a description of selected methane sources in Germany, Poland and Romania, which were the subject of research in this study. The last part presents and discusses the obtained results, starting from the validation of methods used during research works, through the estimation of methane emission rates for visited source, to the study of isotopic composition. At the end of this thesis, chapter 9 gives a summary of this study and general conclusions.

Part I

Theoretical background

2 Fundamentals

2.1 Methane and its characteristics

Methane is the simplest hydrocarbon with the chemical formula CH_4 . It is a harmless and odourless gas, which in a mixture of 5-15% with air is an explosive gas. In addition, methane is a major component of natural gas. The lifetime of methane in the troposphere is about 10 years.

As mentioned above methane is one of the greenhouse gases. It is the second most important greenhouse gas after CO_2 , but because of its greater radiative forcing per molecule, it has a 30 times larger global warming potential (GWP) than carbon dioxide, looking 100 years ahead (IPCC report, 2013). The GWP represents the time-integrated warming effect caused by the immediate release of a unit mass (1 kg) of a given greenhouse gas in today's atmosphere, compared to carbon dioxide (IPCC report, 2013). Over the past decades, there has been a steady increase in atmospheric methane concentrations. Compared to the pre-industrial era, this concentration has increased 2.6 times, from 700 ppb (18th century) to 1880 ppb today (Sherwood et al., 2017). Although there was a short plateau in this increase (2000-2007), since then there has been a steady increase in atmospheric methane concentration, as shown in Figure 1.

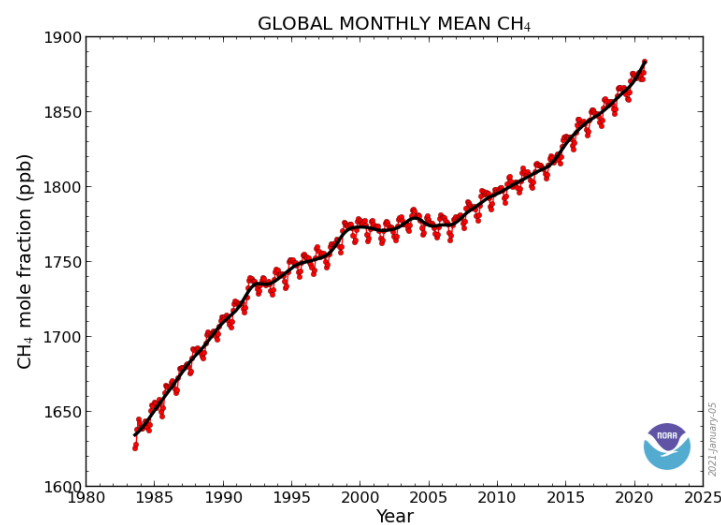


Figure 1: From NOAA. Increase of global monthly CH_4 concentration over last 40 years.

2.2 The sources and sinks of methane and global methane budget

Methane sources can be divided into two categories. The first relates to its origin, and the second to the process by which it is formed. The second category is related to the study of isotopic scaling and is presented in the next section, subsection 2.3. The following description follows mostly Saunois et al. (2020), Kirschke et al. (2013), Frank (2018) and Sherwood et al. (2017).

The origin of methane emissions can be divided into natural methane and anthropogenic methane emission, created by human activity. In order to know and understand the entire methane budget, it is necessary to know its possible sources and how they affect the budget as a whole. Figure 2 shows the split into natural and anthropogenic methane sources with their associated subgroups.

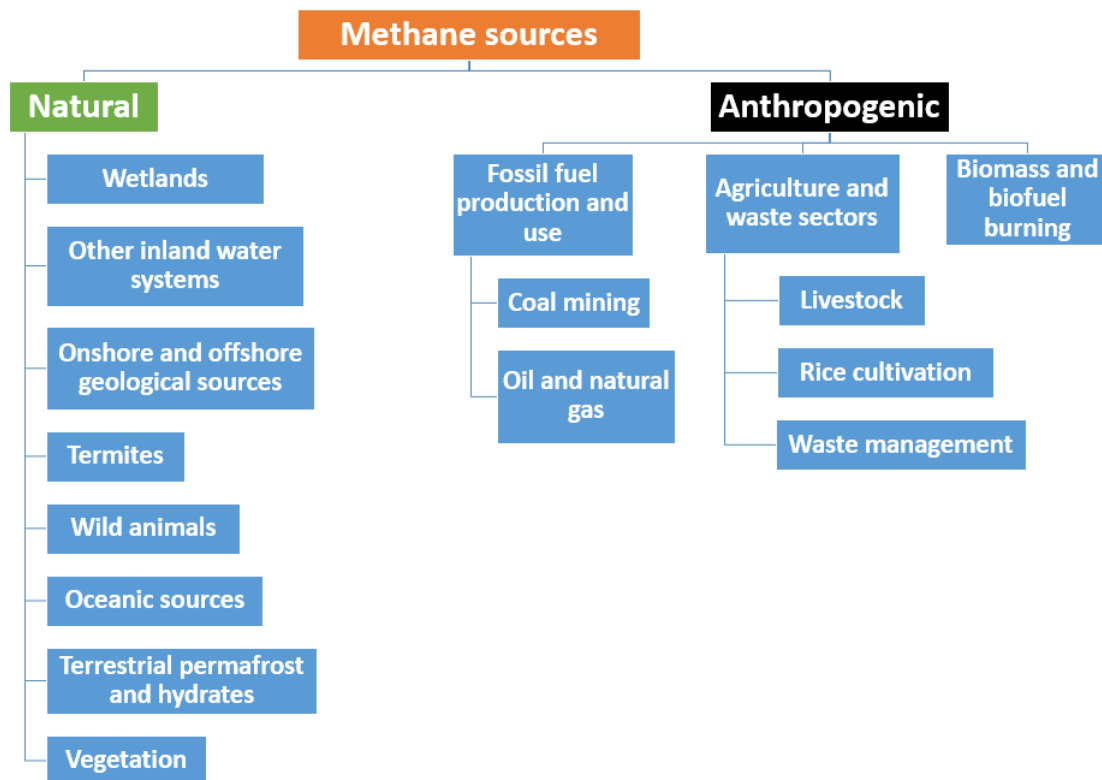


Figure 2: Methane sources divided by origin into natural and anthropogenic. Based on Saunois et al. (2020).

Among the natural sources of methane, the following can be distinguished: wetlands, other inland water systems, onshore and offshore geological sources, termites, wild animals, oceanic sources, terrestrial permafrost and hydrates, vegetation (Saunois et al., 2020). Methane is formed there as a result of the decomposition of organic matter. Approximately 60-70% of natural methane emissions are attributed to wetlands (Kirschke et al., 2013). Because of the large area covered by boreal and tropical wetlands, the un-

certainty of emissions for these sources is still large, as it is calculated as the product of an emission flux density and a methane-producing area or surface extent (Frank, 2018). The average annual methane emissions from all wetlands is $149 \text{ TgCH}_4/\text{yr}$, with a range of $102\text{-}182 \text{ TgCH}_4/\text{yr}$, for the last decade (2008-2017). Methane emissions for the other natural methane sources reported by Saunio et al. (2020) are: $159 \text{ TgCH}_4/\text{yr}$ (other inland water system), $45 \text{ TgCH}_4/\text{yr}$ (onshore and offshore geological sources), $9 \text{ TgCH}_4/\text{yr}$ (termites), $2 \text{ TgCH}_4/\text{yr}$ (wild animals), $13 \text{ TgCH}_4/\text{yr}$ (oceanic sources), $0\text{-}1 \text{ TgCH}_4/\text{yr}$ (terrestrial permafrost and hydrates).

The focus of this work is on anthropogenic methane emissions, which can be divided into three source categories (Figure 2): fossil fuel production and use, agriculture and waste sectors and biomass and biofuel burning.

CH_4 emissions from fossil fuel are mainly from coal, oil or natural gas extraction and transport and use of natural gas. Methane from coal mines comes primarily from ventilation shafts through which methane is released to the surface for safety reasons (to avoid explosions). It can be enriched and used as natural gas, but in many countries it is not captured. Methane can be released from active mines, which are still producing coal and from mines which are closed, but to a smaller amount (Saunio et al., 2020). Coal mines are responsible for producing 40% of the world's energy, and up to 64% of the world's coal mine methane emissions are caused by three major producers, China, the US and India (Saunio et al., 2020). Globally, methane emissions from coal mines are estimated to be $29\text{-}61 \text{ TgCH}_4/\text{yr}$ from 2008-2017, and for the present decade accounted for about 33% of methane emissions from fossil fuels (Saunio et al., 2020). Methane from oil and natural gas can be emitted by drilling in gas fields, production, transportation, storage, gas distribution and end-use. Methane leaks can occur as permanent emissions (leaking facilities) and as a result of maintenance activities. Particularly exposed are old urban gas distribution networks, where it is difficult to locate leaks. Methane emissions from oil and natural gas are estimated (2017) to be between $72\text{ and }97 \text{ TgCH}_4/\text{yr}$, with an average of $80 \text{ TgCH}_4/\text{yr}$ in decade 2008-2017. This is about 63% of global methane emissions from fossil fuels (Saunio et al., 2020).

The second source category of anthropogenic methane is agriculture and waste sectors. It represents about 56% of the global anthropogenic emission and is estimated at $206 \text{ TgCH}_4/\text{yr}$ (Saunio et al., 2020). Livestock production, rice cultivation, landfills, and wastewater treatment are included in this category. Methane emissions here are related to population density, with the largest emissions coming from China, India and Europe. However, there is a disparity between the emissions for the emitters listed above. The total number of cows, sheep and goats is currently over 3.5 billion animals, and each of them is a methane emitter. Manure decomposition must be added to this. The estimated

emissions for livestock and manure management are just over 100 $TgCH_4/yr$ and account for about one-third of all anthropogenic methane emissions. The share of global anthropogenic methane emissions from rice cultivation is only 8%, and about 50% of that comes from Asia. It should be noted, however, that the rice cultivation area is decreasing, and thus CH_4 emission from this source is also decreasing. Waste sector includes landfills (managed and non-managed) and wastewater handling. The share of methane emissions from this sector in global anthropogenic emissions does not change significantly, remaining at 11% in 2000 and 12% in 2017 (Kirschke et al., 2013; Saunio et al., 2020). It is estimated that for the decade 2008-2017 methane emissions from waste management amounted to about 65 $TgCH_4/yr$.

As shown by Saunio et al. (2020), biomass and biofuel combustion resulted in methane emissions of 30 [26-40] $TgCH_4/yr$ between 2008 and 2017. This includes biomass burning in forests, savannahs, grasslands, peats, agricultural residues, and the burning of biofuels in the residential sector. This represents the third type of anthropogenic methane emission, although the magnitude of this emission is much smaller compared to agriculture and fossil fuels methane emission. Biomass burning alone accounts for 5% of anthropogenic methane emissions and is estimated at 17 $TgTgCH_4/yr$ (Saunio et al., 2020). Biofuel burning is estimated slightly less (between 10 and 14 performed) and accounts for about 3% of global anthropogenic methane emissions (2008-2017).

The process of methane removal occurs mainly in the troposphere where it is oxidized by the hydroxyl radical (OH), this represents about 90% of the total removal mechanism. The remaining 10% occurs through photochemistry in the stratosphere, oxidation in soils, and photochemistry in the marine boundary layer. OH radicals are formed by photolysis of ozone (O_3) in the presence of water vapor. OH is destroyed in reactions with CO, CH_4 and non-methane volatile organic compounds. Between 2000 and 2009, methane loss by OH radicals was between 476-677 performed (Saunio et al., 2020). In addition, in the troposphere reactions can occur with Cl, which lead to the oxidation of methane, with a reduction of methane by 11 performed. In the stratosphere, on the other hand, methane losses occur through reactions with excited atomic oxygen, $O(^1D)$. These lead to an average methane loss of 31 performed. This is a value comparable for soil uptake reported by Saunio et al. (2020), for which the mean value is 30 performed for the last two decades (2000-2017). The equations for the chemical reactions occurring during the decomposition of methane are shown below (Frank, 2018):





Figure 3 shows how the methane budget is distributed globally over the last decade 2008-2017. It includes natural and anthropogenic methane emissions (arrows pointing up) and sinks (arrows pointing down) of methane and presents results of two approaches of estimating methane emissions: top-down and bottom-up. The top-down approach includes networks of atmospheric observations of methane, atmospheric inversions inferring emissions and sinks from assimilating atmospheric observations into atmospheric transport and chemistry models (Saunio et al., 2020). In the other hand, bottom-up approaches include process-based models for natural wetlands, inventories of anthropogenic emissions and biomass burning, data-based approaches for other natural sources, and atmospheric chemistry models (Saunio et al., 2020). The first row of numbers indicates the average emissions for a given category, and the numbers in parentheses indicate the uncertainties as minimum and maximum values. Orange indicates anthropogenic methane emissions and green indicates natural methane emissions, while yellow indicates biomass and bio-fuel burning belonging to both categories. The given values are in performed. Using a top-down approach, anthropogenic and natural sources are responsible for 60% and 40% of methane emissions, respectively. In the bottom-up case, the ratio is 1:1, as the natural methane emission estimates are higher. Total methane emissions are between 572 performed (top-down) and 737 performed (bottom-up), while all sinks reduce between 526 performed (top-down) and 625 performed (bottom-up). The difference between the two approaches on a global scale is about 30%, which may be caused by using the same OH distribution from the TRANSCOM experiment for most top-down models, leading to a constrained global budget (Saunio et al., 2020). In both approaches, the atmospheric increase rate, the unbalance of methane emission are not compensated for by the sink process.

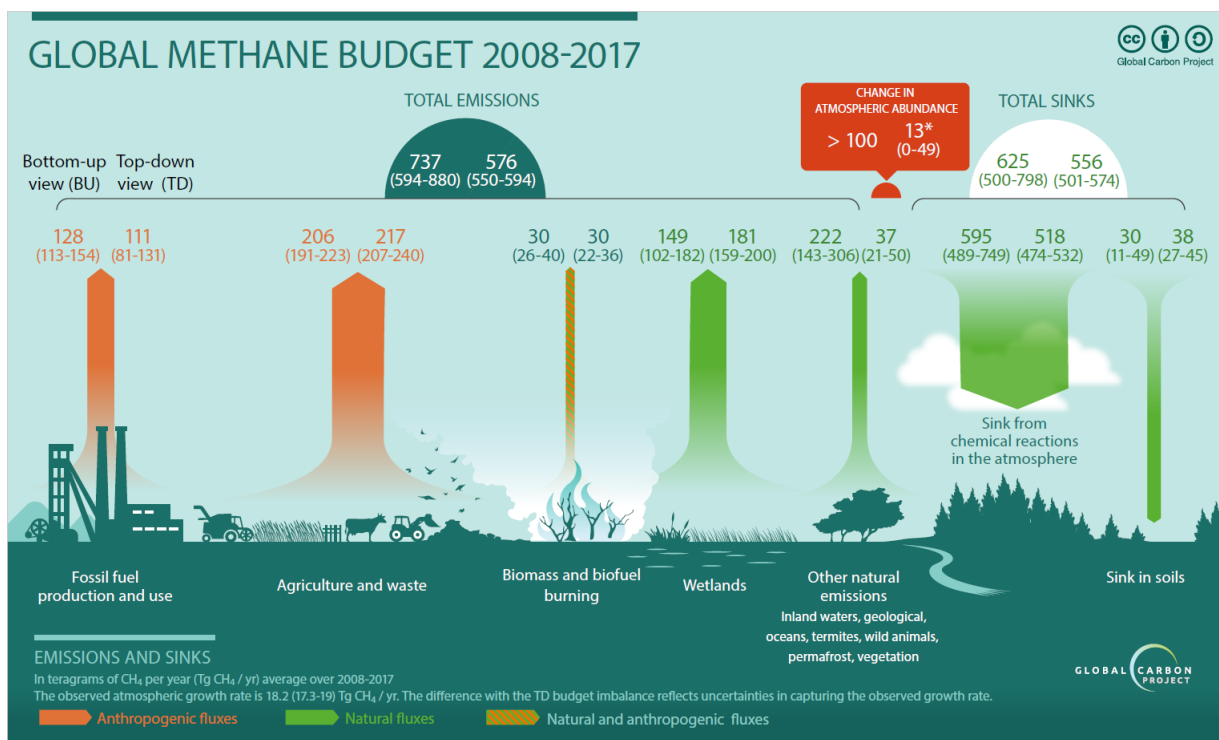


Figure 3: From Saunio et al. (2020). Global methane budget in years 2008 - 2017 in environment including different kind of fluxes (anthropogenic and natural). The numbers on the left represent bottom-down estimates and the numbers on the right represent top-down estimates, while the numbers in parentheses indicate the emission range (performed).

2.3 CH₄ Isotopes

Isotopes are atoms of the same chemical element which are characterized by a different number of neutrons. Isotopes also differ in abundance, the amount in which they occur in the environment. In the case of hydrogen, there are two stable isotopes, such as hydrogen ($H = {}^1H$) and deuterium ($D = {}^2H$), and one radioactive isotope, tritium ($T = {}^3H$). The carbon atom also has 3 isotopes: carbon ${}^{12}C$, ${}^{13}C$ and ${}^{14}C$. The first two are stable isotopes, while the third is radioactive and is used in radiocarbon dating. All the above isotopes and their abundances are shown in the table below.

Table 1: Stable isotopes of hydrogen and carbon (Hitchman et al., 1989).

Atom	Hydrogen		Carbon	
	H	D	${}^{12}C$	${}^{13}C$
Abundance [%]	99.985	0.015	98.89	1.11

The methane isotopic composition is given using delta notation (δ) with following definition for carbon isotope (Keeling, 1958; Mook, 2000):

$$\delta^{13}C_s = \left(\frac{R_{sample}}{R_{standard}} - 1 \right) * 1000 \quad (4)$$

R represents the ratio of abundance of a rare isotope to the abundance of the most common isotope, in the case of carbon it is $^{13}C/^{12}C$ for sample (R_{sample}) and standard ($R_{standard}$) respectively. The unit used to describe a δ is part per thousand, noted as ‰. To report ^{13}C of methane (here it will be reported as $\delta^{13}CH_4$) the VPDB (Vienna Pee Dee Belemnite) international standard is used.

Studying the isotopic composition gives additional information on the origin of methane, since each CH_4 source has its own characteristic isotopic composition of both carbon and hydrogen. There are three main groups of methane origin: biogenic, thermogenic and pyrogenic. This represents a second classification of the methane's origin, here in terms of the process by which it was formed. Biogenic sources contain CH_4 -generating microbes (Kirschke et al., 2013) and include boreal and tropical wetlands, rice cultivation, ruminants and waste decomposition (Brass et al 2010). The isotopic composition for such sources is usually strongly depleted in ^{13}C and D ($\delta^{13}C \sim -60$ ‰, $\delta D \sim -300$ ‰). Typical $\delta^{13}CH_4$ values of biogenic methane range between -70 and -50 ‰. Thermogenic methane was formed by geological processes over millions of years, together with coal and oil as natural gas.. CH_4 from coal, oil and natural gas is rich in heavy isotopes ($\delta^{13}C \sim -40$ ‰, $\delta D \sim -150$ ‰). The isotopic ^{13}C signatures range for thermogenic sources between -55 ‰ and -25 ‰ (Kirschke et al., 2013). Pyrogenic methane is characterized by enrichment in heavy carbon isotopes ($\delta^{13}C \sim -25$ ‰) and depletion in deuterium ($\delta D \sim -230$ ‰) (Kirschke et al., 2013). The isotopic signature ($\delta^{13}CH_4$) range for pyrogenic methane sources is -25 ‰ to -13 ‰, and it is formed by the incomplete combustion of biomass and soil carbon during wildfires and of biofuels and fossil fuels (Kirschke et al., 2013). The isotopic signature of atmospheric air is about $\delta^{13}C = -53.6$ ‰, $\delta^2H = -95$ ‰ (Sherwood et al., 2017). Figure 4 shows a recent plot of $\delta^{13}C$ versus δ^2H for methane for different sources (Sherwood et al., 2017). A distinction has been made between biogenic and thermogenic methane, and symbols are used to indicate which samples were used to create the base. These are both fossil fuels and non-fossil sources.

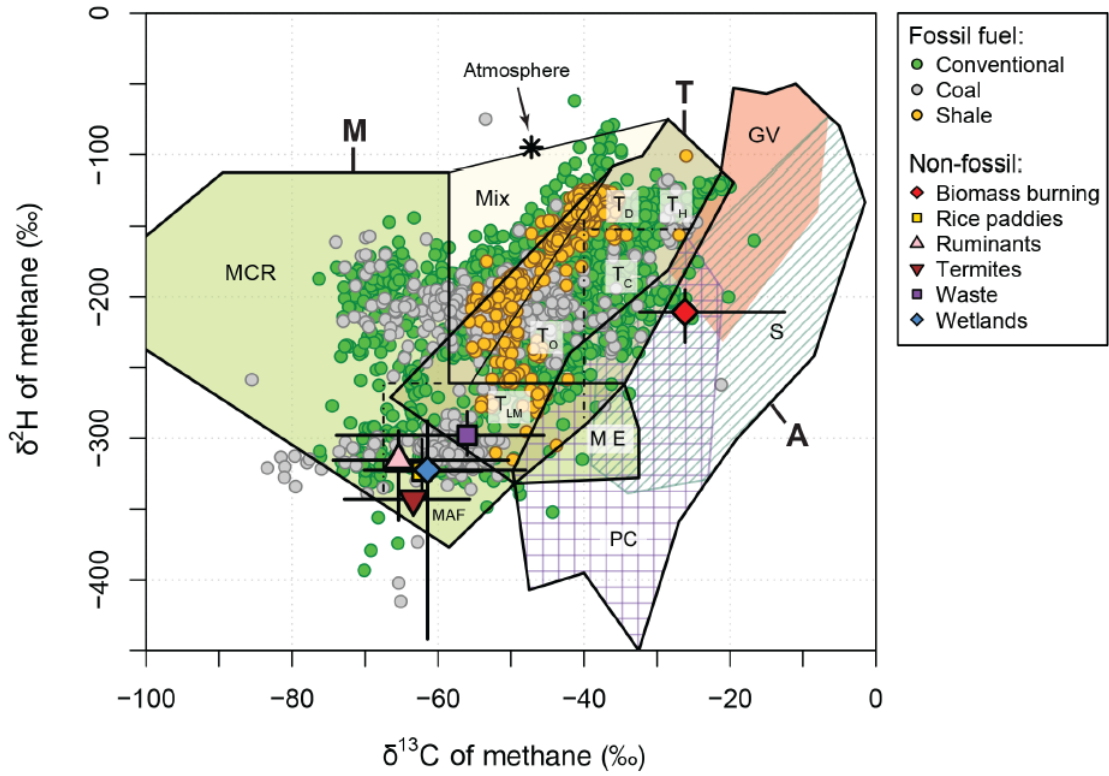


Figure 4: Characterization of methane based on its isotopic composition ($\delta^{13}C$, δ^2H), from Sherwood et al. (2017). M: microbial, T: thermogenic, A: abiogenic, MCR: microbial CO_2 reduction, MAF: microbial acetate fermentation, ME: microbial in evaporitic environment, T_O : thermogenic with oil, T_C : thermogenic with condensate, T_D : dry thermogenic, T_H : thermogenic with high-temperature $CO_2 - CH_4$ equilibration: T_{LM} : thermogenic low maturity, GV: geothermal-volcanic systems, S: serpentinized ultramafic rocks, PC: Pre-cambrian crystalline shields.

The isotopic signature of the methane emitted by source can be determined using one of two methods: Keeling plot or Miller-Tans plot (Keeling, 1958; Miller and Tans, 2003). The first mentioned method is an inverse relationship, while the second is a linear relationship. Both methods assume that the measured methane concentration (CH_{4M}) is the combination of the background methane concentration (CH_{4B}) of the atmosphere and the source concentration (CH_{4S}). This relationship is shown below:

$$CH_{4M} = CH_{4B} + CH_{4S} \quad (5)$$

By taking into account the isotopic signature of each element, the isotopic composition of the measured concentration can be determined:

$$\delta^{13}CH_{4M} = \frac{CH_{4B}(\delta^{13}CH_{4B} - \delta^{13}CH_{4S})}{CH_{4M}} + \delta^{13}CH_{4S} \quad (6)$$

Plotting the $\delta^{13}CH_{4M}$ versus the inverse of the measured concentration (CH_{4M}) gives a linear regression whose intercept indicates the isotopic signature of the source ($\delta^{13}CH_{4S}$).

Multiplying the Equation 6 by the measured concentration (CH_{4M}) yields a formula referred to as the Miller-Tans relationship.

$$\delta^{13}CH_{4M} \cdot CH_{4M} = CH_{4B} (\delta^{13}CH_{4B} - \delta^{13}CH_{4S}) + \delta^{13}CH_{4S} \cdot CH_{4M} \quad (7)$$

As in the case above, the linear regression method is used. However, here the plot shows the correlation of the measured concentration and its isotopic signature with the measured concentration. The isotopic signature of the source is then determined by the slope of the resulting linear regression. More details are described by Miller and Tans (2003).

Hoheisel et al. (2019) studied different fitting methods and compare Keeling and Miller Tans Plots using mobile CH_4 and $\delta^{13}CH_4$ measurements. Taking this results into account here I will analyse my data with the Miller-Tans method, using a York fit.

Figure 5 shows the isotope ^{13}C signature of various sources collected by Hoheisel et al. (2019) based on several publications between 1988 and 2016. The source categories are similar to the CH_4 sources studied in this thesis and provide a comparative basis. Some of the resources presented have been divided into subgroups because they highlight certain aspects. Violet dots for manure indicate the isotopic signature for liquid manure, while green dots indicate manure piles. In contrast, for cows this division occurs because of nutrition, C3-plants are in violet and C4-plants in green. Natural gas is divided according to its origin, purple dots mean natural gas from Siberia, while green dots mean natural gas from the North Sea.

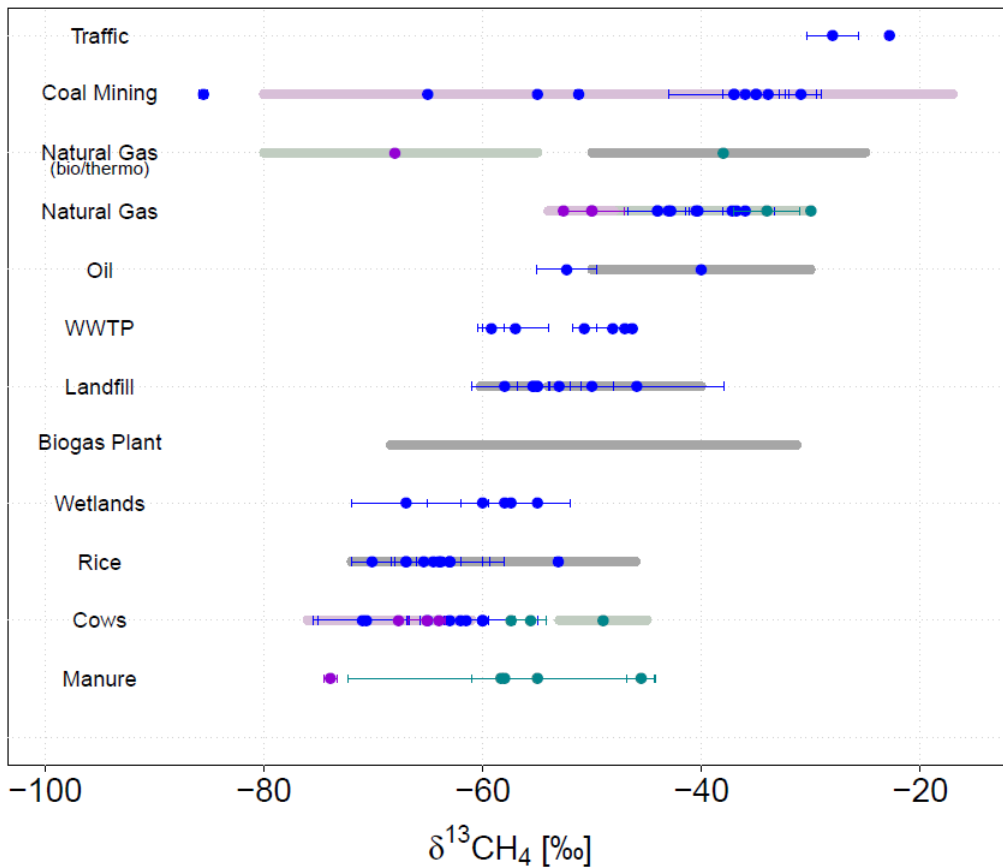


Figure 5: From Hoheisel (2017). Isotope signatures of different methane emitters based on several publications (1988 - 2016). Dots with/without errorbars represents averaged isotopic signature values, while color lines represent ranges of $\delta^{13}CH_4$ reported by authors.

2.4 Emission estimation

This chapter describes the methane emission estimation methods that were used during the measurement campaigns conducted during this dissertation. Two methods were used for field measurements and data analysis: Gaussian Plume Model (GPM) and Other Test Method 33A (OTM-33A). Both methods were also tested with controlled release experiment as described in section 5.

2.4.1 Gaussian Plume Model

The Gaussian Plume Model (GPM) is an atmospheric transport model in which, an analytical solution to the diffusion equation is shown for certain ideal conditions (Abdel-Rahman et al., 2008). The GPM was first reported in the 1930s (Sutton et al., 1932) and then in the 1960s and 1970s by Pasquill (1961, 1974) and Gifford (1961, 1968). It assumes that the atmospheric turbulence is stationary and homogeneous and that the emitter is a source of constant Q force (Hanna et al., 1982) This is one of the models used to determine the emission of a source with a known location. This model is used to estimate emissions on a local scale (less than a few kilometers) under certain constant meteorological conditions (Kumar et al., 2021) and with the assumption of the terrain, that should be relatively flat and open area (Abdel-Rahman et al., 2008). The GPM describe a relation between emission (Q) and measured concentration and it is presented in Equation 8 and in the coordinate system of Gaussian distribution in the horizontal and vertical is shown in Figure 6 (Turner et al., 1970):

$$C(x, y, z) = \frac{Q}{2\pi\sigma_y\sigma_zU} \exp\left(-\frac{1}{2}\left(\frac{y}{\sigma_y}\right)^2\right) \left[\exp\left(-\frac{1}{2}\left(\frac{z-H}{\sigma_z}\right)^2\right) + \exp\left(-\frac{1}{2}\left(\frac{z+H}{\sigma_z}\right)^2\right) \right] \quad (8)$$

where:

- C is the concentration in the location x, y and z
- Q is the emission rate of the source [mass per s]
- U is the mean wind speed
- σ_y and σ_z are the parameters of the normal distribution in y and z direction [m] (other name: horizontal and vertical dispersion coefficients)
- x is the downwind distance from the source [m]
- y is the horizontal distance perpendicular to the wind direction [m]

- z is the vertical direction [m]
- H is the effective height of the plume [m] (release height above ground)

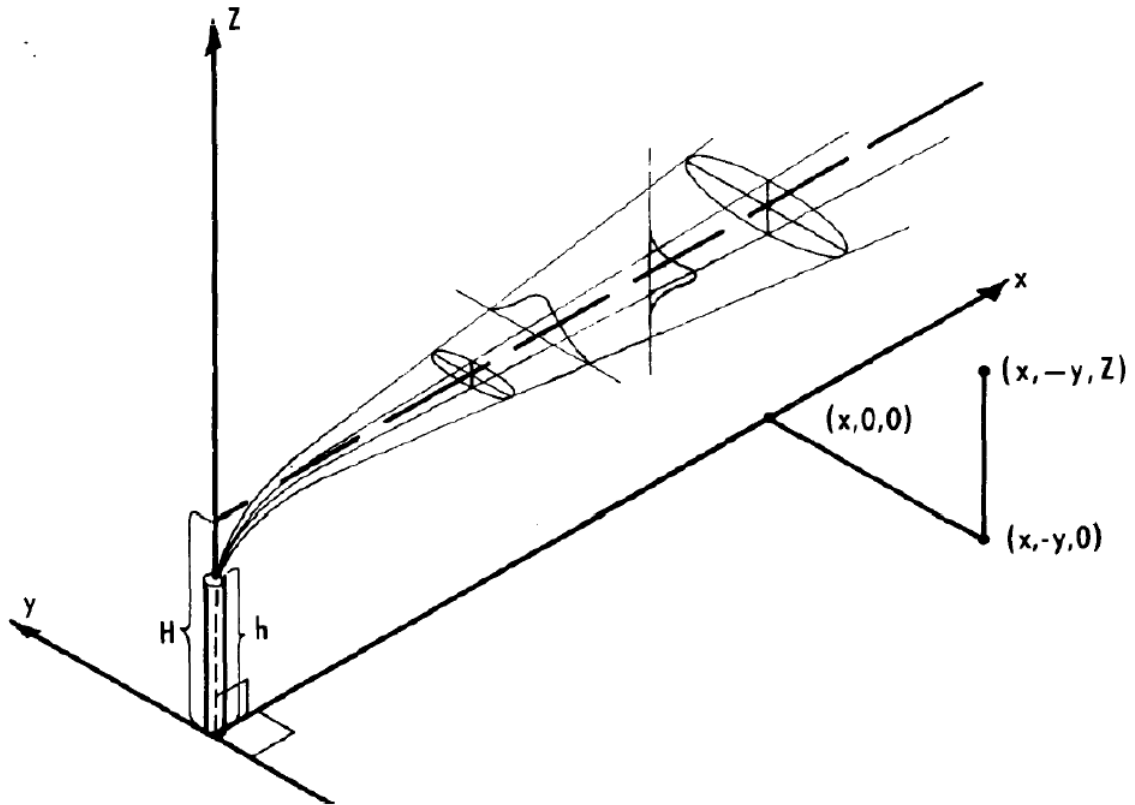


Figure 6: Coordinate system with Gaussian plume of a tracer gas released from point source and transported in the horizontal (y) and vertical (z) direction (Turner, 1970).

The location of point coordinates is determined from the wind direction relative to a known source. In this formula, the last term is responsible for the reflection of the plume at ground level. The values for the dispersion coefficients are mostly determined as a function of downwind distance and stability class, which were determined in experiments in the 1950s and 1960s conducted by Pasquill and Gifford. Initially, the experimental results were classified as values of coefficients in simple exponential equations and suitable for calculations of less than 1 km. They may also work for greater distances, but at that time the database was small to be certain. The following graphs show the relationship between σ_y and σ_z as a function of downwind distance. The solid line indicates the experimental results, while the dashed lines show the expected predictions. Briggs (1973) summarized previous work for dispersion coefficients, using theoretical concepts regarding the asymptotic limits of the formula, and derived the widely used set of formulas given in Table 2. Briggs' parametrization was used to determine the σ_y and σ_z values in the studies of GPM in this dissertation. The formulas given are dedicated to rural measurements, and only

such measurements were conducted as part of this work, so the formulas for urban areas were omitted. Figure 7 shows the variation of sigma values as a function of measurement distance for six stability classes of the atmosphere.

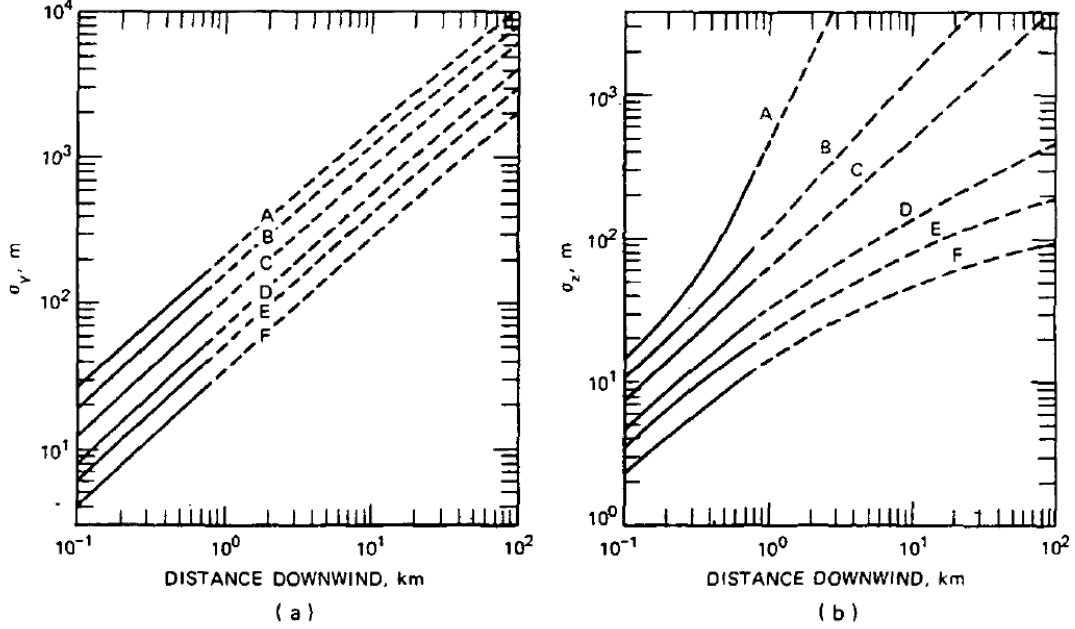


Figure 7: Coordinate system with Gaussian plume of a tracer gas released from point source and transported in the horizontal (σ_y) and vertical (σ_z) direction (Turner, 1970).

Table 2: Briggs parametrisation for stability classes (x is a distance in m). $\sigma_y[m]$ and $\sigma_z[m]$ mean horizontal and vertical dispersion coefficients

Stability class	$\sigma_y[m]$	$\sigma_z[m]$
A	$0.22x(1 + 0.0001x)^{-1/2}$	$0.20x$
B	$0.16x(1 + 0.0001x)^{-1/2}$	$0.12x$
C	$0.11x(1 + 0.0001x)^{-1/2}$	$0.08x(1 + 0.0002x)^{-1/2}$
D	$0.08x(1 + 0.0001x)^{-1/2}$	$0.06x(1 + 0.00015x)^{-1/2}$
E	$0.06x(1 + 0.0001x)^{-1/2}$	$0.03x(1 + 0.0003x)^{-1}$
F	$0.04x(1 + 0.0001x)^{-1/2}$	$0.016x(1 + 0.0003x)^{-1}$

As shown above, the determination of the dispersion coefficients depends on the stability class of the atmosphere. The description of the atmospheric conditions in the model is contained in the stability classes. These contain information about the wind speed during the measurements as well as the solar radiation. The most popular method of determining the atmospheric stability classes is the Pasquill method presented by Pasquill (1961). They have been categorized and assigned the letters A - F. They are described as follows:

- A - Extremely unstable conditions
- B - Moderately unstable conditions
- C - Slightly unstable conditions
- D - Neutral conditions
- E - Slightly stable conditions
- F - Moderately stable conditions

Table 3 and Table 4 present Pasquill stability classes based on wind speed and time of the day. First for classes (A-D) correspond to the atmosphere during daytime. Stability classes E-F correspond to the stability of the atmosphere during night. Class D is a neutral class that can be used both day and night. In addition, the day time stability classes depend on the degree of insolation, which has been divided into 3 categories: strong, moderate and slight. Strong insolation corresponds to a sunny midday in midsummer in England; slight insolation to similar conditions in midwinter. "Night time" is defined as the period from 1 hour before sunset to 1 hour after sunrise. The general recommendation is to use class D when there is cloud cover and then regardless of wind speed.

Table 3: Atmospheric stability classes by Pasquill for daytime insolation (Turner, 1970; NOAA).

Wind speed [m/s]	Strong insolation	Moderate insolation	Slight insolation)
< 2	A	A - B	B
2 - 3	A - B	B	C
3 - 5	B	B - C	C
5 - 6	C	C - D	D
6 <	C	D	D

Table 4: Atmospheric stability classes by Pasquill for nighttime conditions (Turner, 1970; NOAA).

Wind speed [m/s]	Cloudness $\geq 4/8$	Cloudness $\leq 3/8$ cloud
< 2		
2 - 3	D	F
3 - 5	D	E
5 - 6	D	D
6 <	D	D

As shown in the above tables, the choice of atmospheric stability class depends on three parameters: wind speed, insolation and possible cloud cover. The neutral (D) and

stable classes are found at very high wind speeds or during the night, so the most common classes chosen for mobile measurements are A-C, and possibly D.

When data from the analyzer, weather station, and GPS logger are converged, the data analysis process consists of steps that are described in more detail by Kammerer (2019). The first of these steps involves determining the input value of the model. As shown above, the plume propagation formula (Equation 8) contains a number of variables. These include meteorological conditions, the location of the plume in relation to its source, and the source itself, where it is necessary to give its coordinates, height, and its strength, which is called the source's emission. Following Kumar et al. (2021), the wind direction can be determined based on the geographical coordinates between the maximum concentration of the measured peak and the location of the emitter. This allows for the best reproduction of the modelled peak. The wind speed is given from meteorological measurements, and its exact determination is described in the chapter 4, Release test.

Ultimately, the Inverse GPM is used here, in which a value of the emission (typically 1 g/s) is inserted in the Equation 8 and the CH_4 concentration is calculated. Thus the modelled concentration is compared with the results of measurements, namely the comparison of areas of these peaks, which are calculated as the methane concentration above the background multiplied by the distance to the next data point. The background level was determined using the `rfbaseline` function (IDPmisc package), which allows to determine the background conformance value in dependence on its variation, it is a moving background method. Using the relationship below, i.e. knowing the areas of both peaks as well as the modelled emissions, the emissions of the source are determined.

$$Q_{meas} = \frac{\int_{measpeak}}{\int_{modelpeak}} * Q_{model} \quad (9)$$

The emission estimation is done for each recorded peak separately. In this way we get the emission rate values for the whole set of performed transects and from them we calculate the mean and the median with their uncertainties. During the data analysis a quality check was performed inspecting all transects. Cases where the peak was not measured over the entire range were rejected. This means that each transect had to contain a background level, an enhancement, and again a background level. In addition, transects for which peaks were recorded in the event of a vehicle turnaround were also rejected.

2.4.2 Other Test Method 33A

The second method used to estimate methane emissions was the Other Test Method (OTM) 33A developed by the United States Environmental Protection Agency (EPA). This method belongs to a group of Other Test Methods that have been reviewed by EPA's Emission Monitoring Center (EMC) and have been found to be potentially applicable for the emission determination, although they have not yet been approved by the Federal rulemaking process (Thoma et al., 2014). Geospatial measurement of air pollution (GMAP) is a general term that refers to mobile measurements with the use of fast time response instruments and the use of GPS positioning to determine the temporal-spatial air pollution in various uses. A simplified definition of OTM, reads as follows: "Other Test Method (OTM 33) is a general GMAP approach that uses ground-based vehicles to perform remote emissions quantification (REQ) at local scales" (Omara, 2018). OTM33 gives general rules for GMAP-REQ, of which OTM-33A is a submethod used to describe a mobile estimation of emissions from point sources located near-field and at ground level. One of the advantages of the OTM-33A method is the short measurement time and the fact that it allows to estimate the emissions from the source without the use of deployed equipment or site-specific modelling. As with any method, OTM-33A also has some limitations, the practical examples of which will be described a little later. In the method description presented by EPA (Thoma et al., 2014), OTM-33A can be used for one or more of the following three source assessment modes:

1. CM - concentration mapping - used to find the location of unknown sources and/or to assess the relative contributions of source emissions to local air shed concentrations.
2. SC - source characterisation - used to improve understanding of known or discovered source emissions through direct GMAP observation or through GMAP-facilitated acquisition of secondary measures.
3. EQ - emission quantification - used to measure (or estimate) source emission strength.

OTM-33A is a useful approach in applications where the location of the source is unknown. Moreover, it is a useful tool in the case of relatively small emission sources at ground level, and also when needing to make measurements without direct access to the source.

During studies presented in this dissertation, OTM-33A was applied to quantify the emissions from point sources. From the practical side, OTM-33A can be described as a method based on stationary measurements of gas concentration depending on the wind direction. It is a simplified Gaussian model which assumes the propagation of the wind

during the measurements and thus the Gaussian plume is formed after taking into account the gas transport.

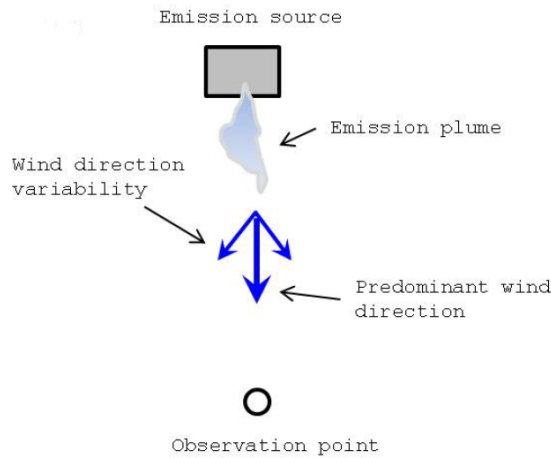


Figure 8: Illustration of stationary field measurements with marked position of the source of the emission and the observation point (Thoma et al., 2014).

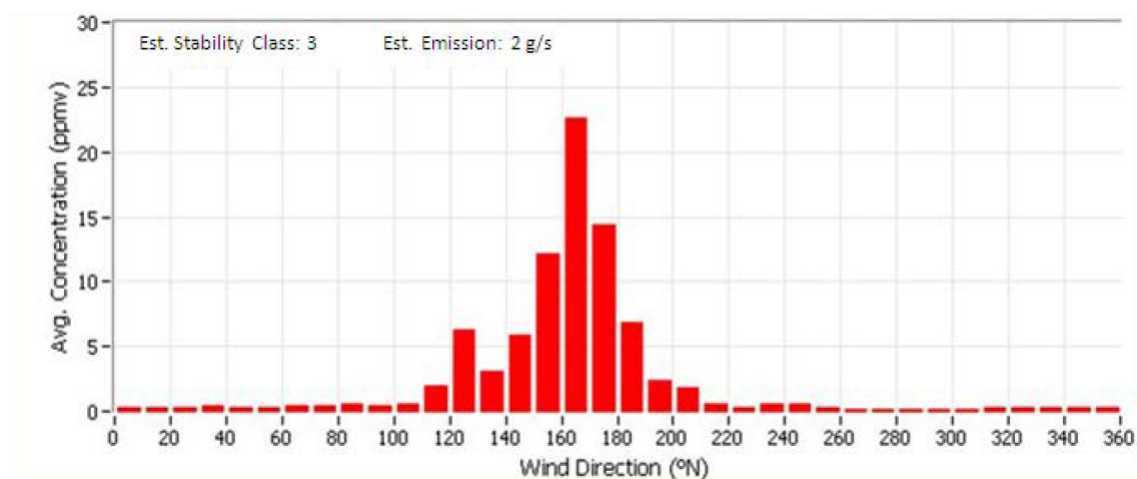


Figure 9: Distribution of gas concentration in relation to the measured wind direction (Thoma et al., 2014).

Figure 8 presents an example of emission quantification. It shows the position of the source of the emission and the observation point. Blue arrows represent the wind fluctuations during measurements. Those fluctuations in the wind direction cause the Gaussian distribution for the gas concentration value relative to the measured wind direction. This means that the highest number of points and the highest concentration of the measured gas occur in the main wind direction. An example of such a distribution is presented as a histogram in Figure 9. The further the wind direction is from the main wind direction, the lower the level of gas concentration that can be measured. It is therefore crucial to locate

the observation point in the headwind direction, which will allow the observation of the full level of gas concentration distribution.

The described method requires certain conditions to be met in terms of instruments and equipment. In situ CH_4 measurement instrument need to record at a frequency of 1 Hz or faster. It is recommended to have both a 2D and 3D weather station with a measuring frequency of 1 Hz or faster and a GPS with high temporal resolution. Additional equipment such as an infrared camera, which will help to precisely locate the gas plume. All the above-mentioned devices will facilitate in equipping the necessary mobile laboratory, which will allow for quick and efficient measurements.

The measurements at a site starts with screening. This involves circling the suspected source and determining in which direction the plume is spreading, with the highest concentration in line with the main wind direction. Mapping the concentrations accurately will allow to better determine where the measurement should be taken. The collection of representative and unrepresentative gas concentration distributions is shown in the images below. They show both a top-down view and a side-down view. As it turns out, both wind direction and velocity have an effect on the measurement, and obstructions can have no less influence. If the mobile device is not aligned with the main wind direction, the distribution of the methane concentration in the plume will be lower, because the tail of the plume will be recorded, not the top of the plume Figure 10. The same is true for the wind speed. If the wind speed is too low, the plume will have a lower concentration as it rises more vertically than horizontally, which is opposite to the situation where the plume is measured at a higher wind speed Figure 11. Figure 12 and Figure 13 show how the measured methane concentration distribution looks when there is an obstacle between the source and the sensor. If this is the case, the observed distribution can be either a reduced Gaussian distribution or a distribution with an undershoot. The positioning of the instrument measuring the methane concentration is also an important factor. Thus, in order for emission estimate to provide a meaningful value, the analyzer should be placed facing the plume if the inlet is mounted on the roof of the car Figure 14, or as was the case for the measurements described below, the analyzer was placed separately facing the plume. According to the description of the OTM-33A method, it should also be applied under appropriate field conditions. This means that the method should not be used if the source is in a forest or an area with many obstacles, but in a flat area without surrounding obstacles Figure 15.

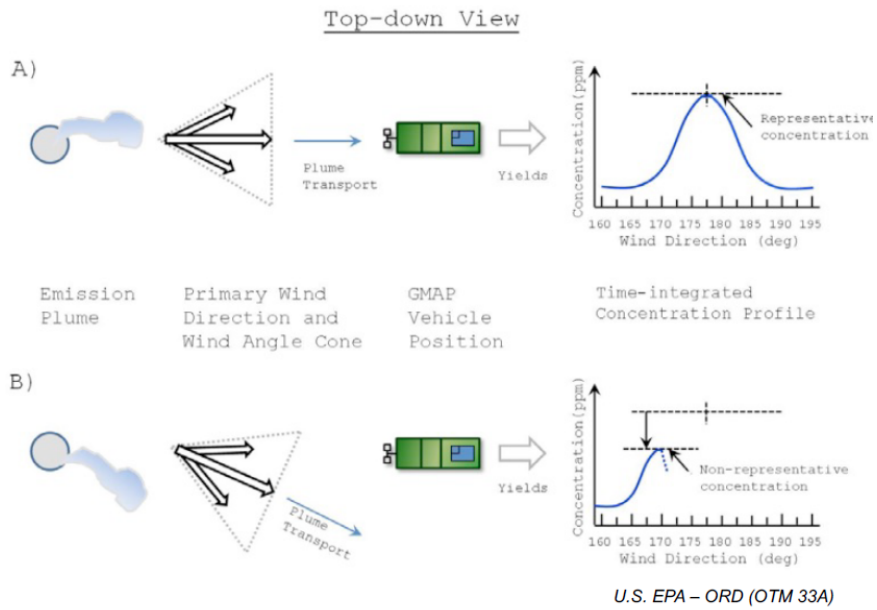


Figure 10: Top-down view. Example illustrating a representative (top) and unrepresentative (bottom) gas concentration profile in terms of wind direction (Thoma et al., 2014; Omara, 2018).

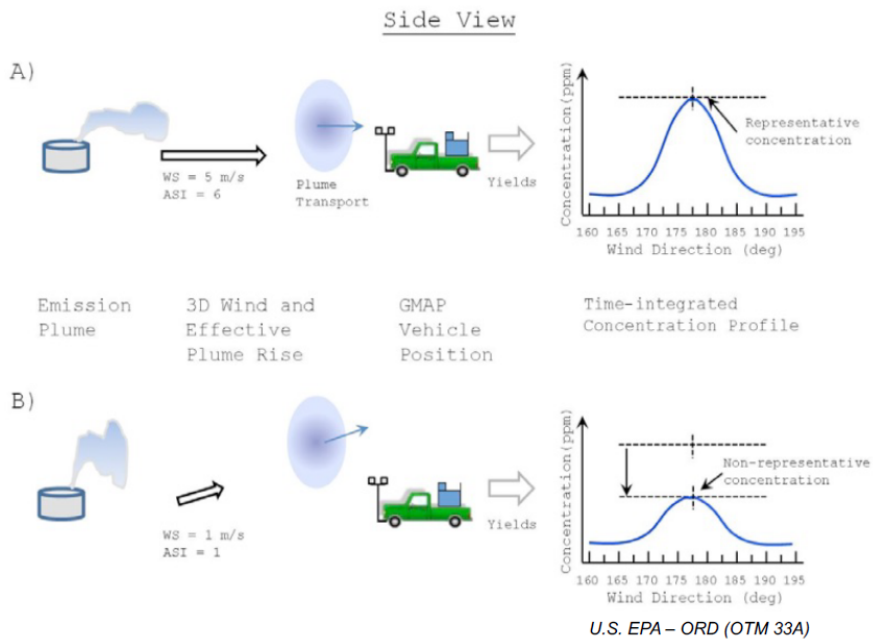


Figure 11: Side view. Example illustrating a representative (top) and unrepresentative (bottom) gas concentration profile in terms of wind speed (Thoma et al., 2014; Omara, 2018).

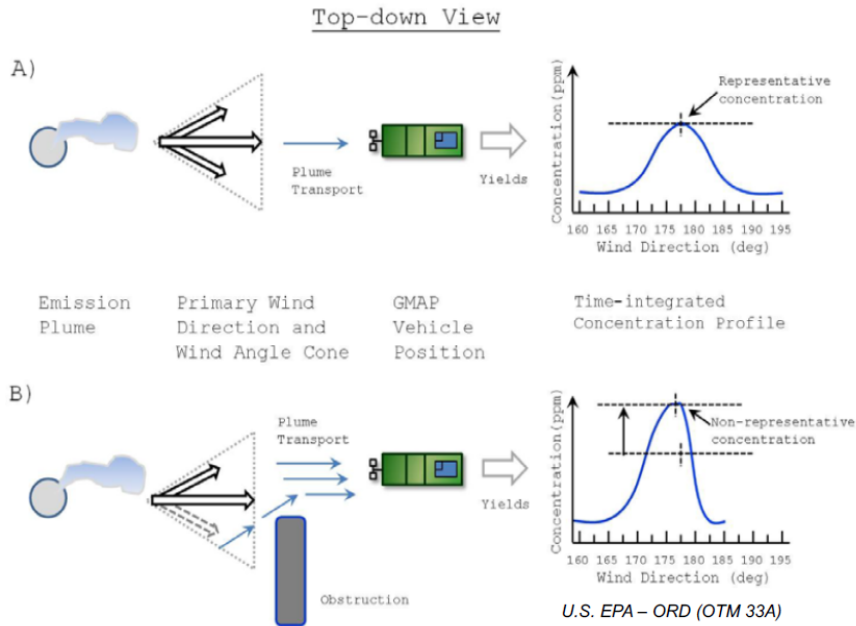


Figure 12: Top-down view. Example illustrating a representative (top) and unrepresentative (bottom) gas concentration profile due to possible obstacles between the source and the receiver (Thoma et al., 2014; Omara, 2018).

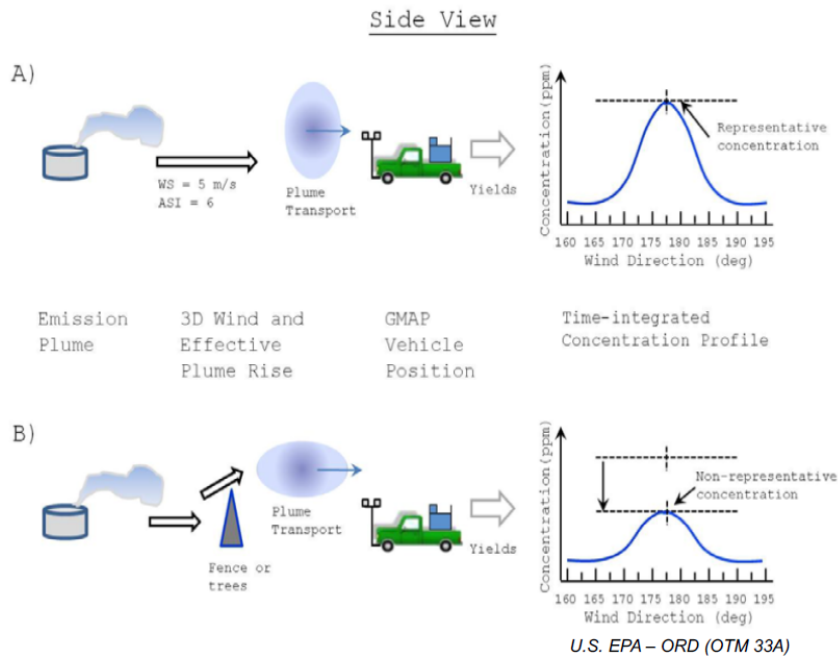


Figure 13: Side view. Example illustrating a representative (top) and unrepresentative (bottom) gas concentration profile due to possible obstacles between the source and the receiver (Thoma et al., 2014; Omara, 2018).

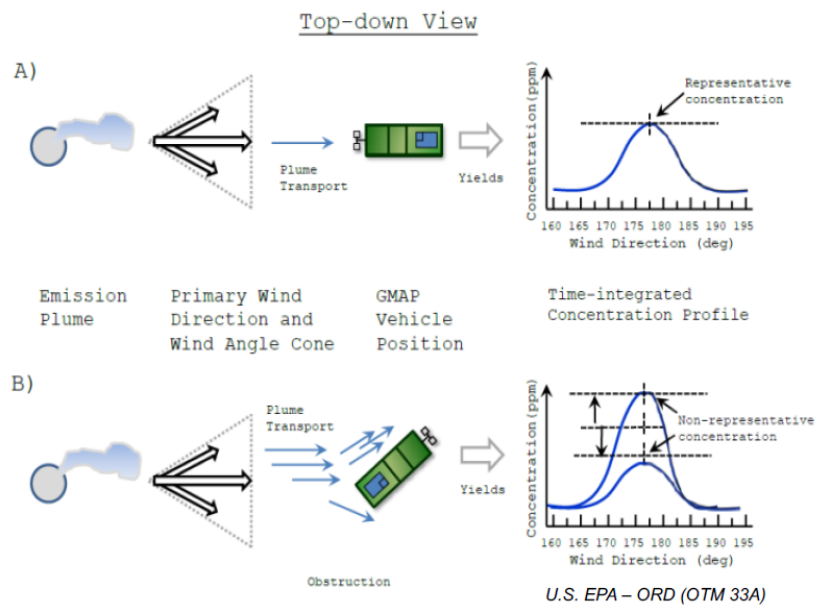


Figure 14: Top-down view. An example illustrating a representative (top) and unrepresentative (bottom) gas concentration profile due to the vehicle’s orientation with respect to the plume transport (Thoma et al., 2014; Omara, 2018).



Figure 15: An example of an acceptable topography (A, top) and an unacceptable topography (B, bottom) for OTM-33A application (Thoma et al., 2014; Omara, 2018).

Certain practical conditions must be met when applying the OTM-33A method. The measurement should take place at a distance of 20 - 200 m downwind from the source. In addition, one measurement should be carried out for at least 15 - 20 minutes.

When all data are merged together (methane results, 2D, 3D and GPS), further analysis consists of several steps. Firstly, the 3D sonic anemometer is rotated to streamlined coordinates. The u, v and w coordinate system is first rotated through the angle formed by the mean u in the u and v directions and second by the mean u in the v and w directions. Next step is to determine average local atmospheric stability class (PGI). The average of the local stability class is based on the stability class calculated using the standard deviation of the wind direction and the so-called turbulent intensity which is the ratio of the standard deviation for the "w" component of the wind direction versus the average wind speed (Thoma et al., 2014; Omara, 2018). The stability class PGI is calculated as the average of the two classes. The possible stability classes and the basis for their determination are presented in Table 5. There are seven stability classes, respectively from extremely unstable to extremely stable, which correspond to the Pasquill stability classes during the day (A - D, Table 3).

Based on measured source distance and the calculated PGI the horizontal and vertical dispersion coefficients, σ_y and σ_z respectively, are determined based on EPA recommendations. Furthermore the average methane background concentration is calculated and subtracted from all methane concentration data. The average methane background is defined as the lowest 5% of all CH_4 concentration data. Then the data are binned every 10 degrees and the average value of the methane concentration is calculated in each bin. If the number of measurement points in a given bin is less than 2% of the total number of points, then the corresponding value of the mean is set to 0. Next step is to perform a Gaussian fit of the mean methane concentration versus binned wind direction to determine the peak methane concentration. Final step is to convert the maximum concentration of methane peak from ppm to g/m^3 and calculate methane emission rate using the equation below.

$$Q = 2\pi \cdot \sigma_y \cdot \sigma_z \cdot U \cdot C \quad (10)$$

Where: σ_y and σ_z are horizontal and vertical dispersion coefficients [m], respectively, U is mean wind speed [m/s], C is the peak methane concentration from the Gaussian curve fitting [g/m^3]. In order to determine the quality of a given measurement and its usefulness, so-called Data Quality Indicators (DQI) were introduced, which allowed for the acceptance or rejection of a given quantification. Data quality indicators for this method include 3 points listed below, and quantification was accepted when all DQI were fulfilled:

1. Fitted peak methane concentration should be within ± 30 degrees of the source direction to identify possible interferences;
2. Average in-plume concentration should be greater than 100 ppb to ensure that there was sufficient plume transport;

3. A Gaussian fit curve with an R^2 value greater than 0.80 to help identify potential interferences and obstructed wind flow conditions to avoid collecting many sources in one plume.

Estimated emission rates were calculated with the R script analysis program dedicated for Point Source Gaussian (PSG) approach.

Table 5: Local atmospheric stability class during stationary measurements based on wind direction and wind speed, (Thoma et al., 2014; Omara, 2018).

Atmospheric Stability Indicator (ASI)	Definition	Standard deviation of wind direction (StdWD)	Turbulent intensity (Turbint)	Average local wind stability class (PGI)
1 (A)	Extremely unstable	$\text{StdWD} > 27.5^\circ$	$\text{Turbint} > 0.205$	$\text{PGI} < 1.5$
2 (B)	Moderately unstable	$23.5^\circ < \text{StdWD} \leq 27.5^\circ$	$0.180 < \text{Turbint} \leq 0.205$	$1.5 \leq \text{PGI} < 2.5$
3 (C)	Slightly unstable	$19.5^\circ < \text{StdWD} \leq 23.5^\circ$	$0.155 < \text{Turbint} \leq 0.180$	$2.5 \leq \text{PGI} < 3.5$
4 (D)	Neutral	$15.5^\circ < \text{StdWD} \leq 19.5^\circ$	$0.130 < \text{Turbint} \leq 0.155$	$3.5 \leq \text{PGI} < 4.5$
5 (E)	Slightly stable	$11.5^\circ < \text{StdWD} \leq 15.5^\circ$	$0.105 < \text{Turbint} \leq 0.130$	$4.5 \leq \text{PGI} < 5.5$
6 (F)	Moderately stable	$7.5^\circ < \text{StdWD} \leq 11.5^\circ$	$0.080 < \text{Turbint} \leq 0.105$	$5.5 \leq \text{PGI} < 6.5$
7 (G)	Extremely stable	$\text{StdWD} \leq 7.5^\circ$	$\text{Turbint} \leq 0.080$	$\text{PGI} \geq 6.5$

Part II

Methodology and research sites

3 Measurement techniques

In this section, measurement techniques and instruments used during measurement campaigns are described. These methods involve determination of methane concentration and methane isotopic composition using two spectroscopic analyser principles, cavity ring down spectroscopy and cavity enhanced absorption spectroscopy. In addition, the methods to sample air and the meteorological data acquisition will be described in detail.

3.1 Cavity Ring Down Spectroscopy

Almost every small molecule in the gas phase has its own unique near-infrared absorption spectrum, just as every human being has a unique fingerprint. In optical absorption, in order to obtain concentration of measured species, a spectral feature (an absorption peak) of a target species is measured (Wahl et al., 2006). Having this "fingerprint" makes it possible to distinguish a given gas on the basis of their spectral profile, because they have one or many wavelengths for which the absorption takes place. The measurement of the concentration of a given molecule can therefore be measured by measuring the strength of the absorption of a given gas.

Cavity Ring-Down Spectroscopy (CRDS) is an analytical technique in which the infrared absorption of a gas sample is measured by quantifying the optical decay rate of a highly resonant optical cell into which the gas sample is introduced (Rella et al., 2015). It allows to perform highly sensitive measurements down to ppb (parts per billion) or even ppt units (parts per trillion) (Rella et al., 2013). In many cases, it can be an alternative to the costly and complicated isotope ratio mass spectroscopy (IRMS) technique. CRDS was first introduced in a paper published by Anthony O'Keefe and David Deacon (1988). This method started out as a technique to measure the reflectivity of mirrors, and was later introduced as absorption spectroscopy (Yeman, 2015).

The CRDS method has a number of advantages, such as those listed below:

- High sensitivity, precision and accuracy with virtually no drift
- Fast, continuous, real-time measurements
- Large dynamic range with high linearity
- Field and laboratory deployable with no consumables

- Installed and operational in minutes
- Rugged and insensitive to changes in ambient temperature, pressure or vibration

The principle of the CRDS measurements is presented in Figure 16. The measurement starts as soon as laser light is introduced into the cavity. It has a specific frequency that is consistent with the resonant frequency of the cavity (length of the cavity is 25 cm). With the application of the mirror system with a high reflectivity of $\geq 99.999\%$, the optical path is extended to 20 km. This increases the detectability of small quantities and thus small absorption coefficient of trace gases in the sample. The temperature and pressure control systems are essential for the stability of the measurement conditions. The analyzers also uses the WS-CRDS (Wavelength-Scanned Cavity Ring Down Spectroscopy) technique. This technique change the length of the laser beam by changing the temperature of the semiconductor junction, which is the so-called laser active volume. This makes it possible to sample the absorption spectrum at different wavelengths for which the decay time is determined. When the light beam is introduced into the cavity, the light intensity increases, i.e. build-up (green curve, Figure 16). It is measured by a detector placed behind the mirror. The laser is turned off when the maximum intensity specified by the manufacturer is reached. The light intensity decays exponentially (ring-down) and the ring-down time is measured, which varies with the selected wavelength. The intensity is described by the exponential decay law:

$$I(t) = I_0 e^{-\lambda t} \quad (11)$$

where I_0 is the intensity at the turn off point and λ is the decay coefficient.

If there is a gas absorbing light in the cavity, an additional loss mechanism in the cavity (absorption) is introduced. This accelerates the decay time of the light intensity compared to a cavity without additional absorption due to the target gas. The CRDS analyser automatically and continuously calculates and compares the ring-down time of the cavity with and without absorption by the target gas and automatically calculates the absorption and the density of measured species. During measurement, the laser is passed through the absorption line and the gas concentration is calculated by using the mathematical fit (Van Pelt, 2008; Kammerer, 2019).

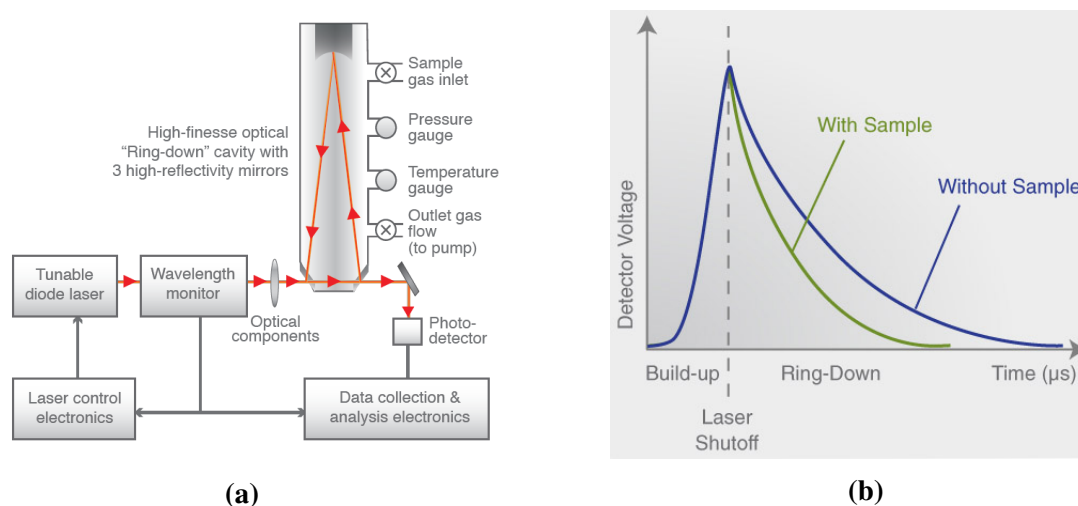


Figure 16: Diagram and principle of analyzer using Cavity Ring-Down Spectroscopy. (a) Schematic of CRDS Analyzer (Saad et al., 2009; Wahl et al., 2008), (b) The scheme of comparison of the cavity with and without sample (Picarro manual).

In this thesis a CRDS analyser Picarro G2201-i (Picarro, Inc. Santa Clara, US) was used. It is a device with dimensions of 43x48x18 cm (Figure 17) and dedicated to measure the concentration of carbon dioxide, methane and also the $^{13}\text{C}/^{12}\text{C}$ isotopic ratio. It is suitable for both laboratory and field measurements. The analyzer can operate in one of three measurement modes: 1) CO_2 only, 2) CH_4 only, and 3) CO_2 and CH_4 combined. The difference in the mode used relates directly to the time dedicated to measuring a given gas, which corresponds to the precision of the obtained results. In most cases the measurements were done in real time using the third mode resulting in a temporal resolution of 3.6 s per measurement.

The CRDS G2201-i instrument, used mainly during mobile measurements, was tested by Dinger (2014) and later by Hoheisel (2017) and Hoheisel et al. (2019), setting up a calibration and correction method. The laboratory system consisted of a CRDS analyser, a 16-port rotary valve, a set of calibration gases and additional equipment (monitor, keyboard, mouse). The rotary valve system allowed for an automatic change of air and calibration gases which was controlled by the instrument. In the laboratory set-up, three gases were connected (high, low and target), respectively to ports 3, 5 and 7. They were measured with a flow of 25 - 35 ml/min. The CRDS G2201-i was calibrated every 5 hours. The measurement of ambient air was carried out on port 1 with a flow of 80 ml/min. The gas flow was observed and monitored using the electronic flowmeter before the sample made its way to the analyzer. The other ports were used for measuring samples from tedlar bags (ports 11 and 13) or for control measurements (port 15).



Figure 17: Cavity Ring-Down Spectrometer (CRDS) - Picarro G2201-i. Instrument to measure a mole fraction and isotopes of CO_2 and CH_4 and concentration of H_2O (G2201-i Analyzer Datasheet)

3.2 Optical Feedback - Cavity Enhanced Absorption Spectroscopy

Optical Feedback - Cavity Enhanced Absorption Spectroscopy (OF-CEAS) was the second technique of measurement used for mobile measurement campaigns described in this dissertation. This is a Cavity-Enhanced Absorption Spectroscopy implementation that exploits optical feedback (OF) to achieve efficient injection of radiation from a continuous wave laser into a high-finesse ($F > 10,000$) optical cavity (Courtilot et al., 2009). The CEAS technique can be distinguished as a second cavity-based technique, where the intensity transmitted by the cavity is measured continuously (Motto-Ros et al., 2008). The OF-CEAS technique is a highly sensitive technique that relies on feedback from a resonant intracavity field to successively lock the laser to the cavity as the wavelength is scanned across a molecular absorption with a comb of resonant frequencies (Manfred et al., 2015). This method was firstly introduced by Morville et al. (2005).

The principle of the OF-CEAS technique will be presented here based on the V-shaped cavity that is used in the device described below and is also considered to be the simplest configuration producing frequency selected OF when the laser frequency enters in resonance with one of the cavity modes (Morville et al., 2005).

A gas measurement is made when the analyzer injects laser light into an optical cavity made up of mirrors 1, 2 and 3, forming a V, as shown in Figure 18. The mirrors are highly reflective, meaning that before a photon leaves the cavity and hits the photodiode of the sample (behind mirror 2) it can travel around the cell many times. By increasing the length of the effective path, which corresponds to enhanced sensitivity, many opportunities for the sample gas flowing through the cavity to absorb light are created. The device increases the laser drive current so that the laser can scan a range of wavelengths that include gas absorption characteristics. Some of the cavity photons are returned back to the laser, creating optical feedback that narrows the laser output. This couples a large portion of the laser power to the cavity and locks the laser frequency exactly in the middle of the cavity resonant mode. During scanning, the device creates a dense grid of fixed

cavity resonant modes that are equally spaced a few kHz apart. The laser discreetly jumps from one cavity resonance mode to the next. The laser frequency scans across the spectral range of interest in about 0.25 seconds, which allows all three gases (CH_4 , CO_2 and H_2O) to be measured. It uses the grid spacing determined in conjunction with the spectroscopic data to determine the exact frequency of each mode. To normalize the measured signal, the OF-CEAS Analyzer uses two "ring down" events - one at the beginning and end of the scan. Absorption is calculated for each resonant mode by comparing the normalized sample photodiode signal to the reference photodiode signal. Then, using a fitting algorithm that compares the measured absorption spectrum with an internally stored high-resolution spectrum, the concentration of each gas is determined (Licor manual).

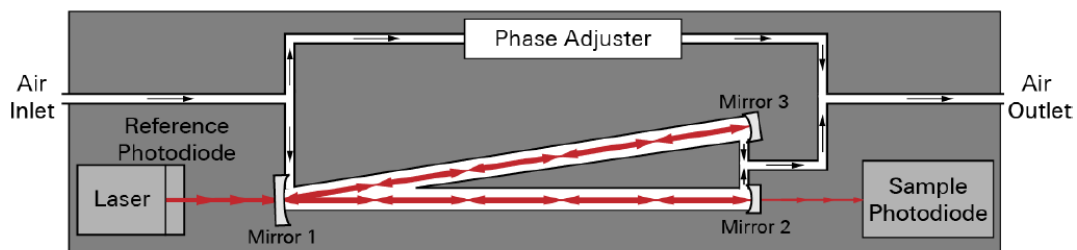


Figure 18: Optical Feedback - Cavity - Enhanced Absorption Spectroscopy, scheme of work (Licor manual).

The second instrument used for mobile measurements was the LiCor LI-7810 manufactured by LI-COR Biosciences, Lincoln, Nebraska, USA (Licor manual). This is a device that uses OF-CEAS. The LI-7810 is built in a small, handy suitcase with dimensions of 51x33x18 cm and weighs only less than 12 kg (see Figure 19). Because of its compactness, the LI-7810 is perfect for field campaigns and can be used for mobile measurements even on bicycles. It is powered by two internal batteries with the option to change batteries during operation, and a set of two batteries can power the device for up to 8 hours. The LI-7810 can be operated at a temperature between -25 and 45 °C, The flow rate is set to 250 sccm. This analyzer is designed to monitor concentration of CH_4 , CO_2 and H_2O with a data acquisition rate of 1 Hz. According to the manufacturer, the LI-7810 can measure methane concentrations from 0.1 to 50ppm. The measurement precision (1 sigma) is equivalent to 0.6 ppb at 2 ppm with 1 second averaging, and 0.25 ppb at 2 ppm with 5 second averaging. Furthermore, the possible drift should be less than 1 ppb per 24-hour period. For CO_2 , the measuring range is 1 - 10000 ppm with a precision (1 sigma) of 3.5 ppm and 1 ppm for 1 second and 5 second averaging, respectively (Licor manual).

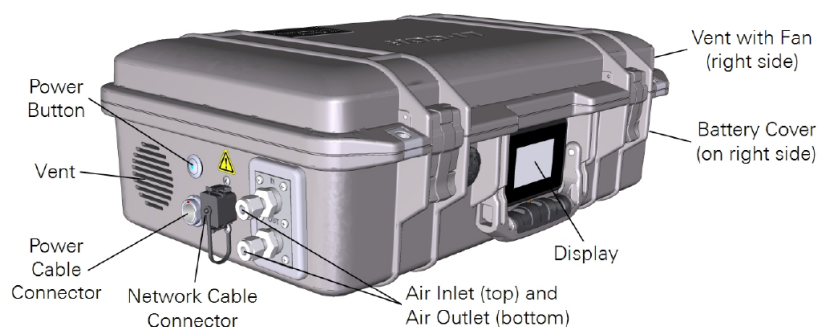


Figure 19: LICOR LI-7810, the Optical Feedback - Cavity - Enhanced Absorption Spectrometer used for mobile measurement to monitor concentration of CH_4 , CO_2 and H_2O (Licor manual).

3.3 AirCore

An AirCore is an auxiliary tool used during mobile measurements. At UHEI, it was developed by Yeman (2015) and then improved by Hoheisel (2017).

The AirCore was first presented in the study of Karion et al. (2010). It was described as 152-m -long, stainless-steel tubing, with an outer diameter of 0.64 cm and a wall thickness of 0.025 cm (Karion et al., 2010). In that study, the AirCore was used for balloon and aircraft measurements as the tube can not only sample the surrounding atmosphere air, but also can preserve a profile of the trace gas. Generally speaking, the AirCore is a tube with specific dimensions (length, cross-section, material from which it is made) that is used to store gas for a short period of time. Depending on the length and cross section of the tube, a limited amount of gas can be stored. In the case of the AirCore used by our group, it is a 25 m tube with an inner diameter of 9.5 mm and a volume of 1.77 l (Yeman, 2015). Such dimensions allowed us to store the gas sample of the last 2 minutes. AirCore itself was an additional tool implemented during mobile measurements, and the entire scheme of the research technique used is presented in Figure 20.

This figure shows the sample flow of air to the analyser. After entering the inlet of the measuring system, the gas sample was distributed into two parallel lines. The upper one, passed the sample directly to the analyser. The lower leg led to the AirCore that can store the air sample. The three-way valve sequence made it possible to select which sample was to be measured. If a plume measured directly was chosen to be reanalysed, the position of the three way valve was turned so that the gas stored in the tube could be measured. Before entering the analyser, the sample was passed through the Nafion dryer. It allowed us to dry the analysed samples, and thus to reduce the influence of humidity on the obtained result (Hoheisel, 2017). Then, the sample was passed to the CRDS analyzer, where the gas concentration and its isotopic composition were measured.

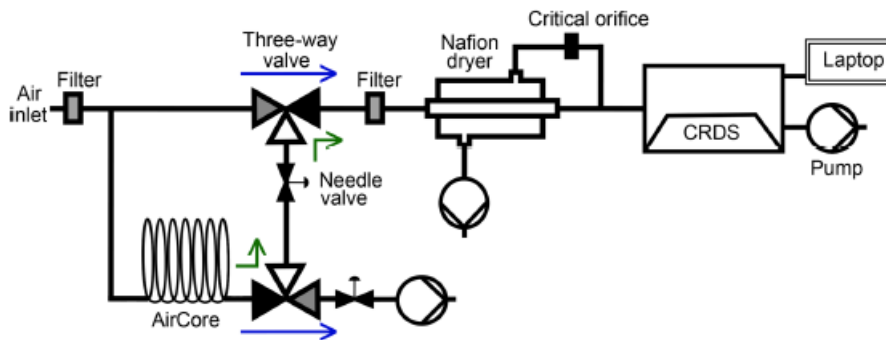


Figure 20: Scheme of AirCore used for mobile measurements (Hoheisel, 2017). The blue arrows indicate the flow of air in the "monitoring mode", while green arrows show the flow of air in "replay mode".

The AirCore offers the possibility of re-measuring the sample. The larger sample volume, in combination with a smaller flow rate through the analyser, allows in the AirCore (replay mode) more measurement points, and thus a better statistic than during monitoring mode. This is especially important when measuring isotopic composition, where the number of individual measurements points in a given emission peak (methane, in this case) is crucial. A comparison of measured peaks using monitoring and replay mode is shown in Figure 21, where the black line indicates the switching from "monitoring mode" to "replay mode". During the "monitoring mode" the measured peak consists of only a few measuring points. When the mode is changed to "replay mode", the number of measuring points increases and thus also the observability of the peak, given that its half-width increases whereas the peak height remains the same. The larger number of data points helps with a more precise fit of the linear function during a Keeling or Miller-Tans plot (see subsection 2.3).

We followed the recommendation by Hoheisel et al., (2019), that a CH_4 peak need to exceed 500 ppb above the background value. When determining the isotopic composition of the peaks with lower enhancements, the source signatures showed a larger uncertainty, making it difficult to identify the origin of methane. If the measured peak exceeded 500 ppb above the background, then the fit error of $\delta^{13}CH_4$ was even below 3 per mille, as shown by Hoheisel et al. (2019) and in Figure 22. In this study, only isotopic source signature calculations with an error lower than 5 per mille were considered.

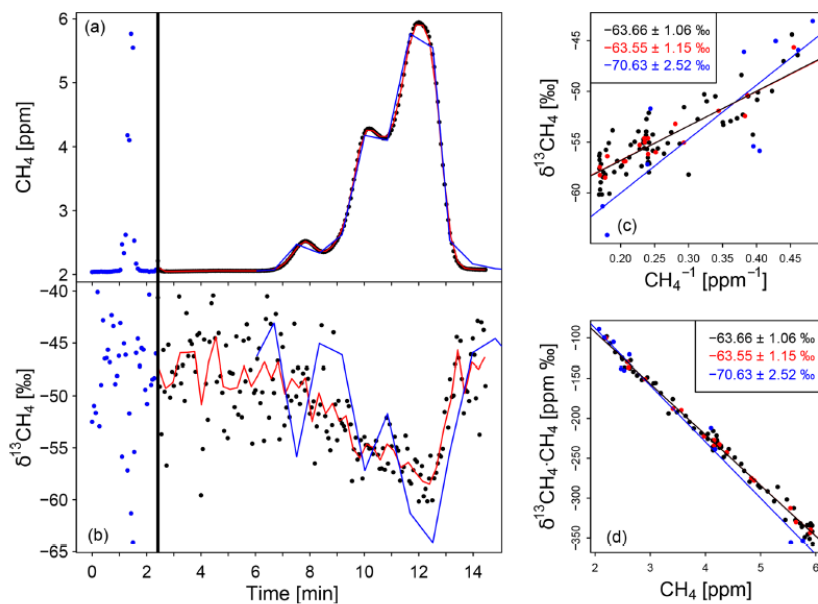


Figure 21: An example of a methane plume measured by Hoheisel et al. (2019). The plots on the left side show the methane concentration and the $\delta^{13}CH_4$, respectively. The vertical black line shows the point at which the measurement was switched from "monitoring mode" to "replay mode". The blue color represents the monitoring mode and the black and red (15 s mean) ones the replay mode. The Keeling plot and Miller-Tans plot for the peak are shown on the right.

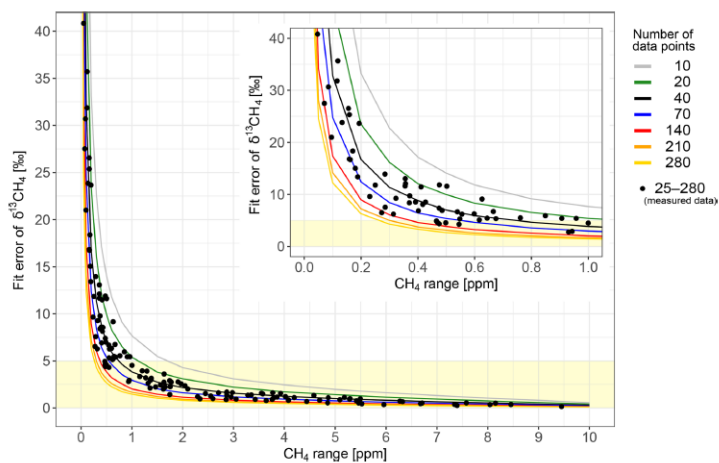
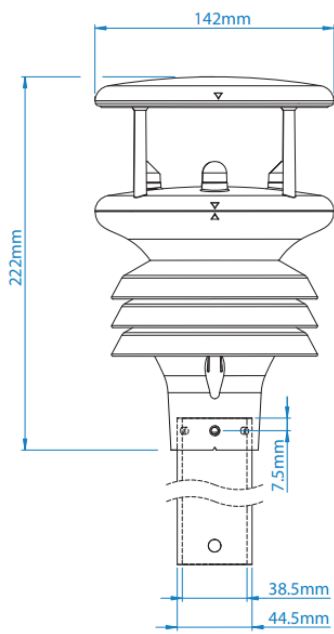


Figure 22: Dependency between peak height above background and the fit error of $\delta^{13}CH_4$ signature from the corresponding measured peak (Hoheisel et al., 2019).

3.4 2D and 3D weather station

The determination of the atmospheric stability classes, described in sections 2.4.1 and 2.4.2, is related to the weather conditions occurring at the time the measurements were taken. It is necessary to know the direction and speed of the wind, and the measurements of sunlight and cloud cover are an additional advantage. Having all the necessary parameters allows for a more accurate determination of the atmospheric conditions. It is needed in GPM as well as in OTM-33A methods, both used in this dissertation.

In order to measure the required weather parameters, 2D and 3D weather stations were used, respectively. The first was the MaxiMet GMX500 Compact Weather Station from Gill (GILL Instruments Ltd., Lymington, UK). For the time of mobile measurements, it was mounted on the roof of the used vehicle (usually the IUP van), otherwise it was stored in the laboratory. It measures basic weather parameters such as ambient air temperature, pressure, humidity as well as 2D wind speed and wind direction. The sampling rate is 1 Hz for each measured parameter. The wind speed is measured with a resolution of 0.01 m/s and an accuracy of $\pm 3\%$ at speeds up to 40 m/s. Wind direction is measured in the range of 0-359° with 1 degree resolution. The accuracy of the wind direction measurement is $\pm 3^\circ$ at wind speeds up to 40 m/s. In the case of temperature measurements, the device works correctly in the range of -40 to +70°C, with a resolution of $\pm 0.3^\circ\text{C}$ and an accuracy of $\pm 0.3^\circ\text{C}$ at 20°C (MaxiMet GMX500 manual). In addition, the MaxiMet has a module for spatial localization and entering geographic coordinates as well as altitude above sea level. As the MaxiMet weather station was mounted on the roof of the van and therefore was in motion during mobile measurements, the wind direction and speed were automatically corrected due to the movement of the vehicle and the data was saved to a file. The MaxiMet weather station sensor and the stations installed on the roof of the institute van is shown in Figure 23. The 2D weather station reading record was overwritten with each successive second to the file on the laptop, which was the weather station's power source via the USB connector.



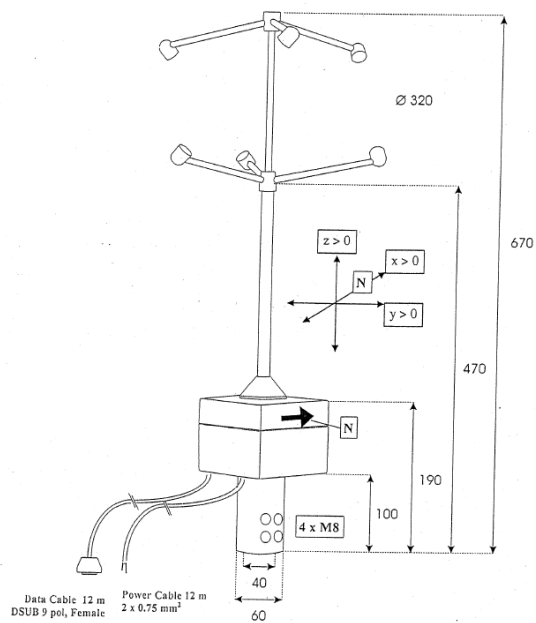
(a)



(b)

Figure 23: Scheme of MaxiMet GMX500 Compact Weather Station (MaxiMet GMX500 manual), own gallery.

The second weather station was a 3D UltraSonic Anemometer (USA-1), METEK (Meteorologische Messtechnik GmbH, Elmshorn, Germany). Compared to the Gill, it was completely stationary and needed external supply, which was supplied by batteries. The USA-1 weather station was mounted on a tripod, the sensors were then set at a height of about 2.5 m above ground level. The 3D weather station sensor itself was set to the north as indicated by the additional compass. The field application of the USA-1 are shown in Figure 24. According to the manufacturer's specification, the USA-1 can work in field conditions in which the ambient air temperature is from -30 to $+50$ °C, in which case its resolution is 0.01K. The wind speed is measured in its 3 components (u, v, w) with a resolution of 0.01 m/s, and also with an accuracy of 0.01 m/s or 2%, with a maximum speed range of up to 50 m/s. The wind direction is measured with a resolution of 0.4° and with an accuracy of 2° at 5 m/s. The METEK can save data in various measurement frequencies, but for the needs of measurement campaigns 1 Hz data were used (METEK manual). Until October 2019, data from the 3D weather station was transmitted from the device via a USB cable after every 20 minutes of measurement, and further measurements were saved on an SD card installed in the station, from which the data was copied after completion of the measurements.



(a)



(b)

Figure 24: Scheme of 3D Ultrasonic Anemometer weather station, manufactured by METEK (METEK manual), own gallery.

Both MaxiMet and USA-1 weather stations were compared to each other by J.Kammerer in February 2019 (Kammerer, 2019). The test was carried out on the roof of IUP, where both MaxiMet and USA-1 were installed for 3.5 days and both were compared to the IUP weather station. The test showed compliance of the USA-1 with the IUP station in the order of 0.99 in the case of wind speed, whereas MaxiMet showed 0.83. Some deviations in the obtained meteorological data were expected, which could have resulted from a certain difference in the position of the compared weather stations. This test shows that the USA-1 station is the most accurate when comparing to the IUP weather station, followed by the MaxiMet station, which underestimates the wind speed.

In addition to the above-mentioned weather stations, in the period between January and April 2018, a Vantage Pro2, fabricated by Davis Instruments Corporation (Hayward, CA, USA), weather station was also used, which measures wind speed and direction with the resolution and accuracy of 0.4 m/s and 1 m/s or 5% and 1° and 3° respectively, for wind speed and direction. However, as it was also shown in the comparative test, it is the least accurate (Kammerer, 2019).

4 Research sites

4.1 Release experiments

To determine the accuracy of GPM and OTM-33A methods in combination with mobile measurements and to work out possible strengths and weaknesses, 5 release tests were conducted over a period of 3 years. Four of them took place in Mannheim and one at Swiss Federal Laboratories for Materials Science and Technology (EMPA) in Dübendorf (Switzerland). The first two tests were focused only on the GPM method, while the test carried out in Switzerland was focused on the OTM-33A with the additional participation of methods using a drone (EMPA) and a small AirCore set (University of Groningen, UG). Details of all tests and the conclusions drawn from them are described in section 5.

The release tests involved the controlled release of methane at a known rate from a high pressure cylinder and then measuring its concentration at various distances from the generated point source. For the release and the measurements it was essential to find a suitable location to conduct the experiment, as well as atmospheric conditions that would allow to actually measure the methane plume. Table 6 shows a list of all the release tests carried out with the basic information described in more detail in section 5.

Table 6: Controlled release test performed performed to verify the quality of quantifications performed using the GPM and OTM-33A.

ID	Date	Country	Place	Method	Data provider
M1	28.11.2018	DE	Mannheim	GPM	J. Kammerer
M2	07.02.2019	DE	Mannheim	GPM	J. Kammerer
D3.	23-27.02.2020	CHE	Dübendorf	OTM-33A	P. Korben
M4	10.09.2020	DE	Mannheim	GPM / OTM-33A	P. Korben
M5	22.10.2020	DE	Mannheim	GPM / OTM-33A	P. Korben

Each of the controlled release tests was conducted in compliance with safety rules. The following equipment was used to perform the tests:

- CRDS (Picarro G2201-i) or OF-CEAS (Licor LI7810) analyser,
- 1-2 cylinders containing 99.999% methane,
- Flowmeter: Yokogawa Rotameter, model RAGL (Yokogawa Deutschland GmbH, Ratingen, Germany) with a measurement uncertainty of 1.6% was used (Kammerer, 2019),
- Mass balance controller: For the Mannheim test an industry weighing scale model DS30K.0.1 (Kern & Sohn GmbH, Balingen, Germany) with a precision of 0.1 g was used. This scale has been tested by J. Kammerer and has an uncertainty of 0.5% (Kammerer, 2019),

- 2D and 3D weather station.

4.2 Field campaigns - Heidelberg

Numerous methane emitters were identified as main or typical emitter in Heidelberg. They are located relatively close to the city, are well accessible and it was possible to visit them regularly to monitor the methane concentration and to determine the methane isotopic composition. The sources listed below are located within a 50 km radius of Heidelberg, but they show a different nature of methane origin, which makes them an interesting object of research. The possibility to take measurements of the gas concentration in the plume was dependent on two factors: the direction of the wind, which needed to be perpendicular (ideally) to accessible roads at the visited site, as well as the wind speed, which needed to be strong enough to measure the plume at the ground level. To plan the measurement campaign and the sites to visit, the direction and speed of the wind were checked according to the weather forecast (AccuWeather) and the weather models (Windy.com). If necessary, the landlords or persons managing the area were informed about the plans to conduct measurements on a given day (this was the case with landfill in Sinsheim).

4.2.1 Dairy farm in Weinheim

The dairy cow farm (DF) in Weinheim is located 18.5 km north of the Institute for Environmental Physics (IUP), near the city of Weinheim. The farm is situated on an area of 0.05 km^2 and has 320-340 dairy cows (Hoheisel, 2017; Hoheisel et al., 2019). There is also a tank for liquid manure on the farm, which holds about 1000 m^3 . In addition to the cowshed itself and the manure tank, the farm has a small biogas plant. Figure 25 shows the location of the buildings on the farm in Weinheim. The point marked by the green pin is the biogas tank, which is feed of a mixture of liquid manure and maize silage (personal communication between A. Hoheisel and the owner of the farm) (Hoheisel, 2017; Hoheisel et al., 2019). A yellow pushpin marks the cowshed where the cows are kept. The biogas plant is located in close proximity to the cowshed (up to 25 m), which may have resulted in the overlapping of the observed peaks (Kammerer, 2019; Hoheisel, 2017). Depending on the direction of the wind, it was possible to observe the separated peaks under ideal conditions. Since was possible to circle the farm from all sides, measurements can be taken regardless of the wind direction. It was also possible to use the road on the other side of the ditch, which gave a fairly wide range of distance in which it was possible to observe the methane peaks from the facility. Most of the measurements were taken on the well-paved road on the north side of the stables when there was a south wind. The research on the isotopic composition of methane for DF in Weinheim was carried out in

2016-2017 by Hoheisel (2017), Hoheisel et al. (2019) and was continued in this study.



Figure 25: Facility in Weinheim. Note that for this location a double source exists, green pin is biogas tank and yellow pin is cowshed.

In total, DF in Weinheim was visited 11 times during 3 years of measurements to capture possible seasonal variability. The first campaign was done on 10th of January 2018, and the last one on 31st of January 2020. As it is shown in Table 7, the number of observed peaks during each campaign varied between 4 and 38. AirCore samples were collected during the first part of the DF measurement campaigns in order to analyse the isotope composition of the methane coming out from the facility.

Table 7: Measurement campaigns performed on the dairy farm in Weinheim with the recorded number of observed peaks and AirCore samples.

Date	Start	End	Number of peaks	AirCore
10.01.2018	15:30:00	16:15:00	4	6
26.04.2018	17:10:00	20:00:00	14	7
04.07.2018	14:45:00	15:30:00	4	1
06.07.2018	16:20:00	18:00:00	5	5
24.08.2018	18:25:00	20:40:00	13	8
25.10.2018	12:15:00	14:00:00	7	8
26.11.2018	16:00:00	17:15:00	6	4
25.01.2019	13:30:00	17:15:00	35	8
02.04.2019	10:10:00	13:30:00	20	10
10.08.2019	11:00:00	14:25:00	25	5
31.01.2020	10:40:00	11:50:00	21	0

4.2.2 Dairy farm in Ladenburg

Another dairy farm is located in Ladenburg - Neubotzheim, a small village located about 6 km north-west of Heidelberg. The whole farm (without counting the agricultural land) has an area of about 0.03 km^2 . A biogas plant is in 110 m distance of the cowshed. In Figure 26. The biogas plant is marked by a green pin while the cowshed is marked with a yellow marker. DF in Ladenburg was also the subject of A. Hoheisel's research (in 2016-2017) and a test field for the AirCore method using a drone by N. Büttner (2019). In 2017 and 2019, 80 to 90 dairy cows and 70 calves were kept on the farm (Hoheisel, 2017; Büttner, 2019). The measurement can only be taken by SW-W wind direction as the road to the north-west of the farm was not suitable due to the hay balls, which exceeded the height of our inlet.



Figure 26: Facility in Ladenburg. Note that for this location a double source exists, the green pin is the biogas tank and the yellow pin is the cowshed.

The DF in Ladenburg was visited 9 times, often on the occasion of other measurement campaigns, as it is very close to the IUP. In addition to the GPM method that was used in most cases, the DF in Ladenburg was also studied for the use of the OTM-33A method (Krümpelmann, 2019). The measured CH_4 peaks in Ladenburg rarely exceeded 3 ppm, which is significantly lower than the 20 ppm obtained in Weinheim. The list of all measurement campaigns performed on DF in Ladenburg is shown in Table 8.

Table 8: Measurement campaigns performed on the dairy farm in Ladenburg with the recorded number of observed peaks and AirCore samples.

Date	Start	End	Number of peaks	AirCore
26.04.2018	15:45:00	16:30:00	4	1
04.07.2018	16:00:00	16:40:00	2	2
25.10.2018	10:00:00	11:20:00	6	8
25.01.2019	18:00:00	19:00:00	6	1
25.07.2019	14:30:00	17:30:00	7	7
09.08.2019	11:00:00	14:15:00	OTM	0
13.12.2019	11:45:00	12:40:00	20	0
31.01.2020	09:20:00	10:20:00	20	0
10.09.2020	15:15:00	15:45:00	12	0

4.2.3 Biogas plant in Pfaffengrund

The Pfistererhof biogas plant in Pfaffengrund is located in the western central district of the city of Heidelberg. This plant is 2.3 km from the IUP and covers an area of about 0.02 km^2 . Figure 27 shows the two access roads, from the north and the south. Therefore, this location can be visited only under south or north wind conditions.

The biogas plant is a long-established Heidelberg family company that has been dealing with the disposal of organic waste for many years. The family has been disposing of leftovers that have been fed to their pigs since 1970. In 2001 a biogas plant was built in order to comply with legal requirements and to optimize their operations. In this plant, the organic residues are biodegraded under anaerobic conditions. A flammable gas mixture (biogas) is created as a degradation product, which is converted into electricity and heat by a combined heat and power plant and, as a by-product, produces an organic fertilizer. The resulting electricity is fed into the transformer station network of the Heidelberg municipal utility (Biogas Plant Pfistererhof).



Figure 27: Biogas plant in Pfaffengrund. Green pin means the middle of the facility.

Table 9 shows the list of measurement campaigns on the biogas plant in Pfaffengrund. It was visited 12 times, from 10.02.2018 to 11.09.2020. Due to the good accessibility independent of the wind direction and high CH_4 peaks of more than 10 ppm, the biogas plant was often measured as a reference site at the beginning of a measurement day.

Table 9: Measurement campaigns performed on the biogas plant in Pfaffengrund with the recorded number of observed peaks and AirCore samples.

Date	Start	End	Number of peaks	AirCore
10.01.2018	17:00:00	17:40:00	6	3
26.01.2018	15:45:00	17:10:00	5	15
26.03.2018	17:00:00	18:00:00	4	3
24.08.2018	15:20:00	17:40:00	6	7
26.11.2018	18:00:00	18:46:00	6	0
17.12.2018	16:45:00	20:00:00	13	10
07.02.2019	11:30:00	14:00:00	14	8
24.07.2019	07:00:00	09:00:00	12	7
10.08.2019	15:00:00	16:00:00	OTM	0
23.08.2019	10:40:00	12:29:00	OTM	0
30.01.2020	09:30:00	10:20:00	15	0
11.09.2020	10:00:00	11:00:00	17	0

4.2.4 Gas compressor station in Gernsheim

The Gas Compressor Station (GCS) is located between Gernsheim and Hähnlein, 40 km north of the IUP. It is both a gas compressor station and a underground gas storage. The entire facility belongs to Open Grid Europe GmbH (OGE). The site is an interesting to study as it is the intersection of two large natural gas pipelines, MEGAL and MIDAL. MEGAL connects the border of Czech Republic to France, passing through southern Germany, transporting mostly Russian natural gas. MIDAL transports North Sea gas to the south of Germany. Due to the fact that they transport natural gas from various regions, a possible leakage, can be attributed to one of the pipelines using the isotope measurements (Levin et al., 1999).

Gas compressor stations are a known CH_4 emitter, even if the operators try to keep it as small as possible. However, Hoheisel (2017) reported methane concentration of up to 25 ppm at the gas compressor station Gernsheim (Hoheisel, 2017; Hoheisel et al., 2019). The presence of multiple gas pipelines, gas compressors and underground storage, presented the additional challenge of identifying the actual source of leakage. Based on this, the centre of the facility was approximated to be the leakage point to simplify further data analysis.

GCS in Gernhseim was visited 8 times, from 10.01.2018 to 13.03.2020. Table 10 shows all mobile measurements performed there including the number of AirCore samples that were taken. The measurement campaigns took place in an easterly wind direction, as the road to the right of GCS in Gernsheim was the best to conduct the measurements.

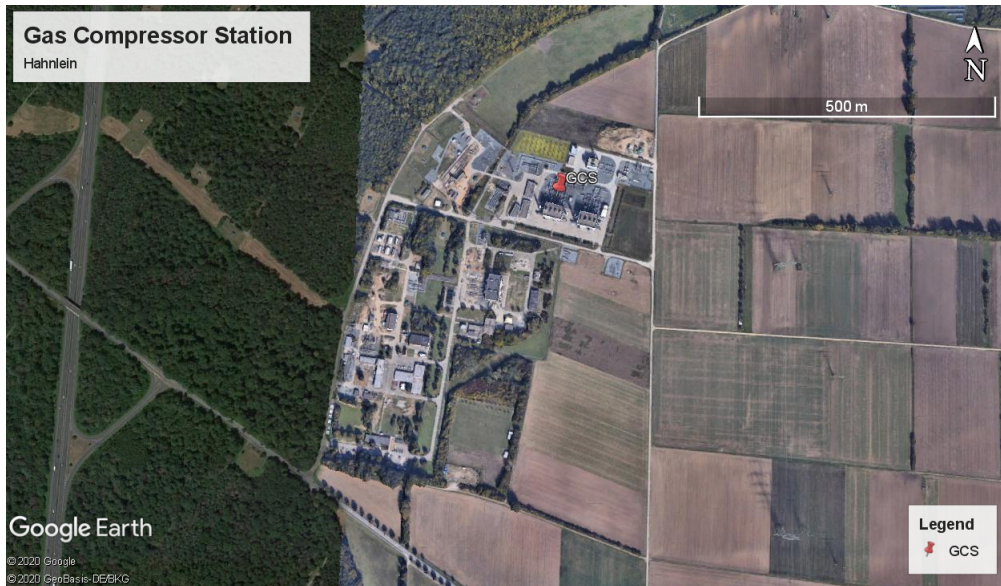


Figure 28: The Gas Compressor Station in Gernsheim. The red pin means indicates the probable source of the methane leak.

Table 10: Measurement campaigns performed on the Gas Compressor Station in Gernsheim with the recorded number of observed peaks and AirCore samples.

Date	Start	End	Number of peaks	AirCore
10.01.2018	14:20:00	15:10:00	4	5
27.03.2018	12:50:00	14:15:00	8	4
06.07.2018	14:00:00	15:50:00	11	1
25.10.2018	14:25:00	15:40:00	8	7
10.05.2019	11:45:00	14:00:00	14	2
31.07.2019	10:00:00	13:30:00	OTM	2
29.01.2020	13:20:00	14:20:00	21	0
13.03.2020	10:40:00	12:29:00	31	0

4.2.5 Landfill in Sinsheim

The landfill in Sinsheim is located north of Sinsheim, 23 km to the southeast of IUP. Thanks to the good contact with the operator, we were always able to drive onto the landfill site with our mobile measuring devices after notification.

The Sinsheim landfill site was operated since 1978 as a opened domestic waste. In 1993, on the basis of a planning approval decision, permission was granted for the expansion of the additional landfill sections. In 2005, the Regierungspräsidium Karlsruhe (Karlsruhe Regional Council) approved the continued operation of the landfill for an indefinite period. Excavated earth, construction waste, road debris, wood ash, foundry sands, waste containing asbestos, mineral fiber waste, sludges from water treatment and similar mineral wastes are placed in the landfill (AVR report, 2016). Currently, the entire landfill is

covered and photovoltaic panels are placed on its surface.

The facility is divided into smaller sectors, of which the main four (DA I, DA IIa, DA IIb, DA IVa) cover an area of 14.5 km^2 . Between 1978 and 1998, approximately 1 million m^3 of domestic waste was deposited in sections DA I and DA II (Yeman, 2015; Hoheisel, 2017; Hoheisel et al., 2019).

As mentioned above, direct access to the site was possible, allowing gas samples to be taken, e.g. for isotopic composition studies. However, as shown in (Figure 29), the only road usable for mobile measurement is east of the landfill. Only during westerly wind, methane emission plumes can be measured on this road. Due to the wind conditions, the Sinsheim landfill was visited only 6 times between April 2018 and January 2020. All campaigns conducted at this facility are listed in Table 11. As with previous sources, the table includes also the number of methane peaks observed during a given measurement campaign and whether AirCore samples were collected.



Figure 29: Landfill on the north of Sinsheim. Red pin means the middle of landfill area.

Table 11: Measurement campaigns performed on landfill in Sinsheim with the recorded number of observed peaks and AirCore samples.

Date	Start	End	Number of peaks	AirCore
26.04.2018	10:12:00	12:30:00	9	5
24.08.2018	13:00:00	14:22:00	14	7
17.12.2018	13:30:00	15:00:00	15	0
10.05.2019	09:00:00	10:40:00	9	10
29.07.2019	08:50:00	09:50:00	7	5
29.01.2020	11:20:00	12:10:00	13	0

4.3 Field campaigns in Poland and Romania

4.3.1 CoMet campaign in Poland

Data from the U.S. Energy Information Administration (EIA) shows that Poland with 1.99 quadrillion BTU (British thermal unit) is the largest coal producer in Europe, and ranks 10th in the entire world. Poland has been a member of International Energy Agency since 2008 and it is known that the coal industry dominates the Polish energy sector about 50% (EIA)

The greenhouse gas emissions in Poland (2017) were dominated with 81% by CO₂, mostly from fossil fuel combustions, and 12% by CH₄. Fugitive emissions from coal and lignite mines contribute to 34.4% of the total CH₄ emissions. The percentage contribution of each greenhouse gas is shown in Figure 30.

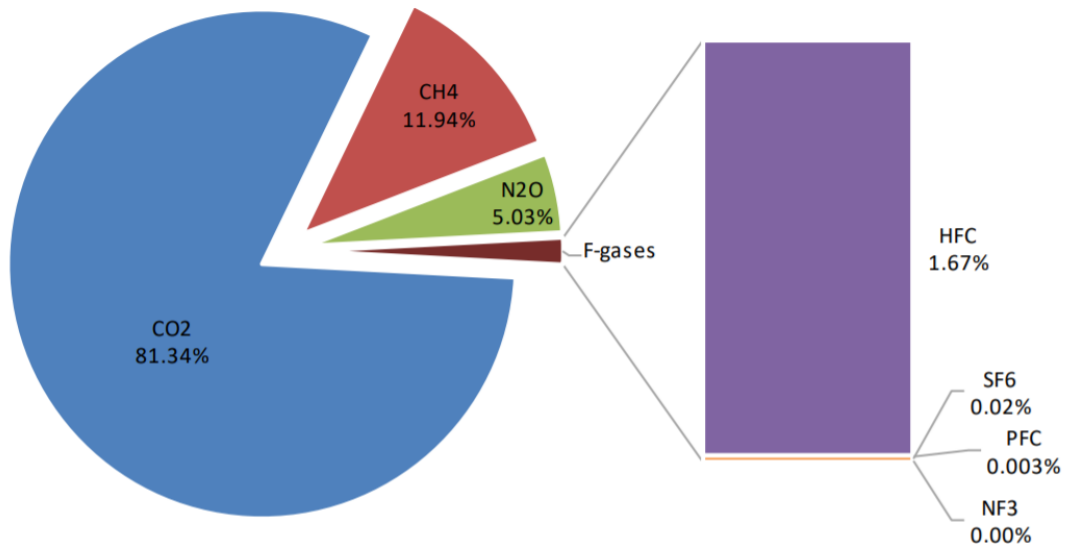


Figure 30: From UNFCCC. Percentage shares of greenhouse gases in the total national emissions in 2017 (excluding category 4. LULUCF)

Our participation to mobile measurements in Poland were a part of the CoMet campaign (Carbon Dioxide and Methane Mission for HALO) (DLR website). The CoMet campaign has several goals but the main one was to develop and evaluate methods for the independent monitoring greenhouse gas emissions and to provide data for satellite validation (Fiehn et al., 2020). The CoMet campaign included several institutes like: DLR (Deutsches Zentrum für Luft- und Raumfahrt, German Aerospace Center), AGH (Faculty of Physics and Applied Computer Science, AGH University of Science and Technology in Cracow, Poland), UG (University of Groningen, Groningen, Netherlands), IMAU (Institute for Marine and Atmospheric research Utrecht, Utrecht University, Netherlands) and

UHEI (Heidelberg University, Heidelberg, Germany) and more than a 100 people participated. The CoMet campaign took place in May and June 2018 and the target region was all of Europe, which is visible on Figure 31. Figure 31 shows map of the measuring area (DLR website). In particular, it shows flight plans, which were made from North Africa to the northern part of Finland, with particular emphasis on the Upper Silesian Coal Basin (USCB) region in Poland.



Figure 31: CoMet campaign logo (on the left) and map of target region on the campaign (on the right) (DLR website).

Measurements as part of the CoMet campaign were carried out in two ways. The first was ground measurements, and the second was airborne measurements. In ground measurements, one can distinguish mobile measurements using CRDS and stationary measurements using Fourier-transform infrared spectroscopy (FTiR). The UHEI group was responsible for isotopic measurements and for supporting airborne measurements to cover their pattern at ground level.

One of the target areas during the CoMet campaign was USCB which is one of the largest sources of methane in Europe. The area of USCB within Poland is around 5800 km^2 . For the purposes of the campaign, the CoMet team created the CoMet v2 inventory database, which is a database of source emissions based on the European Pollutant Release and Transfer Register (E-PRTR) database from 2016. This database contains information on CH_4 and CO_2 emissions for the USCB and the surrounding area. However, the E-PRTR assumes that each coal mine is a one single point source, while the COMET inventory treats each shaft individually, and that is the biggest difference between the two inventories (Fiehn et al., 2020).

The UHEI group visited several coal mines in the USCB region, which are managed by Polish coal mining companies: Jastrzębska Spółka Węglowa S.A. (JSW), TAURON Wydobywanie Spółka Akcyjna, Przedsiębiorstwo Górnicze "SILESIA" sp. z o.o. Short description of visited coal mines is presented in the Appendix.

4.3.2 ROMEEO campaign in Romania

Romania is one of the oldest oil and gas producers, which was one of the first in Europe (1857) to start using oil wells commercially (Craig et al., 2018; Deloitte, 2018). The oil and gas industry is therefore closely related to the economy of Romania.

Romania currently ranks 11th among oil producers, with a resource of 200 million tons of oil, not taking into account the potential of the Black Sea deposits, which are currently being explored (EIR). Looking at the European scale, Romania is the 3rd country in Europe (not including Russia) with significant oil reserves, just behind Norway and the United Kingdom, which at the end of 2015 amounted to 0.6 billion barrels (Craig et al., 2018). Most gas extraction in Romania comes from the onshore fields, while oil in Romania comes mainly from platforms in the Black Sea. The entire oil and gas market in Romania (on land) has about 400 deposits, most of which are small and fragmented. Romania also has the largest number of active wells in Europe.

According to UNFCCC data, Romania is one of the largest emitters of methane from the oil and gas sector in Europe. Figure 32 shows a comparison of methane emissions in Romania from oil and gas compared with other European countries (Germany, UK, Italy, the Netherlands, Norway and Poland). Especially the sectors exploration and also production contribute to a large emission share in Romania.

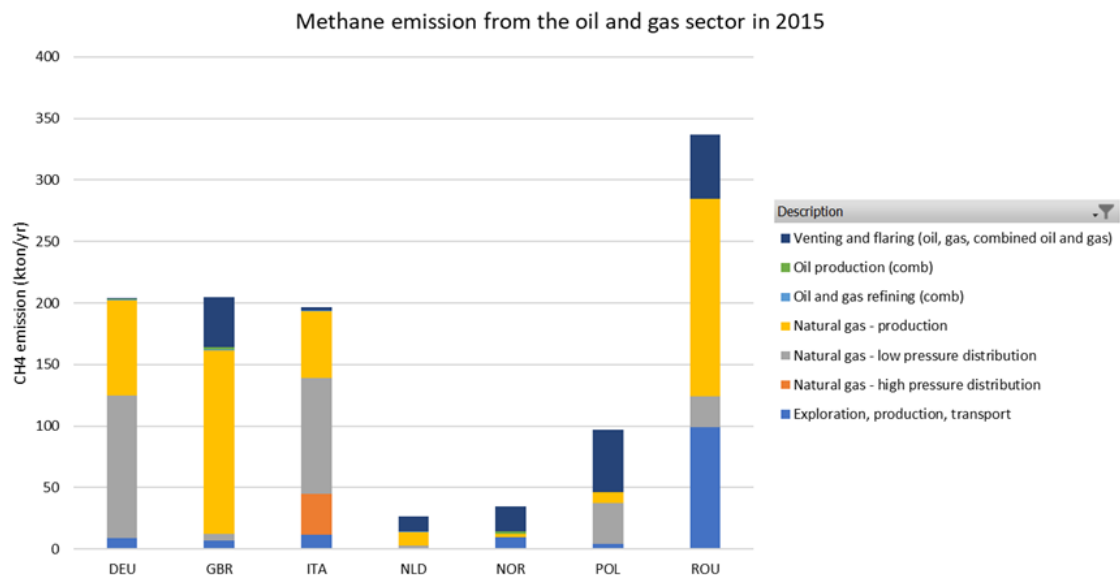


Figure 32: Methane emissions from oil and gas industry for few European countries, in order Germany, the United Kingdom, Italy, the Netherlands, Norway, Poland and Romania (*MEMO*² website).

The ROMEEO project (ROmanian Methane Emissions from Oil & gas) aims with a large measurement campaign to investigate methane emissions from oil and gas production in Romania. The campaign was initiated by the European H2020 project *MEMO*² and

is funded through the Climate and Clean Air Coalition (CCAC) international methane science studies, administered through the United Nations Environment Program (ROMEIO website).

Methane measurements under the ROMEIO project were carried out by 14 institutions from different countries that specialized in different measurement methods. In total, over 70 people were involved in the ROMEIO project (ROMEIO website).

The measurements under the ROMEIO project were mobile measurements with the use of cars, drones and small research aircrafts. The use of various means of mobility allowed for more independence regardless of the terrain and access or lack thereof to selected probable emitters.

Ground based and airborne surveys were mainly carried out in the southern part of the country within the areas whose main cities are Bucharest, Craiova, Pitesti, Ploiesti and Slatina. Figure 33 shows the main research regions. The purple areas are in the west of Wallachia and the red areas in the east of Wallachia, and they corresponded as core research regions to the two research groups Team West and Team East, respectively. Regions 2, 4, 5a, 6, 7 and 8 were selected as the main research areas. Each region highlighted above was made up of smaller ones called clusters. This allowed for more effective planning of measurements each day. Each cluster (and thus, a region) consisted of a different number of sites and had different characteristics. The share of oil and gas wells, respectively, was different, which will be shown in the results chapter (4.2.2.). The target locations for the measurements were provided by OMV Petrom, which was an industrial partner of the ROMEIO project.

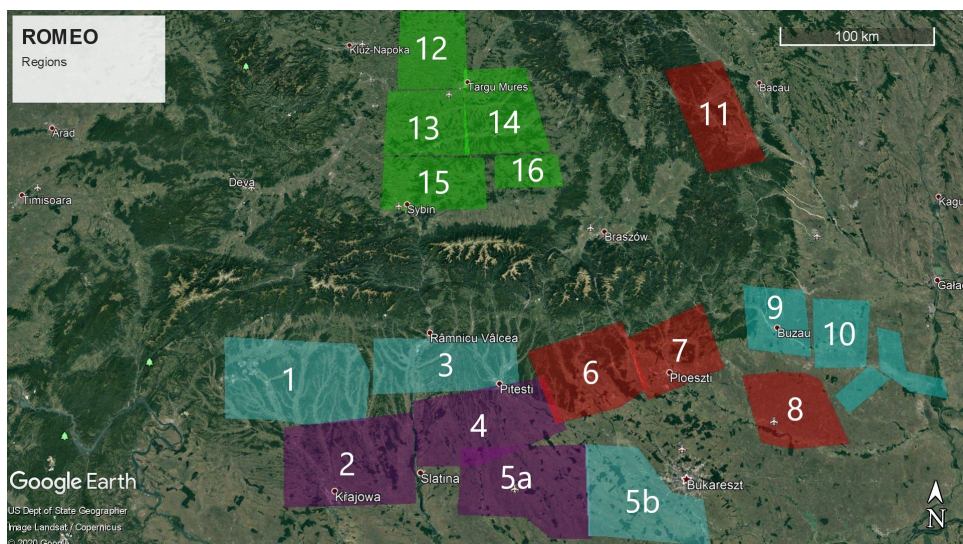


Figure 33: Map of target regions in Romania during ROMEIO campaign

Part III

Results and discussions

This chapter consists of 4 main parts describing and discussing the results obtained in my PhD during the study of regional to local methane emissions in Europe. Starting with the results of controlled CH_4 release tests allow to introduce to the two methods used to estimate the emission rate - GPM and OTM-33A. The release tests with known CH_4 emission can be used to show the strengths and weaknesses of the methods and to estimate the uncertainties. The next part contains the results of methane emission rates for sources around Heidelberg. These results are discussed and compared with other studies from other countries. The next section is dedicated to the mobile measurement campaign in Romania, and presents the results of the analysis of oil and gas emissions. Finally, the results of isotopic compositions of samples collected during mobile measurements in the Heidelberg region and in Poland (CoMet campaign) are presented.

5 Controlled Release Experiments

5.1 Gaussian Plume Model release tests

In practice, the GPM method consists of measuring the methane concentration while making passes (called transects) perpendicular to the direction of plume propagation. This makes it possible to record a peak which shows an enhancement of methane above the background level. These measurements consist of "n" number of transects during which methane concentration and weather conditions are monitored. Caulton et al. (2018) recommend taking at least 10 transects for each source to reliably constrain the atmospheric variability, which was confirmed by Kammerer (2019) with a recommendation of 10-20 transects. Figure 34 (on the left) shows an example time series of 11 transects of methane concentration. While conducting mobile measurements, cross-sections were made that reflected the plume coming from the visited source. With this data set, the GPM method was used to model the measured peak. An example of the model results is shown in Figure 34 (on the right). It shows the concentration above the background of the measured peak (green) and the fitted modelled peak (blue). In addition, the R^2 value was calculated for each pair of measured and modelled peak, which in this case is 0.89 .

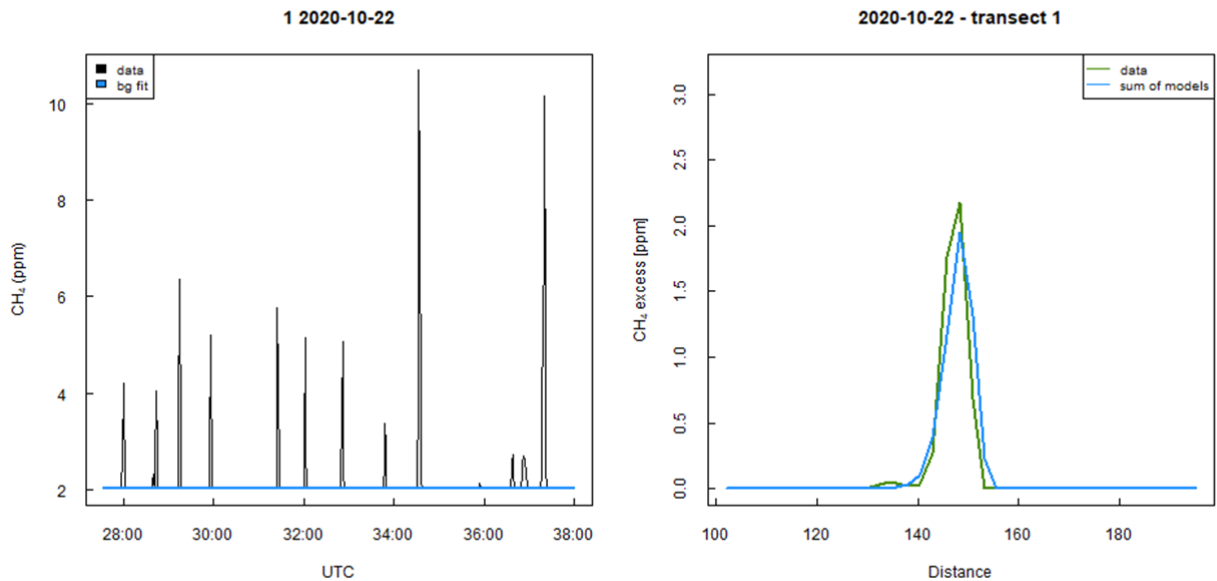


Figure 34: On the left, time series data of mobile measurements during one of the release. Black lines represent methane concentration over time, while blue line indicate background concentration. On the right, comparison of measured (green) and modelled peak (blue).

The methane release experiments during which the GPM method was tested were carried out at the Maimarktgelände Parkplatz in Mannheim (49.470251, 8.516856). This area is located about 13 km northwest of IUP. It was selected because it met the basic site conditions. Although there are many agricultural areas around Heidelberg, they did not allow the use of the full potential. As shown in Figure 35, the Maimarktgelände parking is a flat area with many roads parallel to each other, which allows for the investigation of the plume propagation at different distances. Each successive path is 12.5 m away from the previous one, which means that with a favourable wind, plume concentrations can be measured up to 300 m away. The area is bordered to the north by a local airport that has a weather station, which allowed additional weather parameters to be obtained. Figure 35 shows the location of four points where a controlled release of methane occurred. The predominant wind directions were from the south for tests 1, 2 and 5, and from the north for test 4.

5.1.1 Analysis of Mannheim 1 and Mannheim 2 release test

The first two tests were conducted under the direction of J. Kammerer in the frame of his master's thesis (Kammerer, 2019). The analysis and conclusions of this work are

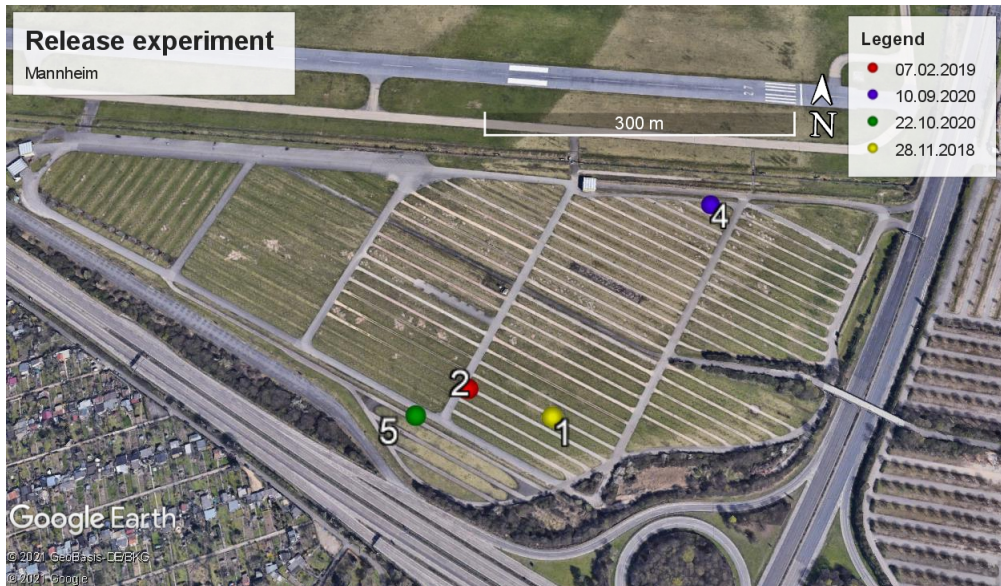


Figure 35: Map for controlled release experiments in Mannheim on Maimarktgelände parking. The pins mark the location where the controlled CH_4 releases were performed. Source: Google Earth.

briefly presented below.

The weather conditions for tests 1 and 2 were very similar. The average wind speed was 2.8 m/s and 2.5 m/s respectively, and the air temperature was around 5-7 degrees Celsius. The Mannheim 1 test was conducted with a CH_4 flow rate of $Q = 0.17 \text{ gCH}_4/\text{s}$ (600 gCH_4/h). The "Mannheim 2" test was performed with an emission of $Q = 0.11 \text{ gCH}_4/\text{s}$ (400 gCH_4/h). For both tests, it was decided to use stability class D for the data analysis due to the cloud cover in both days.

During "Mannheim 1" test, 47 peaks were analysed. The estimated emissions ranged from 0.032 to 0.45 gCH_4/s with a mean and median of 0.15 gCH_4/s and 0.13 gCH_4/s , respectively, which corresponds to 90% or 77% of the true release rate. The standard deviation was 0.098 gCH_4/s (60%). This means that the estimated value understates the true value of emissions.

A similar result was found for the "Mannheim 2" test, in which 29 peaks were analysed. The estimated emissions for those peaks ranged from 0.017 to 0.231 CH_4/s . The mean and median emissions were 0.072 (65%) and 0.068 CH_4/s (62%), respectively, with a standard deviation of 0.043 CH_4/s (39%). As these results show, both tests underestimated the emissions relative to the actual emissions of the released methane. The scatter between estimated emission rates for the individual peaks is significant with range from 16% to 208% for the "Mannheim 2" test. Despite the wide variation in estimated emissions, the average emission and its standard deviation prove the usefulness of the GPM method for estimating emissions from point sources of methane.

The "Mannheim 1" and "Mannheim 2" tests were used to understand and determine possible limits of the GPM method in combination with mobile measurements. Three main aspects were studied: the choice of the stability class, the influence of measurement distance and the number of transects needed for the analysis. While the method of determining the stability class seems to be easy and well categorized, which is a kind of simplification during data analysis, it has a significant impact on the value of estimated emission rates. The performed tests (1 and 2) show that the choice of stability class corresponding to a given wind speed (in this case, class B or C), changes the estimated emissions from overestimating (131% of the actual emission) to underestimating (87%). Especially in cases where the stability class is between two classes, it is recommended to calculate the emissions rate for both stability classes and average the two values or report values for both stability classes. In contrast to the general guideline by Hanna et al (1982), selecting stability class D for cloud cover does not necessarily result in the most accurate emission rates. Another aspect was to investigate the dependence of the estimated emissions on the transect distance from the source. In theory, it was expected that the distance between concentration measurement and release point should not effect on the estimated emission rate. This confirmation would allow measurements to be made at any distance from the presumed source. Transects during the experiments were conducted at distances between 50 and 200 m. The results of the performed tests (especially "Mannheim 2") prove that there is no dependence of the estimated emission on the distance at which the measurement was performed, which was also proven by Rella et al. (2015). Kammerer (2019) studied also the optimal number of required transects. From a statistical point of view, the larger the sample, the more accurate the estimate. However, it is also important that measurements last a certain period of time and weather conditions may change, so the balance between the number of transects that can be made and the time that can be allocated to them is important. The "Mannheim 1" and "Mannheim 2" release tests recommended 10-20 transects.

The results of the analysis of the Mannheim 1 and Mannheim 2 tests performed by J. Kammerer together with P. Korben shows that the combined mobile measurements with GPM works within an accuracy of $\pm 30\%$ in agreement of other studies (Caulton et al., 2018; Kumar et al., 2021). The findings have been used to construct a guideline which was followed during the mobile measurement campaigns.

5.1.2 Analysis of Mannheim 4 release experiment

Using the knowledge gathered so far, we extended the analysis of the GPM method with analysis of background definition, wind speed calculation and statistical analysis. For this purpose, two additional controlled methane release experiments were performed

on 10.09.2020 (Mannheim 4) and 22.10.2020 (Mannheim 5) respectively.

As shown in Table 6 and in Figure 35, the last two controlled release experiments were conducted at exactly the same location as J. Kammerer's measurements. Only the locations of the release point were different, due to the meteorological conditions. In the case of tests 4 and 5, both the GPM and the OTM-33A methods were the subject of the study. Additionally, an experiment to quantify methane emissions from urban areas was attempted to be replicated on the basis of research done by Fisher et al. (2017) and analysed in the study of Wietzel (2021). Tests 4 and 5 involved GPM testing using both a car and a bicycle. Emission rates were tested in the range of 0.028 to 0.11 gCH₄/s (100 - 360 gCH₄/h).

During these tests, several aspects were in the focus, which had not been verified in previous experiments. The first was to verify different ways to determine the background concentration during mobile measurements. Previously tested method "moving background" using `rftbaseline` function (R script) gave satisfactory results. This method calculates the background value as a moving average over a time interval, in this case 2 minutes before and after a given point. With the OTM-33A method a different algorithm of determining the background was introduced. We decided to compare the emission estimates using both methods for determining the background concentration: moving background and the average value of the lowest 5% of measured concentrations. The next aspect was the accuracy of the GPM and the use of the stability classes presented in Table 3 and Table 4. The last main aspect was to test the influence of wind speed averaging on the GPM method. The wind speed is a parameter for the choice of stability class, which then determines the parameters σ_y and σ_z as well as $1/U$ in the Equation 8. Two scenarios of wind speed averaging were applied.

The first one average the wind speed for each transect separately (Transect wind speed, TWS). In this case each measured peak has a corresponding wind speed. The second scenario was to first calculate the average wind speed for the set of made transects (15-30 minutes) and then apply this mean wind speed to each (Mean wind speed, MWS). Presented results were obtained with stability classes based on wind speed. Thus, despite the occurrence of low cloudiness (4/8), class D was used only as a comparison. During most of the mobile measurements only the 2D weather station was used, whereas the 3D weather station was a complementary instrument.

Although the Mannheim 4 test was planned carefully, the analysis of CH₄ and meteorological data showed afterwards that the wind was not very stable. However, this experiment also provided some additional knowledge that allowed us to identify some limitations of the GPM method. During the Mannheim 4 test, 7 "scenarios" were analysed (see Table 12). Each scenario involved a different vehicle, emission, or distance

from the source to the transect. For each scenario, around 10 transects were conducted. All scenarios considered during the M4 test are shown in the table below.

Table 12: Different scenarios for release test M4.

Scenario	Vehicle	Distance [m]	Release rate [g/s]	Transects	Max CH_4 [ppm]
1	bicycle	15	0.056	10	5.38
2	bicycle	5	0.056	9	6.97
3	bicycle	5	0.028	9	3.41
4	bicycle	5	0.11	6	39.51
5	bicycle	15	0.11	8	12.69
6	car	15	0.11	10	6.63
7	car	20	0.11	10	10.75

A total of 62 transects were recorded during the M4 test. During the whole test the average wind speed was 1.71 ± 0.88 m/s for the MaxiMet station and 1.69 ± 0.86 m/s for the USA-1 station. In the case of individual scenarios it varied between 1.07 m/s (scenario 2) and 2.39 m/s (scenario 7). The stability classes A or B should be used in the calculations. The average wind direction was 38 degrees, with a high standard deviation 82 degrees, which at low wind speeds created difficulties in conducting transects. 4 out of 7 scenarios gave emissions estimates comparable to the actual release rate. These were scenarios 1, 3, 5 and 7 and all results are presented in Table 13.

Table 13: Estimated emission for scenarios during release experiment Mannheim 4.

Scenario	Release rate [g/s]	Estimated emission [g/s]	Error to release rate [%]
1	0.056	0.055 ± 0.030	-2
2	0.056	0.028 ± 0.11	-50
3	0.028	0.029 ± 0.022	+3
4	0.11	1.27 ± 44.96	+1000
5	0.11	0.08 ± 0.037	-28
6	0.11	0.048 ± 0.058	-56
7	0.11	0.16 ± 0.06	+45

It is worth noting that in case 3 the uncertainty of the emission estimate was almost 100%, which may be related to the close distance at which the measurement was made. Emissions for Scenarios 2 and 6 were less than 50% of the actual release rate, while for Scenario 4 the estimated emissions were 10 times greater. As in scenario 3, the distance at which the transects were performed was minimal, and although the emission was 3 times larger the observed peaks were 10 times larger compared to scenario 4. Measurements at only 10 m from the source are not suitable for GPM, but these tests were intended to simulate urban methane emissions. In the case of real field measurements, we are always at a minimum distance of 50 m. The release experiment data were further used to test

additional quality criteria. As in the case of the OTM-33A method, where Data Quality Indicators (DQI) are applied, a similar mechanism was developed here for the GPM method. We set a limit of acceptance for the coefficient of determination (R square, R^2) at 0.5. If the coefficient of fit of the model peak to the measurement peak was at least 0.5, the transect with this peak was accepted, otherwise it was rejected. For the M4 test, in each scenario, after applying this limiting factor, the value of estimated emission rate was improved (in the range of 10-300%). Moreover, the application of the R^2 indicator, allowed the automatic filtering of transects for which the modelled peak was not generated.

5.1.3 Analysis of Mannheim 5 release experiment

The Mannheim 5 test was conducted with a constant emission of released methane, which was 0.1 g/s for the entire duration of the experiment. The first part of the experiment (around 3 hours) was designed for the OTM-33A method, while the second part (around 1.5 hour) focused on the GPM method during which 6 scenarios were tested, listed in Table 14. The odd-numbered scenarios were measured on the closest road from the emitter (approximately 10 m), while the even-numbered scenarios were measured on the third road from the emitter (approximately 35 m). The first two scenarios were performed with a bicycle on the first and second road, respectively, away from the emitter, at an approximately constant bicyclist speed (measured less than 10 km/h). The next two scenarios were considered with a car moving with a speed of 10 km/h, and the last two included measurements with a car with a speed of 30 km/h. A total of 68 transects were conducted during the M5 test. The average wind speed during the entire test was 1.95 ± 0.94 m/s, and in the different scenarios it ranged from 1.62 m/s (scenario 1) to 2.19 m/s (scenario 2). Again in this case, the class of stability was either A or B, but looking at the data from the USA-1 station, in each scenario the wind speed exceeded 2 m/s which indicates only class B, with moderate insolation. The average wind direction during the entire experiment was 171 ± 40 degrees.

Table 14: Different scenarios for release test M5.

Scenario	Vehicle	$v_{vehicle}$ [km/h]	D [m]	Release rate [g/s]	Transects	Max CH_4 [ppm]
1	bicycle	10	10	0.1	13	10.68
2	bicycle	8	35	0.1	16	4.32
3	car	10	10	0.1	9	12.79
4	car	10	35	0.1	10	3.99
5	car	30	10	0.1	10	13.51
6	car	30	35	0.1	10	2.86

The first aspect of the data analysis was to define how to determine the background during the measurements. The previously used method (moving background) was one of

the possibilities, which was to be compared with the definition of the background for the OTM-33A method, where the background level is calculated as 5% of the lowest measured values. The data analysis showed that difference in background definition for both methods is negligible. Then emission rates are almost identical (with a maximum difference of up to 8%). However, we have chosen to use the moving background definition when analysing the data, because if there is more than one methane source (such as the Weinheim or Ladenburg farms), the background can be better fitted.

Another aspect of the data analysis was to study how to average the final results and how to report the uncertainties. In the thesis of Kammerer (2019), the mean emission calculated from the number of transects performed. In this case, the standard error of the mean, which is the standard deviation divided by the root of the number of transects (n), was used as the uncertainty of such emission. The second method considered was to report the median of the results obtained, and its uncertainty as the uncertainty of the median calculated from the scaled median absolute deviation (MAD_s) as shown below (Zięba, 2014):

$$u(\text{median}) = \sqrt{\frac{\pi}{2}} \frac{MAD_s}{\sqrt{n}} \quad (12)$$

Figure 36 shows the results of the data analysis for all six scenarios. Boxplots represent the interval in which the measured data are located, i.e., the estimated emissions for each transect. The number of points is written above. This graph represents following values: minimum, maximum, first quartile and third quartile in the data set. The red line represents the actual emission value. The graph shows the results of statistical analysis using the mean and median with their uncertainties. Both statistics give similar results. The mean value is between 2 and 40% above the actual emission and the median is between -10 and +40%. The uncertainties for both statistics are in a similar range of 20 - 50%. Scenario five showed that there is one outlier in the data set. This is a case that can also be expected for real measurements, showing that the median is a better solution for reporting the results. Therefore, unless otherwise stated, the estimated emissions rates presented below are the median with the median uncertainty.

The most important point in analysing the data collected from the M4 and M5 tests was to determine the best way to take the wind speed. As mentioned before, 2 cases were considered, TWS (Transect Wind Speed) and MWS (Mean Wind Speed). Figure 37 shows the dependence of the estimated emissions on the scenarios considered. The red line indicates the actual emission (0.1 g/s). The blue and green points indicate the emissions estimated using TWS and MWS, respectively. Using TWS as a method for determining the wind speed in the GPM model, the estimated emission rates range from -5% to +40%

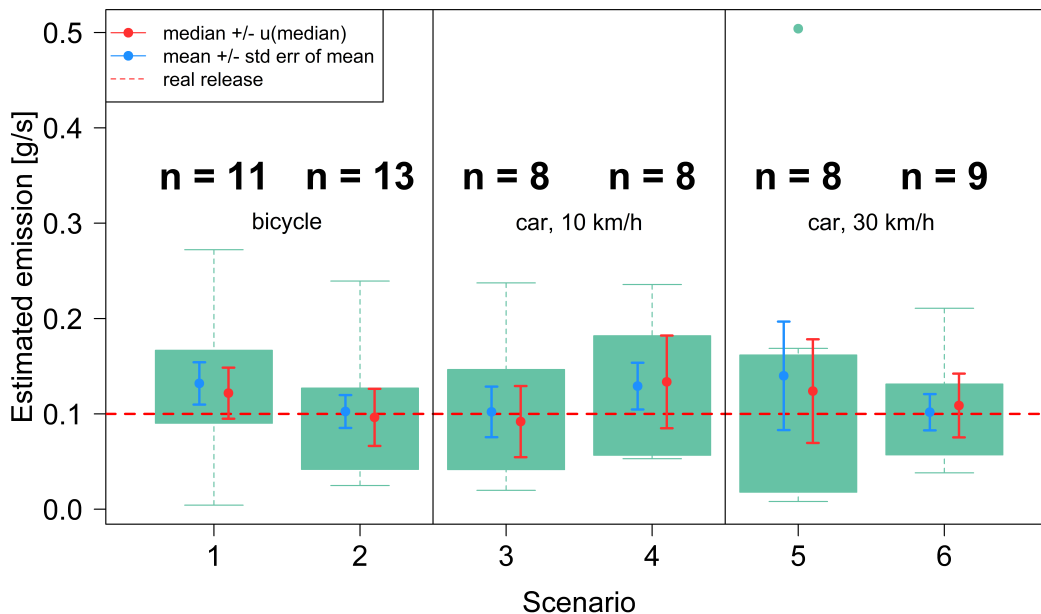


Figure 36: Test of determination statistical description of obtained results. Boxplots represent min, max, first and third quartile values for the data set. Red points corresponds to median \pm u(median), while blue dots corresponds to mean \pm SEM.

of the actual emission. For MWS, it is -15% to + 80%, respectively. Also in the case of estimation uncertainty, it is up to 56% and 75% for TWS and MWS, respectively. The blue and green horizontal line indicate the average emission rate calculated from the collected values, which is 0.116 g/s and 0.126 g/s, respectively, for the selected methods. In order to estimate the emissions during mobile measurements it is more appropriate to use the method of determining the wind speed in the model based on the average wind speed for each transect separately. This will allow a more accurate determination of emissions and will also reflect the atmospheric conditions for each transect independently.

It is worth noting that the emissions estimated for car measurements at 30 km/h do not differ much from the results for measurements at 10 km/h. This shows clearly that the driving speed in such a range does not affect the obtained results. It is more important to conduct measurements at constant speed, which allows to collect measurement points at similar distances from each other and the peak shape will be best represented.

Kammerer (2019) chose stability class D in the data analysis for M1 and M2, following the GPM guideline (Hanna et al, 1982). However, this analysis shows that when generally taken the stability class D for cloudy sky, the emission is estimated at 70% of the actual emission. The M4 and M5 tests confirm this conclusion, since the emission estimated for class D results in a range of 60% to 90% compared to the actual emission.

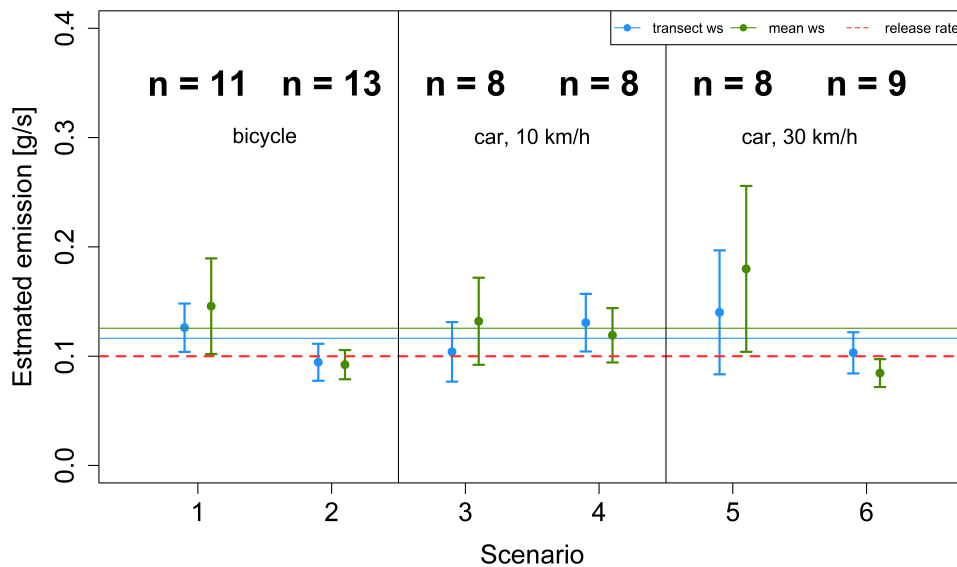


Figure 37: Test of determination wind speed method, transect wind speed (TWS, blue dots and line) and mean wind speed (MWS, green dots and line). Red line corresponds to the real emission rate.

This means that the result is underestimated. Applying a stability class based only on wind speed and do not take care of the cloud coverage in contrast to general GPM rules, would give a more accurate result.

Summarizing all this results collected from the release tests, we can conclude that mobile CH_4 measurements with GPM are a useful tool for estimating local emission rates. The definition of the background is not the most important parameter, but due to the possibility of the occurrence of more than one source, it is better to use the moving background method. Unless otherwise stated, the values of estimated emission rates will be reported as the median with its uncertainty based on the number of transects performed and accepted based on $R^2 > 0.5$. The wind speed input into the model will be the average wind speed for each transect separately (TWS method). The most difficult part of the measurements are the wind conditions. In spite of comparable wind speeds for test M4 and M5, more accurate emission rates were obtained for test M5, with less variability in wind direction. Based on this finding, it is recommended to conduct mobile measurements in conditions where the wind direction vary less than 45 degrees.

The tests carried out in Mannheim were an ideal case with a single well defined point source and a plume dispersion without obstruction. It would be recommended to conduct additional tests, taking into account the presence of certain obstacles (such as trees, buildings) and to release methane at 2 or 3 release points.

5.2 Other Test Method 33A release tests

The OTM-33A method was used in accordance with EPA recommendations (EPA draft method), so measurements took at least 15-20 minutes at a distance of 20-200 m from the source. During this time the concentration of methane and wind direction were measured in the plume. The distribution of the methane concentration with respect to the measured wind direction was plotted as shown in section 2.4.2. These data were then binned and an average methane concentration was calculated for each bin (10 degrees). A Gaussian peak was fitted to the peak created by these average values in each bin and then the Equation 10 was used to estimate the emission rate. An example of the result is shown in Figure 38, where the black points indicate the background - subtracted methane concentration versus the wind direction. The blue points represent the average methane concentration in the bin (if the points in the bin were less than 2% of the total measured data, the average value was set to 0 ppm), and the red points represent the fitted Gaussian peak.

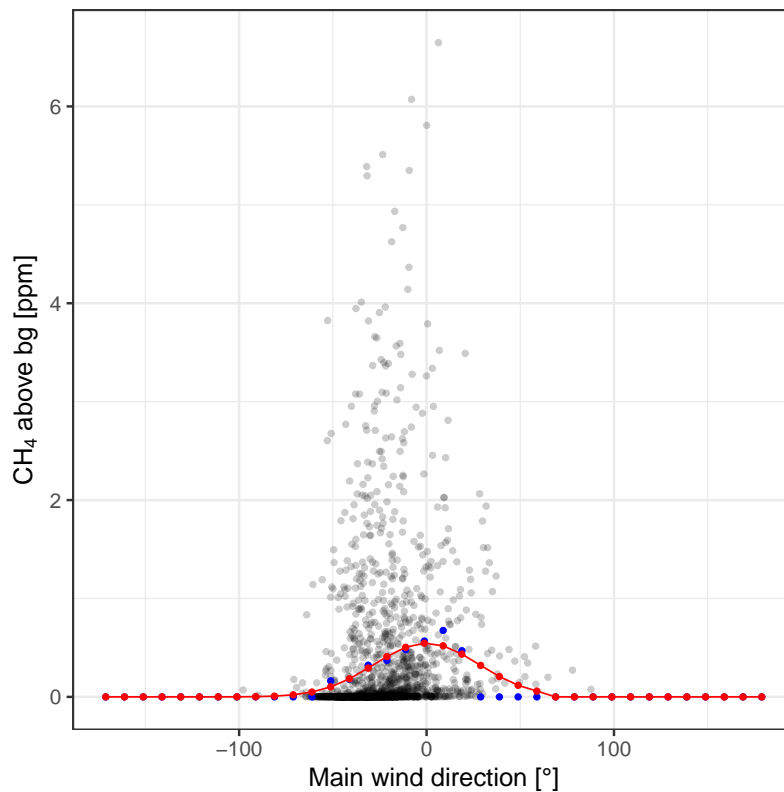


Figure 38: Example of OTM-33A measurement. Background-subtracted methane concentration versus binned wind direction, where 0 degrees corresponds to the main wind direction. Black dots are data points, blue dots are averaged methane concentration values in each bin, red dots represent fitted values from Gaussian fit.

5.2.1 DuREX campaign

The first release test focused on OTM-33A was performed in Dübendorf, on the west from Zurich (Switzerland) in February 2020 (with campaign name DüREX – **D**übendorf **R**elease **E**Xperiment). It was performed in cooperation with other *MEMO*² students from University of Groningen (UG, K. Vinkovic) and Swiss Federal Laboratories for Material Science and Technology (EMPA, R. Morales, J. Ravelid). From 23rd to 27th of February, release tests were done to simulate point source like oil or gas well and to test the OTM-33A method which was applied during the ROMEO campaign (section 7). This opened the possibility to compare the OTM-33A method with mass balance methods with AirCore or in-situ measurements using drone, what is the subject of the publication of Morales et al.(2021)

For the release test EMPA prepared the set-up with flow meters and methane cylinders (92% CH_4). For the OTM-33A method, the methane concentration was measured with a LI-7810 and the meteorological data with a USA-1 weather station (u, v, w and T which are 3 components of wind direction and temperature). Atmospheric pressure was taken from EMPA meteo mast. The gas cylinder with 92% methane was stored in the EMPA van and connected to a 100 m tube was routed at the release point. The flow rates of the release and the measurement periods of OTMs performed during DüREX campaign is summarised in Table 15. Figure 39 shows the location of OTM measurements and release points.

Table 15: Collected OTM-33A data during DüREX campaign with necessary information.

Date	Time [min]	Distance [m]	Latitude	Longitude	Release [g/s]
23.02.2020	180	70	47.389597	8.605456	0.54
24.02.2020	68	57	47.38975	8.605708	0.32
24.02.2020	77	57	47.38975	8.605708	0.32
25.02.2020	60	37	47.389756	8.606039	0.32
27.02.2020	105	46	47.38950325	8.60634326	0.23
27.02.2020	20	26	47.38950325	8.60634326	0.23

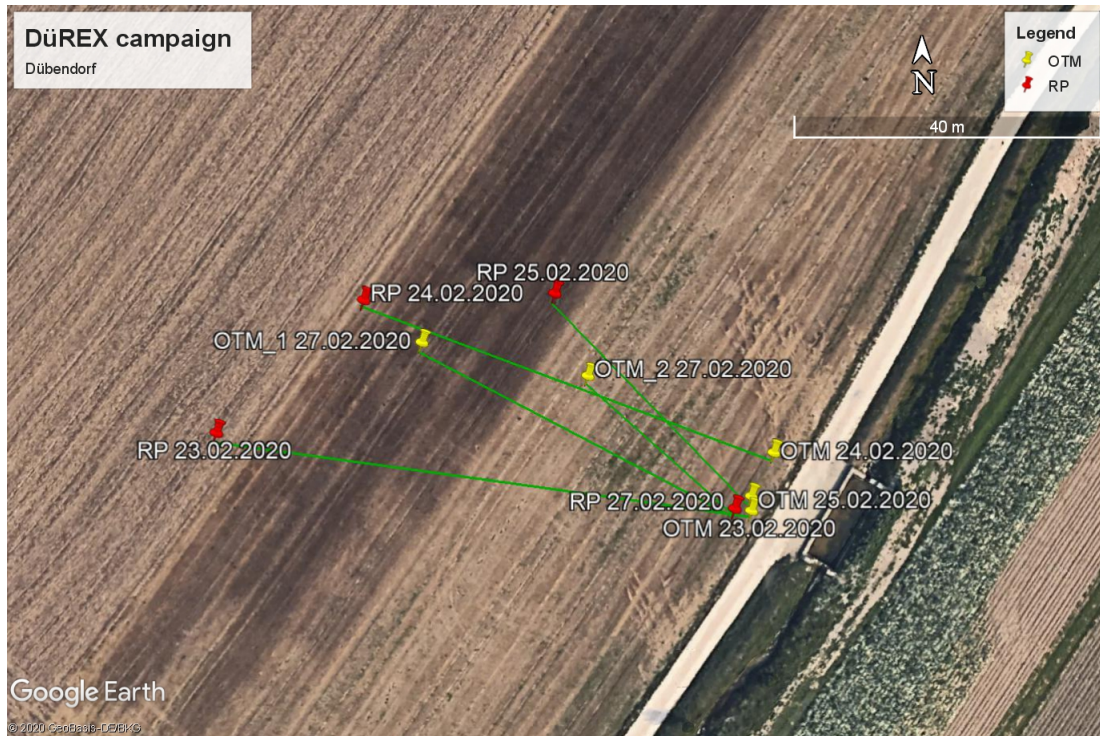


Figure 39: Location of release points (RP, in red) and OTM measurement locations (in yellow).

Data analysis was based on the same procedure as the EPA team (Thoma et al., 2014; Omara, 2018) and described in section 2.4.2. From the original program codes in R (Thoma et al., 2014) parts like additional renaming, not necessary copying of data was deleted. After using double rotation method of three wind components (Wilczak et al., 2001) and calculating wind direction from those, mean wind direction was calculated. Tilt correction algorithms have been developed to correct wind statistics for any misalignment of the sonic anemometer with respect to the local wind streamlines (www.licor.com, EddyPro 7 software). Then the main wind direction has been set to 0 degrees and from now all results are plotted in reference to main wind direction. All data points were separated to 10 degrees bin of wind direction.

During the experiment, the weather conditions were favorable for the OTM-33A measurements. Recorded wind speeds was between 3 and 5 m/s, and mostly above 4 m/s. The wind could blow only in the west-east axis. Due to this excellent conditions the stability class determined for each experiment was usually higher than 3 (see Table 5).

Two examples of OTM-33A measurements are presented in Figure 40a. This graph shows the distribution of the average methane concentration as function of the wind direction and the distribution of the number of measuring points which are well correlated. This confirms, that the measurement set-up is positioned perfectly with the direction of the wind blowing from the methane source. Figure 40b shows a situation that we sometimes

also observed during field campaigns. The discrepancy between the two curves can have three causes. The first is an additional source near the main source, the second is a breeze that gave several readings from another direction causing an infinite Gaussian peak, the third is a misplaced sensor. Here, we can exclude an additional methane source. Gaussian curve is fitted to the average values of methane concentrations in subsequent bins, therefore, in these cases, OTM-33A probably will not be considered correct because the Gauss curve will not fit correctly and the measurement will be rejected at the data analysis stage (by R^2). To avoid such problems in real field measurements, it would be recommended to take a measurement and then make a quick initial analysis for possible repeated measurement.

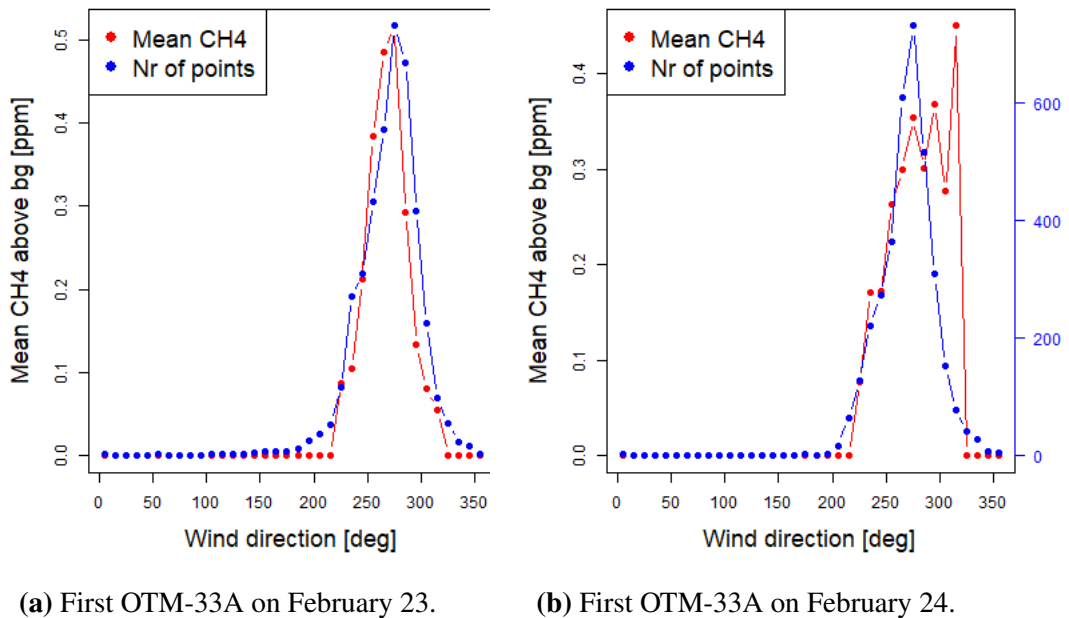


Figure 40: Difference in wind direction bin with maximal mean methane concentration and maximal number of data points in bin. 3a) Ideal case when both curves overlap. 3b) Problematic case with 3 possible reasons.

Once all the necessary values in the Equation 10 were obtained, the value of the emission rate could be estimated. During the first day, one release experiment took place over 3 hours with a release rate of 48.5 l/min (0.54 gCH₄/s). This measurement period is divided to smaller time spans:

- 20 minutes periods (with overlapping, moving 1 minute, 0-20 min, 1-21 min, etc.)
- 20 minutes periods (with overlapping, moving 20 minute, 0-20 min, 0-40 min, etc.)

5.2.2 Validation of stability class averaging

Since the definition of stability classes in the OTM-33A method is averaged from two methods, it was investigated how the choice of stability class affects the obtained result. Figure 41 shows the estimated emission rates. In this analysis, 20 minute running means, with a step of 1 minute were used, resulting in 175 possible cases. If the data analysis used only the WD stability class (orange dots), then the result would always be higher than the actual emissions. If, on the other hand, a turbulent atmosphere class was used, the result would be underestimated (green dots), however, the inaccuracy would be much smaller than in the case of WD stability class. Thus, calculating the average atmospheric class as recommended by the OTM-33A method gives the best approximation to the real release rate (blue dots). In this case, the estimated emission varied between -34% to +92% compared to the real release rate, and 60% of all results are in the range of $\pm 25\%$. Similar results were obtained by Edie et al. (2020) for the OTM-33A method, with 68% of the measurements within 28% of the know release rate. In the same study, Edie et al. (2020) calculated that 85% of the derived emission rates were in the range of $\pm 50\%$ of the know release, and in tests from the DüREX campaign this value was 90%. The average emission rate shown in Figure 41 is $0.60 \pm 0.14 \text{ gCH}_4/\text{s}$, which agrees very well within 12% with real release rate ($0.54 \text{ gCH}_4/\text{s}$).

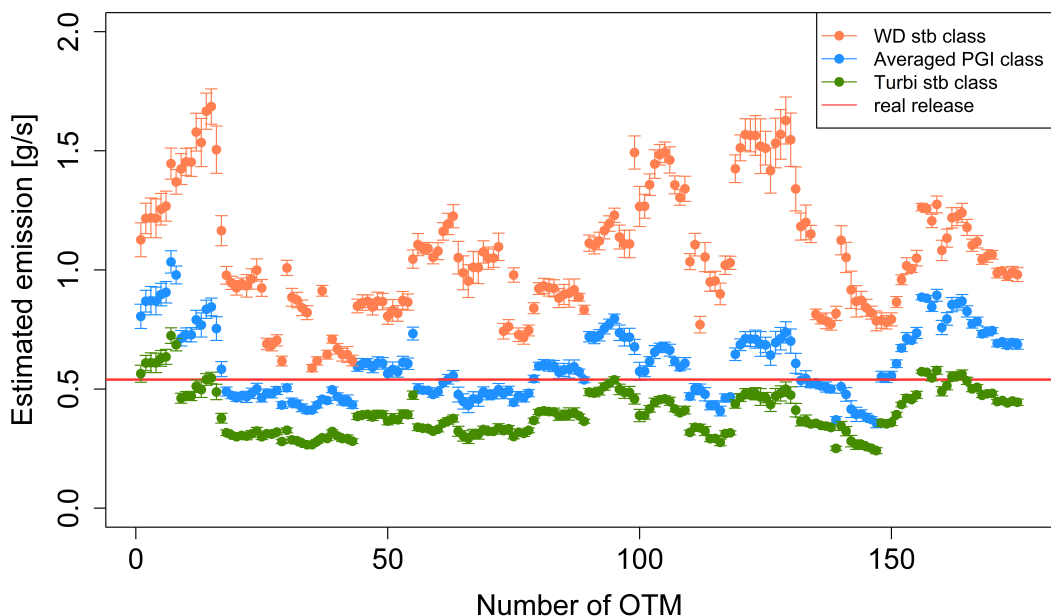


Figure 41: Estimated emission based on different stability classes. Orange dots represent values of emission for stability class based on variability of wind direction, while green dots represent values of emission of turbulent stability class.

5.2.3 Calculation of the uncertainty

In the original version of the OTM-33A method (Thoma et al., 2014), the uncertainty of the measurement is computed only on the uncertainty of the peak fitting of the Gauss curve. This referred to the value of the methane concentration in Equation 10. However, the four additional variables in this equation can also contribute to the uncertainty of the estimated emission rates. Therefore the error propagation was applied and verified for the data collected during the DüREX campaign. The distance between the emitter and the analyzer was determined with the help of the GPS Logger application, which provided coordinates with an accuracy of 3 m. With a measurement error of 3 m, the horizontal and vertical dispersion coefficients can change by 0.6 for σ_y and 0.35 for σ_z . Considering all possible contributions, the uncertainty value of the estimated emission rates increase, from 3-7% to 30-45%, as shown in Figure 42. Taking a full error propagation into account, the estimated emission rates of the release test (Figure 41) agree within the uncertainty with the released CH_4 . This uncertainty is comparable to the uncertainties obtained with the GPM method.

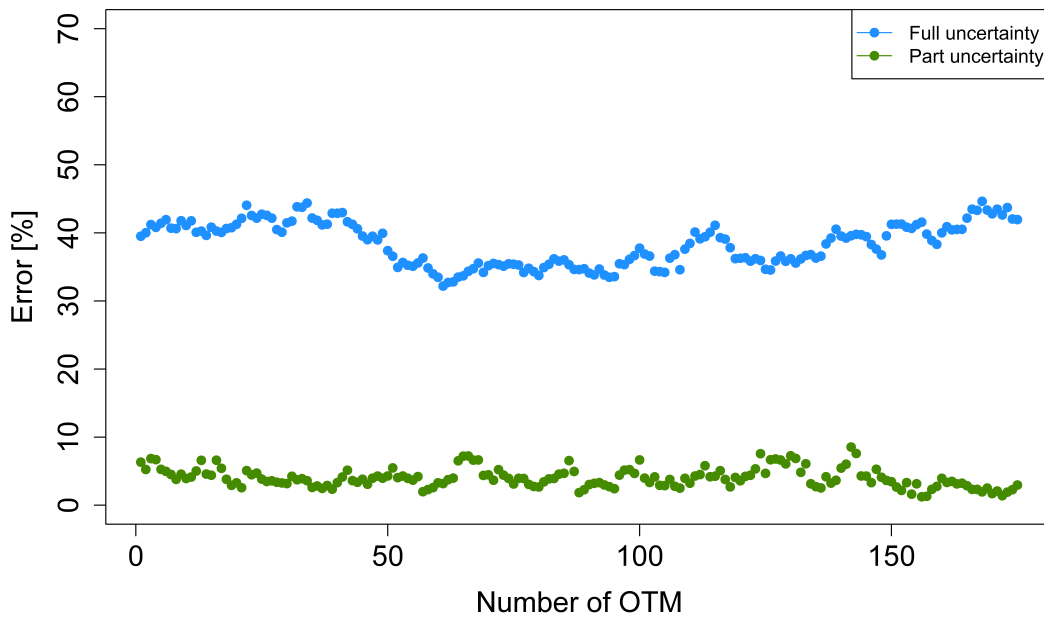


Figure 42: Uncertainty analysis of the estimated emissions after taking into account all component uncertainties. Green points (Partial uncertainty) show the uncertainty range of the emission estimate considering only the uncertainty of the peak, whereas blue dots (Full uncertainty) show the uncertainty of the emission estimate considering all contributions.

With these conclusions, the uncertainty of the estimated emissions was recalculated again. For the 175 possible cases that were separated from the 3 hours of measurement,

about 60% of the emissions were above the real release rate. This shows that OTM-33A overestimates emissions, or at least it does for small values of emissions, but there is not much percentage difference between overestimation and underestimation. Similar conclusions were reached by Edie et al. (2020), who found that the OTM-33A method has a large range of both overestimation and underestimation.

5.2.4 Test of the measurement duration

With the three hour release test we investigated the optimal duration of OTM-33A measurements. The EPA guideline (Thoma et al., 2014) recommends for instruments with 1 Hz data frequency a duration of 15-20 minutes. This is certainly an advantage of such measurements, but the question arises whether such a short measurement time is sufficient. From the 3 hours of measurements, we extracted different time intervals (from 20 minutes to 3 hours) and the emission rate was estimated for each of them. Figure 43 shows the results of the analysis in terms of the duration of the measurement. The blue dots indicate the emission values estimated for a measurement lasting respectively 20 min, 40 min, 60 min, 80 min etc. The green dots represent the emissions for hourly measurements, respectively for the first, second and third hour. A longer time of measurements does not result in more accurate determination of emission rates. Taking into account the estimation uncertainty, each case gives a result comparable to the real release rate. However, the most accurate results were obtained for measurements that lasted 60 minutes. To compare our results from the release test, we used the percentage error described by Edie et al. (2019). Emissions for measurements that lasted an hour have a percentage error of less than 10%. For other time intervals, the error is in the range of 25 - 50%, with the exception of the measurement with $T = 80$ min, for which it was 7%. This leads us to conclude that measurements longer than this period are unnecessary, since they only increase the duration of the measurement and do not improve the result. It seems therefore appropriate to focus more on the repeatability of the measurement, i.e. the number of quantifications performed, rather than on their duration, since looking at the previous graphs, a 20-minute measurement repeated many times gives a good results.

Table 16 shows the emission rates estimated for all OTM-33A method applications listed in Table 15. The last release test did not fulfil the quality criteria, as the mean CH_4 concentration was less than than 100 ppb above background (one of DQI). The stability class in this case was also low (2), indicating a moderately unstable stability class. On February 24-25 methane was released and measured for 60-78 min with release rates of 0.32 gCH_4/s . The results from OTM-33A method agreed within -19% to 48% of the known released rate. However, it should be taken into account the strong winds that exceeded 4 m/s, which makes it easier to estimate emission rates. Similarly, in the case of

the longer OTM-33A measurement, which lasted 180 min, the estimated emission was 0.72 ± 0.28 g/s.

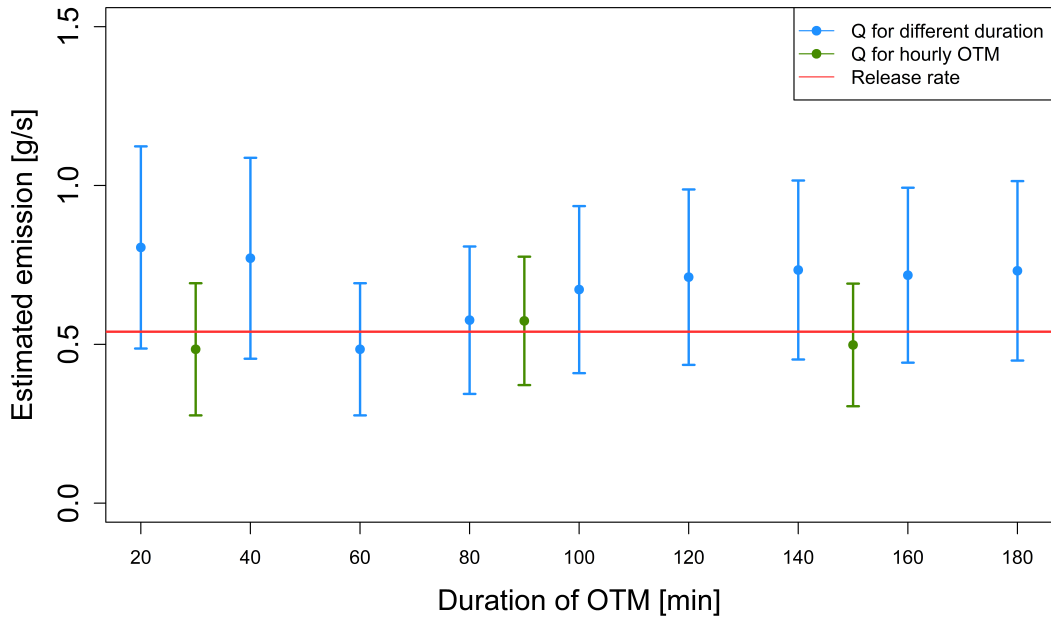


Figure 43: Dependency of estimated emissions on the duration of the measurement. Blue dots represent the estimated emissions for the measurement duration as indicated on the OX axis. Green dots represent emission values for the first, second and third hour of measurement respectively.

Table 16: Emission (Q) estimated for all OTM-33A applications during DuREX campaign listed in Table 15. Test with * does not fulfil the quality criteria.

ID	Release [g/s]	WS [m/s]	Q [g/s]	u(Q) [g/s]	Stb class	D [m]	Error [%]
20200223.1	0.54	4.59	0.72	0.28	4	70	+33.62
20200224.1	0.32	5.49	0.26	0.09	5	57	-19.18
20200224.2	0.32	4.35	0.39	0.15	5	57	+22.15
20200225.1	0.32	5.07	0.47	0.17	5	37	+48.06
20200227.1	0.23	2.02	0.35	0.12	5	46	+53.85
20200227.2 *	0.23	0.73	0.010	0.005	2	26	-95.77

5.2.5 Mannheim release tests

During the last two release tests in Mannheim (M4 and M5), the OTM-33A method was also applied. Here the focus was to investigate if the estimated emission depends on the distance from the source at which the measurement is performed. The results for

the OTM-33A method for the M5 test are summarized in Table 17. Each measurement was taken at a different distance from the source (30 m, 57 m, 92 m, 120 m and 151 m). As written during the analysis of the GPM method, in the case of the M5 test, the wind speed was about 2 m/s. For atmospheric conditions the stability class 4 has been chosen. Methane was released at 0.1 g/s throughout the experiment. From all the performed tests, only the first test (M5_1_1) met all the DQI criteria, the average concentration of methane above the background in the plume was 0.35 ppm (0.1 ppm is the lower limit in DQI) and the fit was $R^2 = 0.85$. However, the estimated emission for this case was 0.06 ± 0.02 g/s, which is 60% of the know release. The test at a distance of 57 m was performed twice (M5_2_1 and M5_2_2), where at the second approach the average wind speed increased by 15%. The first test at this distance gave an emission of 0.03 ± 0.01 g/s, which is only 30% of the known release rate. Comparing the two cases, we can see that the measured average concentration of methane in the plume has increased by 100%, which translates into an increase in the coefficient of fit from 0.48 to 0.64. Although both tests do not meet the recommended DQI, the emissions estimated for the second time gave a result of 0.09 ± 0.03 g/s, which is 3 times higher than the first measurement at this distance. This confirms the assumption made earlier that repeatability of measurements is more important. Interestingly, measurements at 92 m, 120 m and 151 m also failed to meet the recommended DQI. However, despite this, the estimated emission is within $\pm 12\%$ of the know release. Since the concentration of methane in the plume decreases with distance (from 8.69 ppm for M5_1_1 to 2.33 ppm for M5_5_1), a possible solution seems to be to reduce the DQI value, especially for small emissions like the one tested here. Reducing the condition for methane concentration above background from 100 ppb to 50 ppb and $R^2 = 0.7$ for measurements above 100 m, would allow to accept the results as for M5_4_1. With stronger sources this problem becomes negligible because observing the average concentration of methane in the plume at 100 ppb above background will not be a problem.

Table 17: Emission (Q) estimated for all OTM-33A applications during M5 test. The method was tested in different distances.

ID	Release [g/s]	WS [m/s]	Q [g/s]	u(Q) [g/s]	D [m]	R^2	$CH_{4excess}$ [ppm]
M5_1_1	0.1	1.50	0.06	0.02	30	0.85	0.35
M5_2_1	0.1	1.65	0.03	0.01	57	0.48	0.08
M5_2_2	0.1	1.89	0.09	0.03	57	0.64	0.16
M5_3_1	0.1	1.41	0.09	0.03	92	0.76	0.13
M5_4_1	0.1	1.58	0.11	0.04	120	0.70	0.08
M5_5_1	0.1	1.98	0.10	0.03	151	0.58	0.04

5.2.6 Conclusions

In conclusion, the number of performed OTMs is not sufficient to determine all the relationships, and it is recommended to perform additional tests under different weather conditions. Furthermore, additional experiments should be conducted with a higher methane emission rate. Another issue for the future is the distance over which the measurement should take place. EPA recommendations assume a range between 20 and 200 m from the source, but this should be tested depending on the release rate and perhaps this range could be increased or the Data Quality Indicators could be adapted in some range of distance. The performed tests were ideal cases where there were no obstructions between the source and the measurement point, which must be taken into account. However, the OTM-33A method provides an alternative solution to the GPM method, although it is dedicated to point sources such as oil and gas wells. The obtained results indicate that there is no basis for making one long OTM-33A to estimate emissions more accurately compared to a short measurement. However, it is preferable to perform many quantifications at shorter duration. The deciding factor is the repeatability of the measurements. The percentage error is much lower for a shorter experiment time, and the average value of all intervals is closer to the actual release rate than for a 3 hour OTM. It is also better to have a higher wind speed during the real measurements. Taking into account the accuracy of the distance the analyzer is from the source, the uncertainty of the emission estimate increases on average to 40% of the known release rate. It is therefore recommended that the distance between the source and the analyzer location be carefully measured to reduce the uncertainty of the estimated emission rate.

6 Quantification of CH_4 emitters in Heidelberg region

In order to determine the CH_4 emission rates from different emission sources, regular measurement campaigns were carried out in the region around Heidelberg. The sites visited include 2 dairy farms (Weinheim and Ladenburg), a gas compressor station with underground gas storage (Gernsheim), a landfill (Sinsheim), a biogas plant and a wastewater treatment plant in Heidelberg.

The emission rates for the Heidelberger CH_4 sources were estimated using the GPM method, described in 2.4.1. The OTM-33A method was applied only during three test and comparison cases in Heidelberg namely at the biogas plant in Heidelberg and the farm in Ladenburg (Krümpelmann, 2019). Data analysis with the GPM was performed using codes written by Kammerer (2019) which were modified and adapted in this PhD thesis. All codes were written in R and were improved as needed and with new gained knowledge. The results of the analysis are presented using figures and tables below.

Figure 44 shows the frequency of yearly measurement days for the different CH_4 sources. It is divided into two periods when the researchers conducted Hoheisel (2017), and measurements conducted in this study (after 2018), as indicated by the black line. Mobile measurements were carried out only under stable atmospheric conditions. Bad weather conditions such as thunderstorms and rainfall were avoided for safety. In order to ensure driving safety the mobile measurements were also only carried out during daylight hours.

The data analysis begins with the merging of all individual data series: from the analyzer (G2201-i or LI-7810), from the GPS recorder, from the two weather stations (2D and 3D). If weather data were missing, they were replaced by values obtained during later measurements at a similar time.

All local CH_4 sources are shown in Figure 25- Figure 29 where the assumed emission release points used for the data analysis are marked. In the case of the farms in Ladenburg and Weinheim, two potential sources, the cow shed and the biogas plant were included in the GPM. As described in the chapter (subsection 5.1), an additional quality parameter included in the analysis, must be $R^2 > 0.5$. This additional parameter allows further automation of the data evaluation. Transects for which the peak was measured during a turnaround or if the model did not generate a peak were automatically rejected. However, in the case of two sources (farm and biogas), this quality check does not work properly, because of the size and location of two peaks and the inability to determine the value of R^2 . Therefore, in the case of Ladenburg and Weinheim the value of the correlation coefficient did not constitute automation of the analysis process, and each measured and modelled peak was inspected separately and manually.

Measurements for which the isotopic composition was also studied were characterized

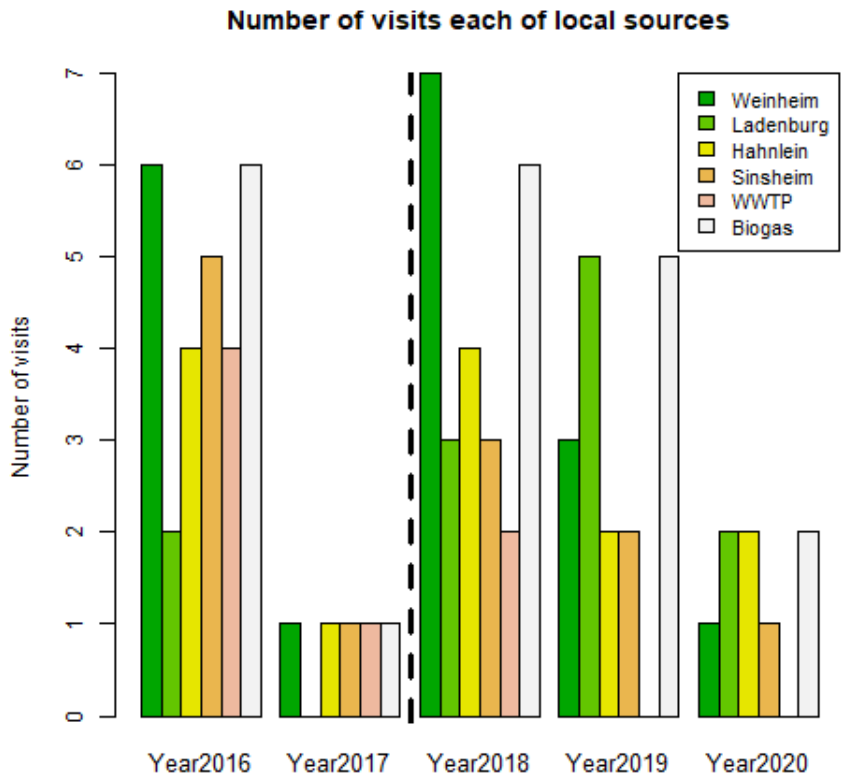


Figure 44: Barplot presenting frequency of visited sites around Heidelberg between 2016 and 2020. The black dashed line divides the period into measurements carried out by Hoheisel (2017) and during this study.

by a high variability of methane concentrations, because the amplitudes were usually increasing from background value to 50 ppm of CH_4 in a short time interval, so that it was necessary to determine the background as for the OTM-33A method (5% of the lowest values).

All data are presented using graphs and tables. The tables contain information as shown in Table 18, if not stated differently, estimated emission will be presented as $Q_{med} \pm u(Q_{med})$ [g/s].

Table 18: Description of the values used in the tables summarizing the measurements for a given source.

Variable	Description	Unit
date	date of mobile measurements	YYYY-MM-DD
class	stability class used for data analysis	A - F
WS	wind speed	m/s
$u(WS)$	uncertainty of wind speed	m/s
WD	wind direction	degrees
$u(WD)$	uncertainty of wind direction	degrees
N	number of accepted transects	
N_{all}	total number of transects	
C_{min}	minimal concentration of observed peak	ppm
C_{max}	maximal concentration of observed peak	ppm
Q_{min}	minimal estimated emission for each campaign	gCH_4/s
Q_{max}	maximal estimated emission for each campaign	gCH_4/s
Q_{med}	median of estimated emission	gCH_4/s
$u(Q_{med})$	uncertainty of median	gCH_4/s
Q_{mean}	average emission	gCH_4/s
$u(Q_{mean})$	uncertainty of average emission	gCH_4/s

6.1 Dairy Farm in Weinheim

The dairy farm in Weinheim has been visited 11 times between 10.01.2018 and 31.01.2020. A total of 154 transects have been analysed for this facility. The estimated emissions with uncertainties are shown in Figure 45 and summarized in Table 19. The biogas plant near the dairy cow barn made the calculation of CH_4 emissions from the dairy cows alone difficult. Typically, the peaks of both sources overlap to form a double peak, which can even in some cases not be distinguished. Therefore, the results presented here apply to the entire facility. In the case that the atmospheric stability class determination cannot be made uniquely and 2 classes would be possible, the calculated CH_4 emission rates for both classes are presented.

The concentration of the measured methane peaks ranged between 2.08 and 30 ppm, driving in a similar distance of the farm. This shows already a large variability, which is not expected from the emission of the dairy cows. The estimated emission rates range from 2.3 gCH_4/s to nearly 30 gCH_4/s (Figure 45). On most measurement days, CH_4 emission rates between 2 and 6 g/s were determined, while on two measurement days significantly higher emission rates were determined. The first one took place on 26.04.2018 and the second one on 02.04.2019. Both of these campaigns were considered for two stability classes. Additionally, analysis of the measurements from 02.04.2019 were performed in two cases because the time series shown previously in the Figure 48 (Kammerer, 2019)

shows that the first 8 peaks had significantly lower concentrations (up to 5.45 ppm), than the next 12 peaks (up to 29.99 ppm). Both emission rates are presented in Figure 45 with light green points and dark green points, respectively. The remaining emission rates do not exceed 10 gCH₄/s, and their average is then 4.72 ± 1.89 gCH₄/s.

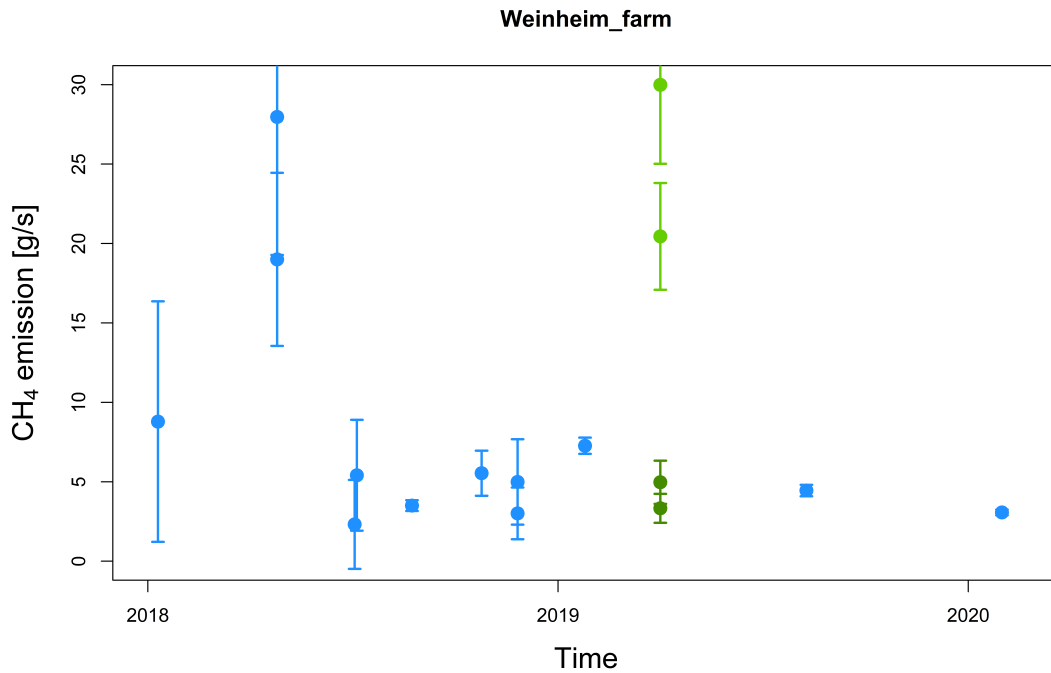


Figure 45: Estimated emission rates for the Weinheim farm. The light green and dark green points indicate 8 and 12 peaks for measurements on 02.04.2029 respectively.

Even without considering the two cases of very high emissions, the average emissions of the whole farm are higher than calculated with emission factors used by the national emission inventories. According to the UBA 2020 report, the CH₄ emission factor for dairy cows depends on the milk production of the cows and is on average for Germany 137 kg/cow/year (0.004 g/cow/s). With the above emission factor for dairy cows, the methane emissions from 340 cows on this farm should be 1.5 g/s. The CH₄ emission rates measured in this study are 3 times higher. Even taking into account the CH₄ emissions from manure of 22 kg/cow/year, the total emission without biogas plant would be less than 2 g/s. Assuming that CH₄ emissions from cows are relatively well studied, it follows that more than half of the emissions from the Weinheim dairy farm would be from the biogas plant.

Table 19: Results of GPM for Dairy Farm in Weinheim.

date	2018-01-10	2018-04-26	2018-04-26	2018-07-04	2018-07-06	2018-08-24	2018-10-25	2018-11-26
class	C	C	D	B	B	D	B	A
WS	3	3	3	3	2.83	2.19	2.09	0.76
u(WS)	-	-	-	-	1.83	1.15	1.2	0.58
WD	-	-	-	-	314.08	234.84	312.15	8
u(WD)	-	-	-	-	48.38	30.78	67.22	50.18
N	3	10	10	2	2	9	4	5
N_{all}	4	14	14	4	5	13	7	6
C_{min}	6.13	7.78	7.78	2.08	4.2	3.28	3.51	3.02
C_{max}	14.26	29.99	29.99	5.03	4.48	6.76	4.65	11.7
Q_{min}	4.05	12.06	8.66	0.54	3.19	2.36	2.99	2.32
Q_{max}	18.44	57.86	38.07	4.1	7.64	6.14	6.76	20.91
Q_{med}	8.79	27.97	19	2.32	5.41	3.5	5.54	4.99
u(Q_{med})	7.57	8.69	5.45	2.8	3.49	0.34	1.42	2.69
Q_{mean}	10.43	31.55	21.74	2.32	5.41	3.73	5.21	8.69
u(Q_{mean})	4.23	5.37	3.55	1.78	2.22	0.35	0.89	3.52
date	2018-11-26	2019-01-25	2019-04-02	2019-04-02	2019-04-02	2019-04-02	2019-08-10	2020-01-31
class	B	C	B	B	C	C	B	C
WS	0.76	2.5	5.5	3.13	5.5	3.13	3.37	2.91
u(WS)	0.58	0.95	1.62	1.62	1.62	1.62	1.63	1.06
WD	8	188.7	192.32	192.32	192.32	192.32	226.14	225.89
u(WD)	50.18	25.8	36.97	36.97	36.97	36.97	33.67	22.81
N	5	35	12	8	12	8	25	21
N_{all}	6	35	12	8	12	8	25	21
C_{min}	3.02	4.1	4.38	2.75	4.38	2.75	2.88	2.79
C_{max}	11.7	11.22	28.79	5.45	28.79	5.45	4.31	4.08
Q_{min}	1.4	4.79	8.89	2.17	5.69	1.42	2.15	2.01
Q_{max}	12.59	13.25	49.13	7.43	32.4	4.93	8.25	4.73
Q_{med}	3.01	7.27	29.99	4.97	20.45	3.33	4.45	3.07
u(Q_{med})	1.63	0.51	4.97	1.36	3.36	0.91	0.36	0.18
Q_{mean}	5.22	7.82	29.58	5.04	19.84	3.34	4.96	3.18
u(Q_{mean})	2.13	0.4	3.73	0.69	2.5	0.46	0.29	0.15

6.2 Dairy Farm in Ladenburg

The Ladenburg farm was visited 9 times to evaluate the CH_4 emission rates. All results are presented in Figure 46 and Table 20. During one of the measurements OTM-33A method was used, which is marked in red in the Figure 46 and in the Table 20 as *. Similar to the farm in Weinheim, at this farm is also a biogas plant installed. In some cases it is difficult to separate the CH_4 emission peaks of the stables from those of the biogas plant. Emissions from both sources were therefore modelled together and the estimate represents emissions for the entire facility. The CH_4 concentrations peaks recorded during mobile measurements were usually between 2.5 - 4 ppm, with one exception of 11.5 ppm. These values were comparable for all mobile measurements, indicating relatively constant emissions for the entire facility. Similar CH_4 concentration of the peaks were also measured by Hoheisel et al. (2019). The range of estimated CH_4 emission rates is 0.54 ± 0.34 to 1.98 ± 0.20 gCH_4/s . Emissions estimated using the OTM-33A method gave the second lowest values of 0.7 ± 0.04 gCH_4/s . Based on all results, the average emission rate for the entire facility is 1.26 ± 0.47 gCH_4/s .

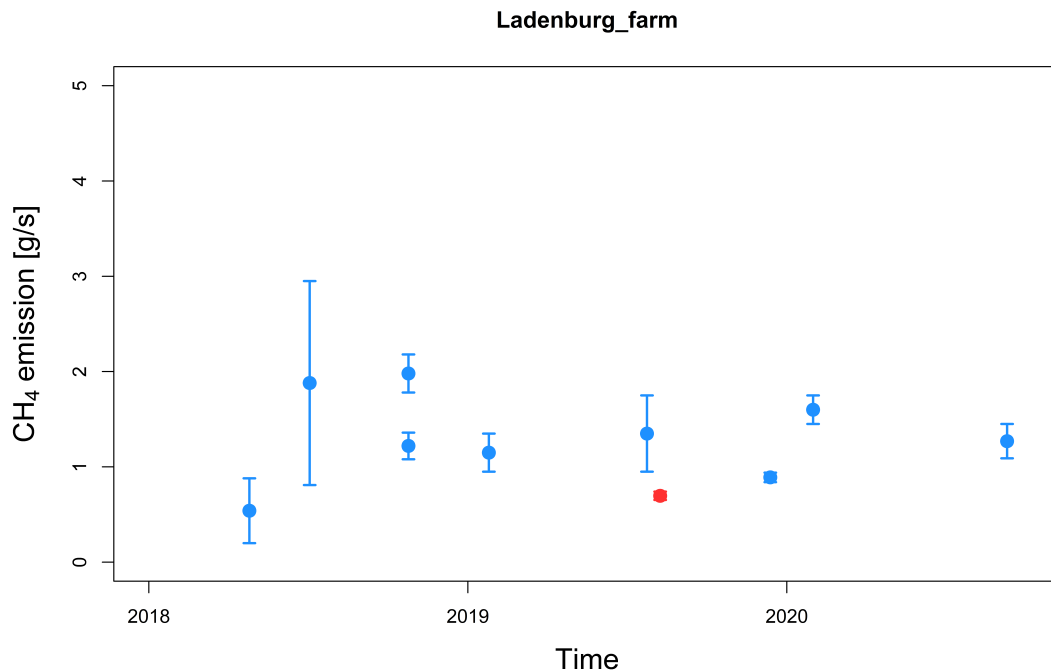


Figure 46: Estimated emissions for the Ladenburg farm. The red point indicates the estimate made using the OTM-33A method.

Using the UBA guideline for UNFCCC reporting, (UBA report) we can again calculate the the CH_4 emission for a farm with 90 cows in Germany. For this farm in Ladenburg the emission rate rate for 90 cows sum up to 0.40 gCH_4/s . When taking into account the

methane emission factor for calves (0.0016 g/cow/s), which is taken as a factor for the other (non-dairy) cows, this results in an additional 0.11 gCH₄/s (for 70 calves). Manure management will result in additional emissions of about 0.08 gCH₄/s. The total emission from "bottom up" approach is 0.6 gCH₄/s. This is therefore half of the average estimated emissions (for Weinheim it was a ratio of 1:3). However, the Ladenburg farm is a source without significantly higher emissions. Compared to the Weinheim farm, this is a smaller farm in terms of number of cattle and associated tanks, which suggests that the emissions for this facility will be lower, even if they are scaled up against each other.

Table 20: Results of GPM for Dairy Farm in Ladenburg. Date with "*" means measurements made using OTM-33A.

date	2018-04-26	2018-07-04	2018-10-25	2018-10-25	2019-01-25	2019-07-25	2019-08-09*	2019-12-13	2020-01-31	2020-09-09
class	B	B	A	B	C	A	B	C	C	B
WS	2.00	2.00	1.75	1.75	2.63	1.70	2.60	3.43	2.49	2.03
u(WS)	-	-	0.99	0.99	1.39	1.06	-	1.65	1.19	1.02
WD	-	-	227.55	227.55	158.91	47.06	-	210.42	205.75	236.76
u(WD)	-	-	34.45	34.45	43.63	77.96	-	34.18	28.98	36.63
N	3	2	4	4	4	5	-	17	13	9
<i>N_{all}</i>	4	2	6	6	6	7	-	20	20	12
<i>C_{min}</i>	2.31	2.76	2.72	2.72	2.59	4.11	bg	2.31	2.6	2.96
<i>C_{max}</i>	2.61	3.87	3.60	3.60	2.83	11.49	2.70	2.83	3.71	4.52
<i>Q_{min}</i>	0.33	1.20	1.71	1.03	0.58	0.70	-	0.52	1.13	0.55
<i>Q_{max}</i>	2.18	2.56	2.35	1.45	1.38	3.20	-	1.21	2.37	1.95
<i>Q_{med}</i>	0.54	1.88	1.980	1.220	1.150	1.350	0.697	0.890	1.600	1.270
u(<i>Q_{med}</i>)	0.34	1.07	0.200	0.140	0.200	0.400	0.044	0.050	0.150	0.180
<i>Q_{mean}</i>	1.02	1.88	2.00	1.23	1.06	1.55	-	0.90	1.59	1.27
u(<i>Q_{mean}</i>)	0.58	0.68	0.13	0.09	0.17	0.44	-	0.05	0.10	0.14

6.3 Biogas plant in Pfaffengrund

As mentioned in the description of the biogas plant at Pfaffengrund, it was a source where very strong methane signals could often be measured, with peaks very clearly above the measured background. This site was visited a total of 13 times between 10.01.2018 and 11.09.2020. During 11 visits the GPM method was used and during two visits the OTM-33A method was applied. Emissions estimated with the OTM-33A are shown in red in the figure and with "*" in the table.

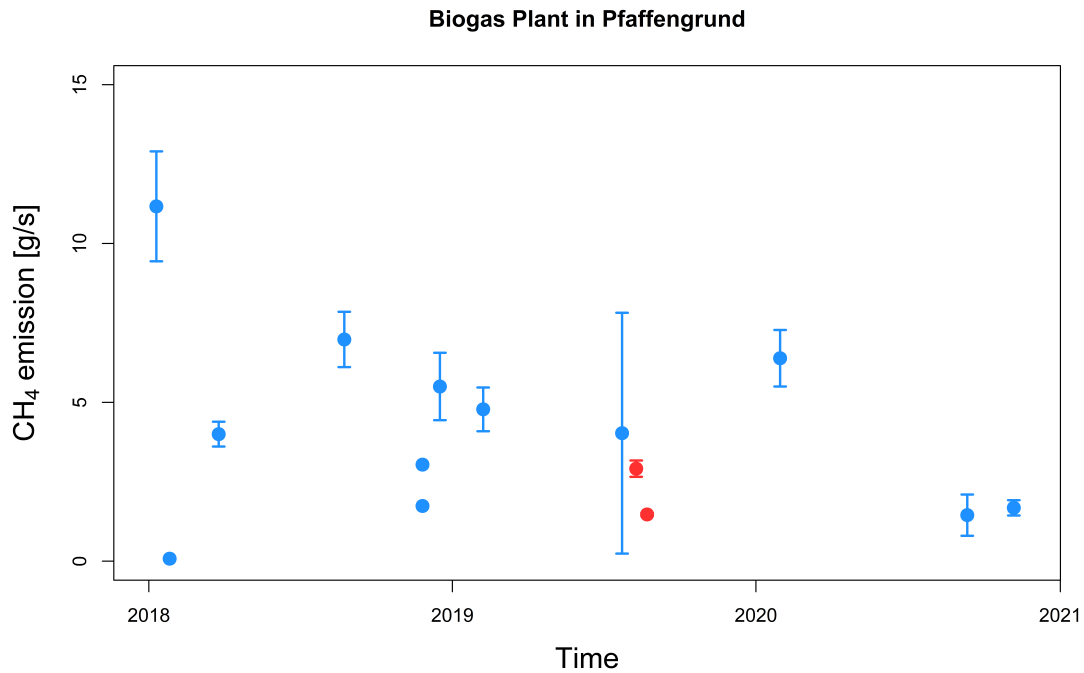


Figure 47: Estimated emissions for the biogas plant in Pfaffengrund. The red point indicates the estimate made using the OTM-33A method.

Figure 47 shows the estimated methane emission rates for each measurement campaign. It illustrates that the CH_4 emission rates from this biogas plant shows large variations, from 0.08 to 11.17 gCH_4/s . Recent mobile measurements have been carried out by Seyfarth (2021), where first 12 transects were carried out and then the OTM-33A method was applied. The estimated methane emission rate from the GPM method was $1.68 \pm 0.24 gCH_4/s$, while the OTM-33A analysis showed emission rate of $1.75 \pm 0.04 gCH_4/s$. As for the Ladenburg farm, the OTM-33A method estimated one of the lowest emission rates, $2.91 \pm 0.26 gCH_4/s$ and $1.47 \pm 0.05 gCH_4/s$ for first and second OTM-33A measurement performed in August 2019. The mean emission rate for this facility, is $3.94 \pm 2.90 gCH_4/s$. The emission rate of 1 g/s reported by Yeman (2015) fits in the order of magnitude, however the average emission rate obtained in this study is almost 4 times higher. This value is more comparable to that obtained by Bakkaloglu et al. (2021), where 10 biogas plants in the UK were visited. The average emission for these biogas plants was $4.42 gCH_4/s$ (org. $15.9 kgCH_4/h$). When comparing this to the value obtained by Scheutz et al. (2019), the average emission estimated for 23 Danish biogas plants was $2.89 g/s$ (org. $10.4 kg/h$), so the average emission for the biogas plant in Pfaffengrund is 36% higher. The difference probably depends on what is stored in the biogas plants and what the biogas is produced from.

Table 21: Results of GPM for Biogas plant in Pfaffengrund. Date with "*" means measurements made using OTM-33A.

date	2018-01-10	2018-01-26	2018-03-26	2018-08-24	2018-11-26	2018-11-26	2018-12-17
class	C	C	B	B	A	B	B
WS	3	3	3	2.38	1.15	1.15	1.5
$u(WS)$	-	-	-	1.29	1.02	1.02	0.97
WD	-	-	-	225.51	344.2	344.2	136.3
$u(WD)$	-	-	-	41.67	71.65	71.65	46.26
N	4	1	4	5	1	1	8
N_{all}	6	5	4	6	6	6	13
C_{min}	10.38	2.21	5.19	2.04	2.14	2.14	5.4
C_{max}	22.4	2.21	6.86	11.34	2.14	2.14	19.15
Q_{min}	4.99	0.08	3.61	0.14	3.04	1.74	1.96
Q_{max}	13.75	0.08	4.57	9.16	3.04	1.74	8.59
Q_{med}	11.17	0.08	4	6.98	3.04	1.74	5.5
$u(Q_{med})$	1.73	-	0.39	0.87	-	-	1.06
Q_{mean}	10.27	0.08	4.05	5.92	3.04	1.74	5.64
$u(Q_{mean})$	1.86	-	0.22	1.53	-	-	0.76
date	2019-02-07	2019-07-24	2019-08-10*	2019-08-23*	2020-01-30	2020-09-11	2020-11-06
class	C	A	B	B	B	B	C
WS	2.15	1.35	3.6	3.7	1.72	2.75	2.2
uWS	1.18	1.01	-	-	0.8	1.4	0.15
WD	159.9	45.9	-	-	130.93	321.02	180
$u(WD)$	56.53	88.72	-	-	76.04	42.73	-
N	7	5	-	-	15	9	12
N_{all}	14	12	-	-	15	17	12
C_{min}	6.76	2.09	bg	bg	8.94	2.18	2.3
C_{max}	12.02	18.75	3.2	7	51.93	6.16	3.3
Q_{min}	2.74	0.27	-	-	3.25	0.11	0.64
Q_{max}	6.53	14.61	-	-	11.79	5.66	3.64
Q_{med}	4.78	4.03	2.914	1.472	6.39	1.45	-
$u(Q_{med})$	0.69	3.79	0.257	0.051	0.89	0.65	-
Q_{mean}	4.56	6.85	-	-	6.51	2.07	1.68
$u(Q_{mean})$	0.46	2.64	-	-	0.58	0.67	0.24

6.4 Discussion of results for farms and biogas plant

The agriculture and waste sector accounts for 30% of anthropogenic methane emissions, and 50% of emissions from this sector (115 Tg CH_4 /year) come from enteric farm and manure (Saunois et al., 2020). The problem for the estimation of emissions from facilities such as dairy farms is the emissions coming directly from the cows as well as emissions from manure management. In addition, as in the case of the Weinheim and Ladenburg farms, the biogas plant is another source with some methane emission rate.

There is a wide variety of manure management practices on dairy farms, and intensification favors manure management. This trend increases the potential for CH_4 (as well as N_2O) emissions, as well as the need for mitigation. However, methods for estimating emissions from manure are not well suited to describe farm-level management, and the effects of changes in manure management or processing are not easily quantified, which is also a barrier to future emissions regulation. To accurately estimate CH_4 emissions from manure and CH_4 mitigation potential, it is important to separately estimate losses during storage in barns and outdoor storage. Better mapping of temporal and spatial variability can provide assistance in quantifying manure treatment and management effects and mitigation potentials (Petersen, 2018). According to a recent study (Arndt et al., 2018), CH_4 emissions from manure should be measured monthly or more frequently throughout the year to verify manure management predictions. A study done for two dairies showed that emissions from these farms can be reduced by changes in manure management practices (Arndt et al., 2018).

A decrease in methane emissions from ruminants could be also achieved by reducing animal products such as beef and dairy products. However, this involves a social consensus that would need to be achieved. Data presented by the Minus Methane Project (2019) show that emissions for cows depend on the composition of their diet. Methane emissions increase when cows are fed coarse or fibre-rich diets, so one way to reduce methane emissions is to change the composition of the diet (Jayasundara et al., 2016).

The farms in Weinheim and Ladenburg are typical dairy farms for this region, operating a biogas plant. Due to the close location of the stable and the biogas plant, it is partly difficult to separate the CH_4 concentration peaks. Sometimes we see double peaks with varying contributions. The key to estimating accurate emissions for a farm is to distinguish between the effect of the biogas plant and the farm on emissions from the entire facility.

Despite the similarities in the two farms, they show different emission rates. When compared with the emission factors reported by UBA, the emissions for both farms exceed the expected values. Therefore it is crucial to estimate the impact of emissions from biogas plants. While the Ladenburg farm does not show much variation, the Weinheim

farm had two events with significantly higher emissions. However, excluding these two special cases of higher emissions, the Weinheim farm maintains a rather constant emission value. Therefore, it can be assumed that emissions from these sources are relatively constant throughout the year, and thus the share of each source (biogas plant and cowshed) in the emissions mix does not change. As described above, one of these occurred during measurements by Kammerer (2019). The variation of methane peaks versus time of mobile measurements is presented in Figure 48. The time-dependent methane concentration measurements are shown in blue, while the CO_2 concentration is shown in black. Wider peaks following narrower ones indicate AirCore measurements.

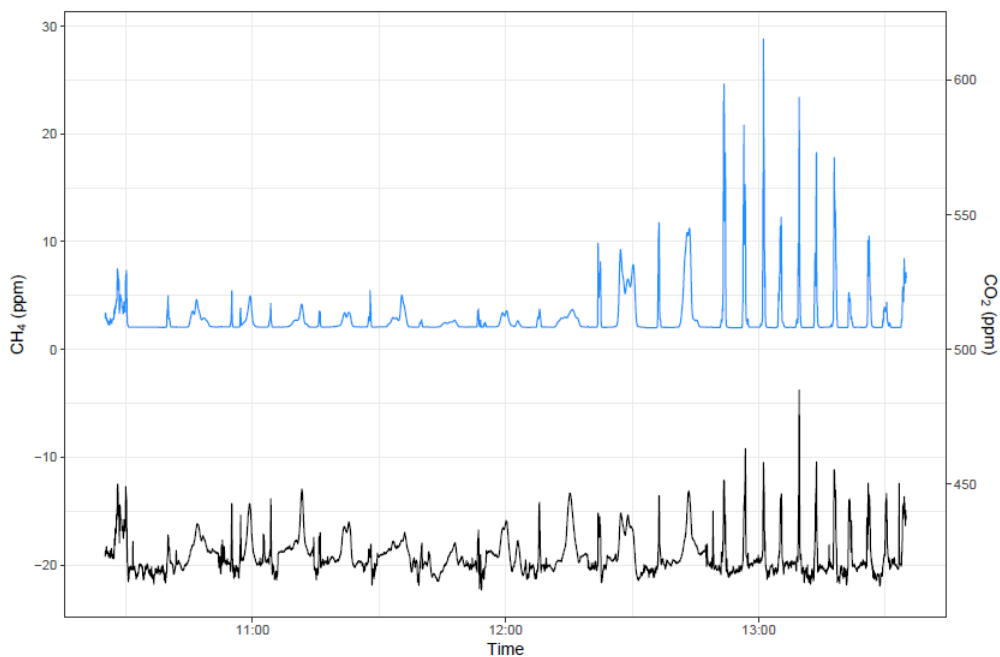


Figure 48: Time series of CH_4 and CO_2 measurements in Weinheim, 02.04.2019 (Kammerer, 2019).

It can be seen that during the first part of the measurement the CH_4 concentration is relatively low and does not exceed 5 ppm. However, after 12:20 the CH_4 concentration peaks increases to 15-30 ppm..

One possible explanation for this could be a leak in the biogas plant. However, this is not very probable, because in cases like that such an anomaly would be observed more frequently and certainly there would not be such a variation in the concentration of measured plumes within one day. Liebetrau et al. (2017) and Reinelt et al. (2019) also conducted methane emission studies for biogas plants. Based on their research, they provide an explanation for the increased emissions from biogas plants. It may come from pressure relief valves of the gasholders. This is closely related to safety issues. Long lasting pres-

sure relief valves could be an explanation of larger methane emission from biogas plant (Liebetau et al., 2017; Bakkaloglu et al., 2021). These occasional events would explain the sudden increase in measured concentration in the plume and thus the spike in methane emission rates.

Another possible explanation observed by Reinlet et al. (2019) is the ambient air temperature. In the summer months, when the temperature is higher, they observed increased emission rates. As shown in the graphs of emissions for the farms in Ladenburg and Weinheim, despite measurements carried out at different correlations, no increase in emissions can be seen during the summer months compared to the winter months.

Monitoring the emissions of the Pfaffengrund biogas plant leads to the same conclusion. There was no correlation between the estimated emission rates and the period of measurement, which would be characterized by a higher or lower air temperature. Moreover, in this case the emissions are highly variable and do not show any particular characteristics.

An additional question is why such high values in the emission rates were measured only for the Weinheim farm. A possible explanation is the technological aspect of the biogas plant. As presented by Liebetau et al. (2017), monitoring and maintenance can help to reduce emissions from biogas plants. The monitoring frequency needs to be adapted to any potential emission sources on site. One proposed solution for emission reduction is upgrading biogas plant technology. The use of newer technology should help to better monitor possible increases in emissions. From personal communication, it is known that the biogas plant in Ladenburg is younger than the one in Weinheim, which could explain the lack of emission anomalies for the smaller farm.

As mentioned when describing the results for the Pfaffengrund biogas plant, the obtained average methane emission rates based on all measurements are comparable to those obtained by Bakkaloglu et al. (2021) and higher than those presented by Scheutz et al. (2019), however in the same order of magnitude. Bakkaloglu et al. (2021) studied 10 biogas plants, while Scheutz et al. (2019) studied emissions from 23 biogas plants, but spent only 1 or 1 to 4 measurement days per plant. In these two works, to estimate methane emission rates, the GPM method and the Tracer Gas Dispersion method (TGD) were used, respectively.

As part of the Heika campaign, Seyfarth (2021) conducted mobile measurements for the Pfaffengrund biogas plant (results described earlier) and the Emter Öko biogas plant located in Bavaria. It was monitored during three days of measurements using the GPM method and a total of 40 transects were performed (31 accepted for analysis). The analysis of the collected data showed emission levels between 2.8 ± 1.4 and 6.3 ± 0.5 gCH₄/s. Also these values are in good agreement with those obtained for the biogas plant in Pfaf-

fengrund.

Mobile measurements on the farms in Weinheim and Ladenburg and biogas plant in Pfaffengrund should be continued. To answer for all questions some actions should be considered. One possible solution would be to consult with the owners of these sites to discuss the results. In addition, campaigns should be conducted more regularly to catch possible anomalies like the one in Weinheim. In addition, the LI-7810 portable analyzer should be used detailed inspection of the biogas tank. Sampling for isotopic composition analysis should also be carried out at every possible opportunity to allow a more accurate comparison between direct samples and values obtained from plume measurements. Perhaps this will allow determination of the contribution to the plume of emissions from the biogas plant and cowsheed. In the case of the Ladenburg farm, it is possible to take advantage of favourable weather conditions and make measurements on the road between the biogas plant and the cowsheed. This will allow to determine the contribution of the emissions from the biogas plant to the total facility emissions. Isotopic measurements could help distinguish plumes from two sources, such as a farm and a biogas plant, but only with a high frequency analyzer. The CRDS analyzer used in this study recorded every 3.7 seconds, leading to a small number of points in the plume, so the maximum concentration may not have been observed. The use of the LI-7810 analyzer, increased the number of measurement points but does not give information about the isotopic signature. Nevertheless, the biggest problem is the overlapping of plumes from both sources. It would be useful to conduct research at a facility that does not have a biogas plant in the vicinity, or at a greater distance than the ones in Weinheim and Ladenburg.

Over all, the primary goal should be to implement a regular monitoring plan for the above-mentioned sources. As proposed by Liebetrau et al. (2017), the most important task for emissions quantification should be data reproducibility and as representative data as possible, since only with a combination of comparable data and a large number of sampled sites the emissions from this sector can be better understood. Methane emission levels from biogas plants should even be monitored daily to capture the emission and dispersion pattern due to on-site activities and different meteorological conditions at different time scales (Bakkaloglu et al., 2021).

6.5 Gas Compressor Station in Gernsheim - results and discussion

The gas compressor station in Gernsheim - Hähnlein has been visited a total of 7 times. Emissions from this source were successfully estimated for each measurement campaign and the results are presented in Figure 49 and Table 22. A total of 97 plumes were analysed, of which 45% were accepted. Due to the lack of access to the site and the inability to identify the exact source, it was assumed that the emissions originated from the gas compressor station center. Due to the nature of this source, there should ideally be no emissions indicating a possible leakage of the system. The maximum CH_4 concentration of the measured peaks decreased over time as the peaks reached concentrations above 13 ppm during the first measurements, while the last mobile measurements performed showed a maximum peak concentration of about 2.5 ppm, a value beyond which no Air-Core samples were taken. However, during the campaign in early 2020, the wind velocity exceeded 4 m/s, which allowed us to conduct a larger number of transects (20 and 30 for the January and March measurements, respectively). For the measurements of 25.10.2018, data analysis was performed for both possible stability classes; however, only for class B the emission was estimated, although only on the basis of one accepted peak and it was 1.66 g/s. The low wind speed must be taken into account. The overall low number of measurements for GCS is due to the usually unfavorable wind direction which disallowed conducting transects where representative plumes would have been measured. The estimated CH_4 emission rates are in the range 0.38 to 3.42 g CH_4 /s. However, high emissions were observed only once during the first measurements. Afterwards, lower emissions (up to 1.66 g CH_4 /s) were observed. Average methane emissions are 1.2 ± 1.0 g CH_4 /s including the results of the first measurement campaign, and 0.88 ± 0.49 g CH_4 /s without it. This is comparable in order of magnitude to the emission for the GCS in Sandhausen which was 1.35 ± 0.14 g CH_4 /s obtained by Yeman (2015), which due to the difficulty of conducting measurements was not studied in this study, even though this facility is near Heidelberg (10 km).

In the Figure 49 a decreasing trend can be observed, indicating that less and less methane is emitted from this source. The reason for this emission reductions may be attributed to the fact that over the last 2 years the facility was expanded and construction works may have been connected with tightening of the installation. In 2015, GCS in Gernsheim reported methane emissions of 112 tons/year to the European Pollutant Release and Transfer Register (E-PRTR). This value corresponds to emission rate of 3.5 g CH_4 /s reported directly by GCS and only for the year 2015. For the more recent periods, no emission values have been reported in the E-PRTR database, so we can assume that only in 2015 the GCS did exceed the reporting threshold of 100 t/year methane emissions. The averaged emission rates for the years 2018, 2019 and 2020 are 1.8 g CH_4 /s, 1 g CH_4 /s and

0.48 gCH₄/s which correspond to an annual CH₄ emission of 55.6 t CH₄/y, 31.5 t CH₄/y and 15.3 t CH₄/y. The annual averaged CH₄ emission of the GCS determined in this study are below the threshold of 100 t CH₄/y, and confirm with an independent methodology that the threshold for E-PRTR reporting has not been exceeded.

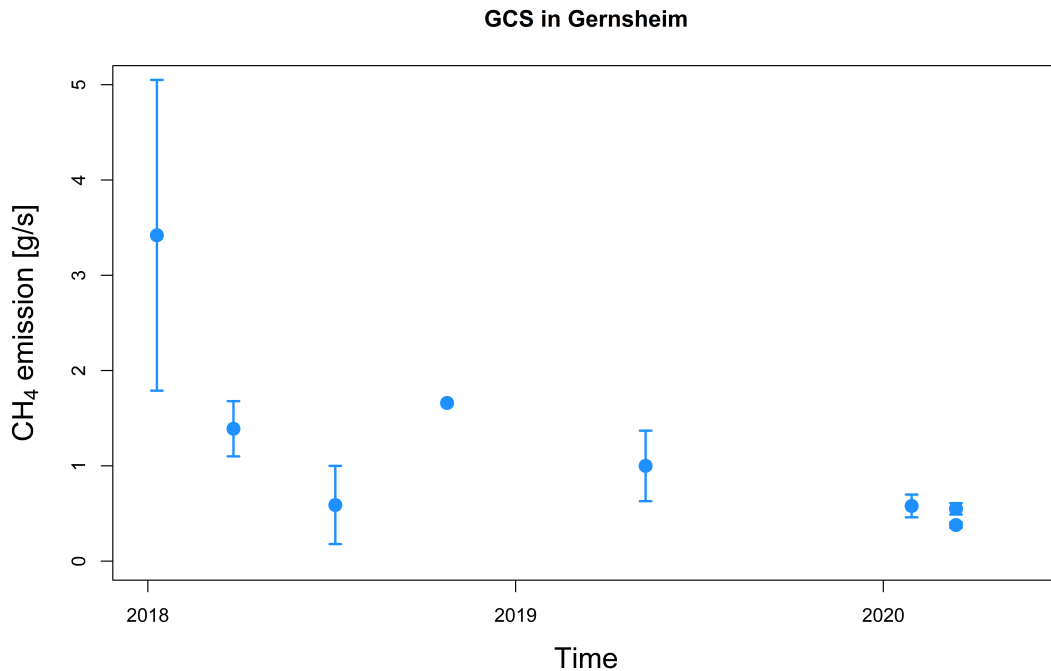


Figure 49: Estimated methane emission rates for the Gas Compressor Station in Gernsheim.

The study of Defratyka (2021) quantified the CH₄ emission rate of two gas compressor stations in the Ile de France region (Paris, France). The CH₄ emission rates from the gas compressor stations varies between 0.15 ± 0.05 gCH₄/s for site C and 0.7 ± 0.14 gCH₄/s for site A. Both gas compressor stations have two compressors and use the same technology. The emission rates of the GCS in Gernsheim are similar to the ones of the Ile de France region. However, it should be noted that the Ile de France measurements were taken once without revisiting, which does not allow for long-term emissions. However, these emissions are 3-10 times lower than average emission for GCS in Gernsheim, which may be caused by size of given GCS and also type of installation, which in Gernsheim is larger facility, with a intersection of two pipelines and an underground gas storage in comparison to GCS C.

Table 22: Results of GPM for Gas Compressor Station in Gernsheim.

date	2018-01-10	2018-03-27	2018-07-06	2018-10-25	2018-10-25	2019-05-10	2020-01-29	2020-03-13	2020-03-13
class	C	B	B	A	B	B	C	C	D
WS	3.00	3.00	2.25	1.63	1.63	2.52	4.27	5.75	5.75
u(WS)	-	-	1.59	0.94	0.94	1.34	1.82	2.08	2.08
WD	-	-	296.14	277.00	277.00	247.88	266.17	235.38	235.38
u(WD)	-	-	61.94	50.08	50.08	42.46	27.96	26.96	26.96
N	3	5	3	0	1	6	6	9	11
N_{all}	4	8	11	8	8	14	21	31	31
C_{min}	7.65	2.37	2.07	-	5.30	2.25	2.20	2.21	2.21
C_{max}	13.29	4.14	2.49	-	5.30	3.53	2.56	2.66	2.66
Q_{min}	2.40	0.59	0.33	-	1.66	0.56	0.38	0.40	0.21
Q_{max}	5.47	1.69	0.92	-	1.66	1.73	1.05	1.23	0.84
Q_{med}	3.42	1.39	0.59	-	1.66	1.00	0.58	0.55	0.38
u(Q_{med})	1.63	0.29	0.41	-	-	0.37	0.12	0.06	0.03
Q_{mean}	3.77	1.22	0.61	-	1.66	1.08	0.65	0.65	0.43
u(Q_{mean})	0.9	0.21	0.17	-	-	0.2	0.1	0.08	0.05

Discussion

The gas industry consists of four main stages: production, processing, transmission/storage and distribution (Mandal et al., 2017; Harrison et al., 1997). Gas compressor stations together with control venting and fugitive emissions belong to the third stage (transmission/storage) and account for 24% of methane emissions from the gas industry in the European Union, rising to 39% in Germany (DVGW). This makes it reasonable to monitor methane emissions from sources like gas compressor stations. Furthermore, majority of emissions in the transmission/storage sector come from compressor station processes (INGAA). By concept, such installations are designed to increase the pressure in the pipe in which the natural gas flows. Their construction and function is therefore linked to a network of connections between pipelines, which all must be tight in order to prevent leakages. While the GCS in Gernsheim does not emit large quantities of methane into the atmosphere (about 31 t per year), this is just one example. Considering the length of the pipelines and the distances between the various compressor stations, many methane leaks can be expected. However, it is nearly impossible to monitor methane emissions over hundreds of kilometers of pipeline, therefore quantifying emissions from a gas compressor station is very important. The need for such measurements is even greater because gas compressor stations can also be "super-emitters", characterized by much higher methane

emissions (Zimmerle et al., 2015; Subramanian et al., 2015). A problem that arises in estimating emissions from GCS is the difficulty of determining the location of the leak, which was also observed in this study and by Defratyka (2021)

Methane emissions from GCSs can be reduced in several ways. These include: replacing rod packing on reciprocating compressors, performing leak surveys and minimizing releases prior to scheduled maintenance (INGAA). It is therefore crucial to closely monitor the methane emissions and the operating system of a facility. Each of the solutions mentioned above has certain assumptions. Rod packing should be exchanged regularly after a certain number of working hours or after a certain period of time (INGAA). Conducting regular leakage surveys seems to be most beneficial, allowing for regular monitoring of emissions and rapid response. It is also very easy to apply. Simply use a portable analyser or infrared camera, for example, which will allow you to quickly locate the source of the emissions. An important consideration, however, is the size of the gas compressor station and the multitude of connections that can make such measurements difficult or time-consuming.

6.6 Landfill in Sinsheim - results and discussion

At the landfill in Sinsheim only six measurement campaigns took place between 26.04.2018 and 29.01.2020. Most of them were focused on isotope measurements, but some transects were successfully used to estimate methane emission rates. A point source of methane emissions located in the central part of the facility was used for the analysis with the GPM. A total of 67 transects were analysed, and only 21 of these (31%) could be used to estimate emission rates. Almost 70% of the measured peaks had to be discarded as the concentration was measured parallel to the direction of the plume, therefore disallowing fitting the Gaussian peak. The first five campaigns were conducted inside the landfill, on the road perpendicular to the wind direction and using the road network on the site, as no significant methane enhancement was observed on the external road (Figure 29), and therefore only background concentrations were recorded there. Only the last campaign (29.01.2020) allowed to measure peaks with concentrations up to 2.3 ppm on the road about 350 m away from the landfill center point. The higher wind speed, exceeding 4m/s, was also only measured for the last campaign, while previous measurements were conducted at relatively low wind speeds (about 1m/s).

As shown in Table 23, the measured methane concentrations at landfill did not show large signal amplitudes, ranging from background levels to nearly 9 ppm. And for the three campaigns, peaks of only 2.3 to 4 ppm could be observed. Low peak concentrations often prevented collection of AirCore samples.

Figure 50 shows the values of estimated CH_4 emission rates for the days on which

the measurement campaigns were carried out. The emission range is between 0.10 ± 0.01 and 3.28 ± 0.72 gCH_4/s . All results are summarized in Table 23. The average methane emission rate based on the performed measurements is 1.38 ± 1.30 gCH_4/s . The variability in the methane emission rates for this landfill over 3 years is almost 100% of the estimated emissions. This is due to the small database with large variation in emissions for individual measurement campaigns. The latest measurement campaign (29.01.2020) was performed under nearly ideal conditions. There were 13 transects, all on the road outside the landfill area (Figure 29), and 8 of them were accepted, giving an estimated emission between 1.67 and 4.71 gCH_4/s with a mean emission rate of 3.28 ± 0.72 gCH_4/s . This is also the highest obtained estimation value.

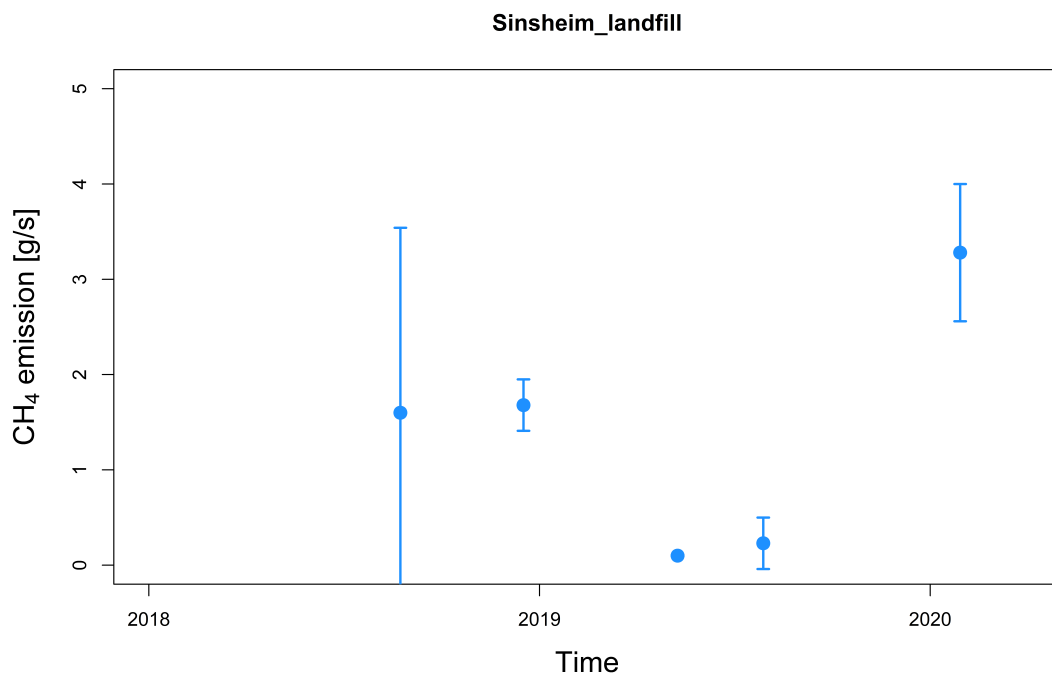


Figure 50: Estimated methane emission rates for the landfill in Sinsheim.

A previous study to estimate emission rate for the landfill in Sinsheim was performed by Yeman (2015). Analysis of the data at that time showed an emission rate of 6.5 gCH_4/s . This is almost double the highest emissions estimated during the last campaign and 5 times higher than average methane emission calculated in this study. This difference may be due to the fact that in 2015, the landfill was not completely covered, which is the case now. This would indicate that the landfill cover insulates well and no higher emissions are occurring. Similar conclusions were found by Defratyka (2021), studying a large landfill (consisting of an open and a closed part). A tracer gas dispersion method was used to conduct measurements of 20 transects. The estimated methane emissions were 18.89 ± 3.61 gCH_4/s . This is 4 times lower than the value reported by Ars et al. (2017). It was

most likely caused by the expansion of the gas collection network and also by covering the closed part with a geomembrane (Defratyka, 2021).

The recent increase of CH_4 emissions at the landfill Sinsheim is most likely due to the newly built compost plant on the landfill area.

Table 23: Results of GPM for landfill in Sinsheim.

date	2018-04-26	2018-08-24	2018-12-17	2019-05-10	2019-07-29	2020-01-29
class	B	B	B	B	B	C
WS	2.00	2.65	1.95	1.66	2.08	4.56
u(WS)	-	1.10	1.04	1.30	0.97	2.31
WD	-	252.23	258.56	246.63	290.36	257.91
u(WD)	-	40.07	41.83	69.36	46.95	36.40
N	0	3	3	3	4	8
N_{all}	9	14	15	9	7	13
C_{min}	-	2.52	2.32	2.26	2.33	2.14
C_{max}	-	8.72	2.43	4.07	7.05	2.31
Q_{min}	-	0.08	1.05	0.09	0.01	1.67
Q_{max}	-	2.81	1.85	0.56	0.55	4.71
Q_{med}	-	1.60	1.68	0.10	0.23	3.28
u(Q_{med})	-	1.94	0.27	0.01	0.27	0.72
Q_{mean}	-	1.50	1.53	0.25	0.25	3.36
u(Q_{mean})	-	0.79	0.24	0.16	0.14	0.39

The E-PRTR database has no reported emission data for the landfill in Sinsheim, which implies, that the on-site calculated emissions is below the reporting threshold of 100 t CH_4 /Year or 3.2 g CH_4 /s. In 2017, methane emission rates of the nearby landfills Mannheim and Heilbronn are reported with 4.72 g CH_4 /s and 3.32 g CH_4 /s respectively (E-PRTR inventory).

The decreasing emission rates after the measurements in 2015, is typically for a covered landfill. Emissions have increased over the last 3 years, most likely due to the newly built facility, the compost plant, which represents a possible new source of methane emissions.

The emission estimates shown in Figure 50 include the measurement period between two winters. It shows increased emissions in winter, compared to decreased emissions in summer, which would indicate seasonality of emission rate for this landfill. Several studies confirm this possibility. Research at landfill in Hamburg shows that environmental factors (soil temperature and moisture, ambient pressure) affect methane emissions

(Rachor et al., 2013). They influence the biological processes of methane oxidation or the physical processes of gas transport, resulting in higher emissions in winter and lower emissions in summer (Rachor et al., 2013). Lee et al (2018) has shown that oxidation efficiency increases with temperature. Similarly, Chanton et al. (2000) concluded that methane emissions are higher in cold months and lower in warm months.

Discussion

Methane from waste and wastewater treatment is the third largest source of emissions and accounts for up to 30% of total methane emissions in Germany. In this sector, landfills are responsible for 90% of methane emissions (UNFCCC). In the US in 2014, methane emissions from landfills accounted for 26% of total anthropogenic emissions (Saunois et al., 2020). On a European scale, they account for 15% of anthropogenic methane emissions (Saunois et al., 2020). The importance of estimating methane from this source and its reduction is even greater as the world's population continues to grow year on year, thus increasing the amount of generated waste, which often poses problems with disposal.

Since 2009, EU landfills have been required to control gas emissions and have been obligated to reduce emissions till 2016 to less than 65% of 1990 levels. This is being mitigated by separating at source and treating the separated biodegradable waste in composts, bio-digesters and paper recycling (Saunois et al., 2020).

In addition to basic waste segregation, covering the landfill area with a layer of bio-product or a geomembrane can reduce methane emissions (Chanton et al., 2000). As shown by Ars et al. (2017) and Defratyka (2021) methane emissions can be reduced by up to 25%. Compared to the methane concentrations on the soil cover of the landfill, where the bio-product has not been installed, the methane removal efficiency of the bio-vapor has increased from 35–43% in winter to 86–96% in summer (Lee et al., 2018). However, one must keep in mind the seasonal variation in methane emissions due to oxidation, which increases emissions in winter and decreases in summer. Environmental conditions such as soil moisture and air pressure and temperature affect methane emissions, which affect the biological process of methane oxidation or the physical gas transport process (Rachor et al., 2013; Lizik et al., 2013; Lucernoni et al., 2017; Zhan et al., 2020). However, weather conditions are not the only factor affecting emissions estimates and differences in emission pathways through the landfill cover should be taken into account (Rachor et al., 2013).

Next step to reduce methane emissions from landfills into the atmosphere was to start collecting it and use it as a renewable energy source, thereby mitigating climate change. Also, from an economic perspective, it will create additional revenue and jobs, EPA. Methane recovery from landfill in Germany has increased from 6% in 1980 to 22% in

2018 (UNFCCC).

It is crucial, as with all other sources, to regularly monitor the methane emission rates which, as mentioned, vary with the season and also with whether the repository is covered and whether it is active or not. From private communications with the Landfill, it is known that the Landfill has a network of measurement points where information of methane concentration from those point have been kept regularly since 2012 as one way to better control methane emissions from the landfill.

The estimated methane emissions for the landfill in Sinsheim are lower compared to others in the Rhein-Neckar region. However, it would be recommended to estimate emissions for other landfills to create a reliable database, knowing that inventories have a large uncertainty due to the size of landfills and possibility of multiple sources.

7 Romanian oil and gas wells

The results described in the chapter below refer to the measurements made mainly by UHEI, AGH (Cracow, Poland) and UU (Utrecht, the Netherlands) during the ROMEIO campaign. The data evaluation of the raw data measured during the campaign, were centrally evaluated within the framework of my doctoral thesis. The data collected and their analysis presented below is a paper draft under preparation on CH_4 emissions from oil and gas production in Romania, to be submitted to Environmental Science and Technology journal in July 2021.

Over the last decade, many studies on the quantification of the methane emission rates of oil and gas wells and facilities have been carried out in the US (Mitchell et al., 2015; Zavala-Araiza et al., 2015; Omara et al., 2018; Robertson et al., 2020). However in other regions there are only limited studies which quantified emission rates from oil and gas producing sectors. On a global scale CH_4 emissions from oil and gas extraction contributes to 22% of the anthropogenic emissions (Saunio et al., 2020).

According to the emission rates reported to the United Nations Framework Convention in Climate Change (UNFCCC), Romania, Germany and Italy are in the European Union the countries with the highest CH_4 emissions from the oil and gas sector. (UNFCCC). Romania alone contribute to 13% of the European CH_4 emissions from the oil and gas-producing sector. However, this information is subject to large uncertainty because the reported emission rates are calculated using standard emission factors, and independent measurements of methane emission rates from oil and gas production in Romania are lacking. In order to address this this questions the ROMEIO project (ROmanian Methane Emissions from Oil & gas) aims to quantify emission rates using atmospheric measurements. From 30th of September until 20th of October 2019 a three-week measurement campaign with up to 70 participants from 14 research institutes was carried out in Southern Romania. In this study we present the results of mobile in-situ measurements performed with five cars equipped methane analysers from Heidelberg University, AGH Krakow and Utrecht University in cooperation with INCAS (Bucharest, Romania) and UBB (Cluj-Napoka; Romania) Two of the cars were only used for “screening”, i.e. to locate possible methane emitters and to identify appropriate locations for further quantifications according to the requirements for the Other Test Method 33A (OTM-33A) and Gaussian Plume Method (GPM). The observation datasets were processed centrally at University Heidelberg to apply a Gaussian Plume Model or the OTM-33A method (Other Test Method 33A, EPA) to calculate methane emission rates for individual oil and gas wells and facilities. The screening data is used to develop an estimation of the number of CH_4 emission rates below the detection limit and integrate this information in this study.

7.1 Methodology

7.1.1 CH_4 calibration scale

The UHEI group was responsible for data analysis of measurements performed during campaign (GPM and OTM-33A). At the beginning of the campaign all research groups were together at the INCAS headquarters to discuss the measurement strategy and compare the instrumentation. First all instruments were tested and installed in five cars. The different methane analysers were calibrated at the beginning of the ROMEO campaign with gas mixtures from 10 different high-pressure cylinders spanning a methane concentration range between 2 and 130 ppm (Appendix). The high CH_4 mole fractions of most of these cylinders fall outside of available calibration scales. Therefore, the scale of the calibration gases was checked at University of Groningen by dilution experiments and a common scale was established for the ROMEO campaign. Based on the reported data for the calibration tanks, the data from all instruments were harmonized to this scale, using instrument-specific calibration functions provided by University of Groningen. During the campaign, the analysers were calibrated regularly using 1-2 high pressure cylinders, to detect possible instrument drift.

7.1.2 Instrumentation and measurement vehicles

The UHEI research group in cooperation with UBB and INCAS equipped two cars with in-situ methane analysers. The equipment of one car (UHEI_1) is described in detail in the following, the differences of the other vehicles are shown in Table 24. UHEI_1 was equipped with Licor Li-7810 and it was mainly used for quantification using the OTM-33A or Gaussian plume modelling approach. The air inlet line was mounted at the roof rack 2.5 m above ground. Air was flushed through the inlet line and the analyser with a flow rate of 250 ml/min, causing a delay time of typically 8 s. This delay time was measured each day before the start of the measurements and corrected during data evaluation to synchronize the clocks of methane analyser, GPS and weather station. Meteorological data were collected with two anemometers: a 2D weather station (Gill MaxiMet GMX500) and a 3D sonic anemometer (USA-1, Metek). The 2D weather station was mounted on the roof rack, and recorded temperature, humidity, pressure, wind speed and wind direction and GPS coordinates during driving. When performing transects for Gaussian plume modelling or stationary measurements downwind of the plume, the 3D sonic anemometer was installed close by. Geographic coordinates of the car were recorded by a 2D weather station in addition to the GPS logger application (www.basicairdata.eu) installed on a smart phone. It was used to determine the exact position of the analysers during stationary measurements. In some cases, the downwind methane plume was not

accessible by car, then the lightweight CH_4 analyser was installed outside the car next to the 3D sonic anemometer. The second car (UHEI_2) was equipped with a Cavity Ring Down Spectrometer (CRDS, Model G1301, Picarro Inc). As we had no additional weather station, and the frequency of the analyser was only 0.2 Hz this mobile devices was only deployed for screening possible emitters. The other three cars were equipped by UU and AGH using the same measurement methods and setups but with different instruments. Table 24 summarizes the information on used instruments of the 5 equipped cars used during the campaign.

Table 24: Specification of in-situ analysers used for quantifications and screening including methane and meteorology measurements.

Methane analyser						
	UHEI_1	AGH_1	IMAU	UHEI_2	AGH_2	IMAU
Instrument	LI-7810	LGR M-GGA-918	Picarro G4302;	Picarro G1301	Picarro G2201-i	Picarro G2401
Measured species	CH ₄ , CO ₂ , H ₂ O	CH ₄ , CO ₂ , H ₂ O	CH ₄ , C ₂ H ₆ , H ₂ O;	CH ₄ , CO ₂	CH ₄ , CO ₂ , H ₂ O	CH ₄ , C ₂ H ₆ , H ₂ O, CO
Measurement interval [s]	1	1	1 <5	<5	<4	<5
Precision (1sec, CH ₄)	<1 ppb	4ppb	30 ppb;		5 ppb (30 sec average)	<1ppb
Meteorology instrument						
3D Windsensor	METEK Ultrasonic anemometer USA-1	3-axis ultrasonic anemometer 'Young, Model 81000V'	Campbell CSAT3 3-D Sonic Anemometer	Campbell Scientific	TriSonica™ Mini Wind and Weather Sensor	-
2D Windsensor	Gill MaxiMet GMX500	-	Gill MaxiMet GMX200	-	-	-

7.2 Site selection

Every day before and after the measurements, a meeting of all teams took place to discuss the planned measurements. This was done in order to allocate each research team appropriately, so as not to duplicate the position and quantify, or at least check the largest possible number of sites. Each day had to be carefully planned also in terms of the prevailing weather conditions, because the key factor was the speed and direction of the wind. Thus, visiting individual clusters depended on the expected weather conditions predicted by weather forecasts and a group of modellers cooperating with the ROMEO team.

In order to know what method of target quantification (GPM or OTM) should be used in a given place, it was first necessary to apply emission screening. This method allowed to quantify how much methane was produced from a given borehole, and above all, whether there was any gas leakage that could be measured. This method consisted in driving around a given source (if possible) and determining which quantification method (GPM, OTM-33A or drones) is the most appropriate. This significantly simplified the entire measurement process, as the emission screening cars provided for further information the places corresponding to the given method. Then the team closest to one quantification could proceed to the next quantification. If a given source did not show methane emissions, i.e. places where the concentration was at the background level, they were defined as non-detects and recorded with accurate comments in the database of all available sites, where emission screening data such as measured concentration, wind direction, road accessibility and most suitable method were recorded. A CH_4 calibration gas was analysed every morning and evening in order to correct for instrument drifts. All clocks were also synchronized in the measuring instruments used, i.e. in instruments for measuring gas concentrations, 2D and 3D weather stations and a GPS position recorder. Additionally, every evening the data from the measuring instruments were copied to avoid unexpected circumstances such as damage of the equipment.



(a) Pumping crane for pumping oil. Here an example of big one, around 10m height.



(b) Gas installation. Usually a kind of tubes connections in the cross sign

Figure 51: Different installations visited during mobile measurements (source: Own gallery). Normal view when driving a car in Romania, in the regions visited by the ROMEIO team.

During the ROMEO campaign, OTM-33A and Gaussian plume methods were applied 140 times (118 times OTM-33A and 22 times GPM) on 112 different locations. Due to missing meteorological data, two measurements had to be rejected from further analysis. Figure 53 shows the distribution of the surveyed sites in each region. In region 5A we determined the methane emission rates of 40 oil and gas wells, representing 35% of quantified wells in our study. This disproportionate preference for Region 5A can be explained by the flat topography, easy access and favourable wind conditions with stable wind speed and wind direction, compared to measurement days in other regions. Figure 52 shows a comparison of two regions, 5a and 6. The first one is flat and the possible sources are more accessible compared to those in region 6, where the terrain is hilly and forested.

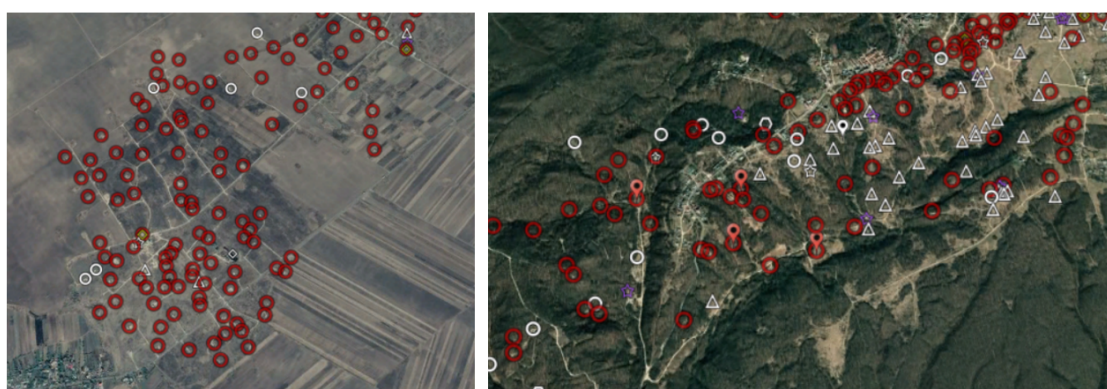


Figure 52: Comparison of two visited regions, 5a (left) and 6 (right).

Wind conditions were the largest limiting factor to meet conditions for application of the GPM or OTM-33A method. Based on meteorological forecasts, the daily average wind speed for each day between 7:00 a.m. and 7:00 p.m. at a height of 2m, did not exceed 2 m/s for half of the duration of the ROMEO campaign. If we distinguish between different types of production infrastructure, Figure 53 (right panel) shows that 75% of the measurements were carry out close to oil wells and facilities and only 15% on gas wells, reflecting the dominance of oil production infrastructure in the target region. Most of the studied wells are active and still pumping or collecting oil and gas (Figure 53, left panel). In order to measure as many different sites as possible, we normally visited each site only once during the campaign. 7 sites were measured several times either with different instruments/cars, on different days or at different times during one day.

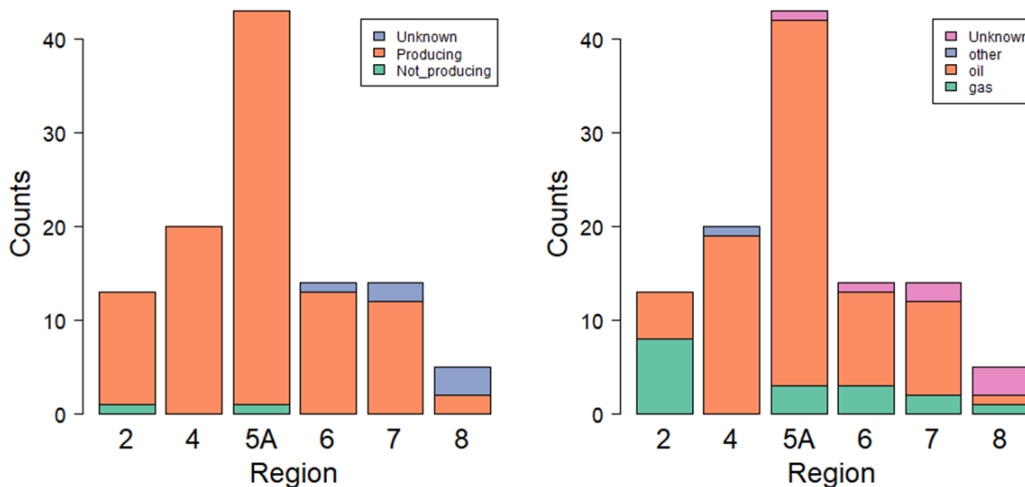


Figure 53: Distribution of visited sites based on information given by OMV: differentiates according to the given production status (left panel) and to gas or oil (right panel).

7.3 GPM results

The GPM was applied when the OTM-33A could not be applied or when topography allowed to drive transects instead of installing the instruments on the field. In most cases GPM was not applied for bigger facilities with several possible emitting points. On Oct 1st, we performed a comparison measurement with the cars UHEI_1, AGH_1 and UU driving transect measurements for GPM at an oil facility. The three cars drove 10-12 transects along the road crossing the CH_4 emission plume. All analysed plumes show methane enhancement between 0.4 – 4.9 ppm above the background. The emission rates estimated for this oil gathering facility from measurements made by UHEI_1, AGH_1 and UU are 0.16 ± 0.03 g CH_4 /s, 0.18 ± 0.02 g CH_4 /s and 0.19 ± 0.02 g CH_4 /s, respectively (numbers are means of individual transects \pm standard error of mean). The good agreement shows that CH_4 emission rates derived from measurement of the different cars during the ROMEO campaign compare well.

A total of 22 GPM applications were carried out at 20 sites in all regions. Measurements from two sites were rejected during data processing as they did not fulfil the quality criteria. The number of transects driven ranges between 3 and 22 per site. The plume crossings were performed at a distance between 11 to 160 m and the maximal observed methane enhancement after subtracting the background was between 2 to 1074 ppm. Figure 54 shows the calculated methane emission rates for the 20 sites for oil wells (green), gas wells (orange) and other facilities (blue). The shaded area marks the results for the

comparison at the oil park, described above. The determined CH_4 emission rates vary between $0.08 \pm 0.04 \text{ gCH}_4/\text{s}$ and $25.8 \pm 8.5 \text{ gCH}_4/\text{s}$ for the individual sites.

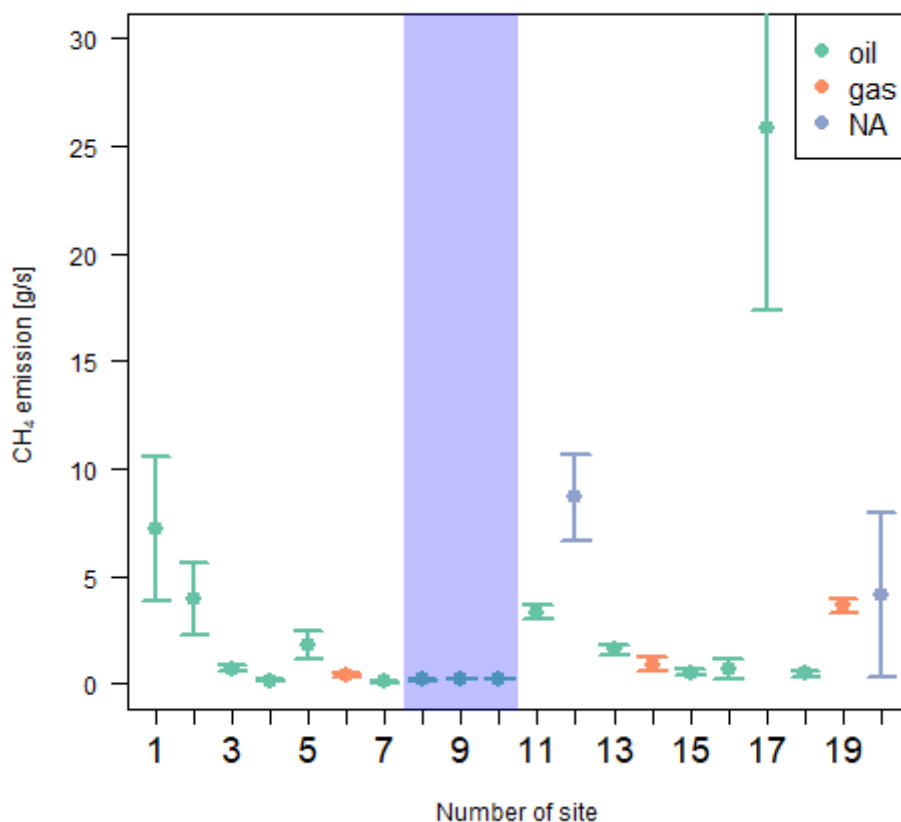


Figure 54: Calculated CH_4 emission rates for 20 sites using a Gaussian Plume Model. Green dots show emission rates for oil well, orange for gas well and blue are for unknown type of the source. The shaded area marks a comparison measurements with parallel measurements by 3 teams (ROM4080).

7.4 OTM-33A results

Other Test Method 33A was applied for 97 sites. 65% (77 quantifications) of all OTM-33A (118 cases) measurements fulfil the Data Quality Indicators (DQIs), which is comparable to the studies of Brantley et al. (2014) and Robertson et al. (2017), where around 70% of the field measurements were accepted. Similar to the GPM evaluation, most OTM-33A measurements were applied for oil wells or facilities (Figure 55). Measurements for OTM-33A were performed in distances between 15 to 190 m from emitters, with an average distance of 35 m. Measured CH_4 concentration reached up to 1600 ppm above background, but for most sites, we measured between 2 and 200 ppm CH_4 . The calculated

range of CH_4 emission rates derived with OTM-33A is comparable the range derived from GPM results with values between $0.03 \pm 0.01 \text{ gCH}_4/\text{s}$ and $20.2 \pm 10.1 \text{ gCH}_4/\text{s}$

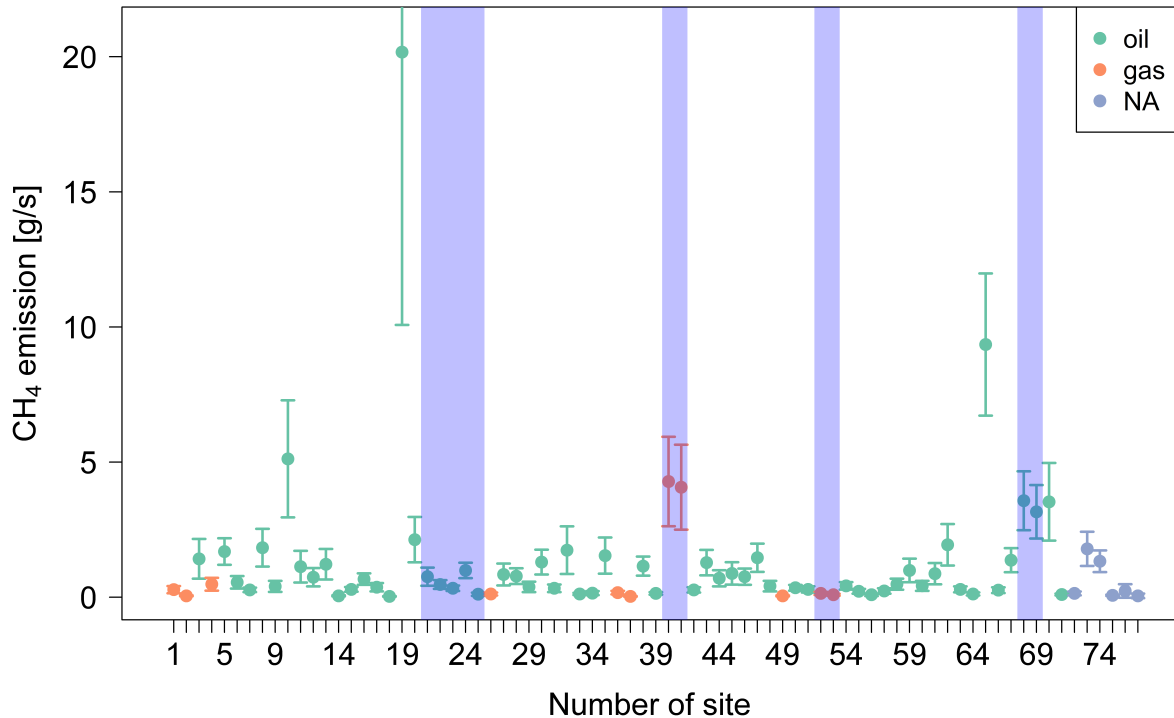


Figure 55: Calculated emission rates by Other Test Method 33A. Green, orange and blue dots represent CH_4 emission rates for oil, gas and unknown type of the source site respectively. The shaded areas mark sites with several application of OTM-33A.

7.5 Revisited sites

During the campaign, several sites were measured by several cars or visited several times and are marked by shaded area in Figure 55. The first field comparison of OTM-33A was performed on ROM2090 by the cars UHEI_1 and AGH_1. Both methane analysers were installed in the field in a distance of 46 and 43 m from the gas well, respectively. The measured CH_4 enhancements were similar, resulting in a very good agreement of the CH_4 emission rates with $0.17 \pm 0.07 \text{ gCH}_4/\text{s}$ for each instrument. The ROM2563 (gas well) was an ideal site, where we have compared OTM-33A and GPM three times during the measurement campaign. On November 3, 2019 UHEI_1 and AGH_1 measured simultaneously using the OTM-33A method and estimated CH_4 emission rates of $4.28 \pm 1.66 \text{ gCH}_4/\text{s}$ and $4.07 \pm 1.57 \text{ gCH}_4/\text{s}$, respectively. The second measurement on November 9 did not fulfil the quality criteria but show already during measurements much smaller CH_4 enhancements. The use of the GPM method at the end of the measurement campaign

estimated the emission rates of $0.41 \pm 0.07 \text{ gCH}_4/\text{s}$ which is a factor 10 lower than the first approach. This decrease in CH_4 emission rate can be explained by the intervention of a service team from the operator, which repaired the leak after we reported the large CH_4 emission rates. It should be mentioned here that the determined emission rates are only a snapshot during our measurement campaign, which does not mean that a particular oil well has a constant methane leakage. Repeated OTM-33A measurements have been applied 6 times on an other oil well in the region 6 during 3 days of measurements. Five measurements out of six fulfil the DQIs. The determined CH_4 emission rates for this studied oil well range between 0.11 ± 0.06 and $0.99 \pm 0.29 \text{ gCH}_4/\text{s}$.

7.6 Emission rates below the detection limit

The screening data were used for estimating emission rates that are below the detection limit of the OTM-33A method. Sites where the screening cars were clearly downwind, but where no methane enhancements were detected or the enhancement was below 200 ppb CH_4 and therefore below the limit for OTM-33A were marked as BG (background) or with the measured concentration up to 2.2 ppm CH_4 , respectively. All screening measurements were performed within 8-30 m of the source, the distances noted in the list, were only roughly estimated, but can be later measured using the GPS coordinates. Brantley et al. (2014) determined the lower detection limit of the OTM-33A method as $0.01 \text{ g CH}_4 / \text{s}$ which corresponds to a downwind average in-plume mole fractions greater than 0.1 ppm CH_4 . In this study the lowest emission rate determined was $0.03 \text{ gCH}_4/\text{s}$.

Similar to the study of Robertson et al. (2020), we also calculated the number of oil and gas wells that are below the detection limit in order to include them in the representative mean values for the regions. However, we used the much larger database of screening data. We have chosen the screening data measured by UHEI_1 and UHEI_2, as the documentation on files was the most complete. In total 532 screening of wells were performed by the two cars equipped with instrumentation of Heidelberg University. 42 of these measurements could only be carried out upwind the well or had other implausible entries in the comment column and were therefore not used for further evaluations. In addition, we excluded the 28 sites which were classified as "disposal_injection" as we have not quantified any of this site types. Of the 462 remaining screening data, 98 were flagged as "BG" (background, indicating now discernible CH_4 elevation), and 61 had a low mole fraction excess of 0.050-0.29 ppm. These 159 screening data that are below our detection limit for the OTM-33A method correspond to a proportion of 35%. This percentage of emission rates below the detection limit is comparable to the result of Robertson et al. (2020), who found a share of 38% in a study of CH_4 emissions of oil and gas wells in New Mexico. We have tested different scenarios with subsets of our data, such as screenings

performed by the UHEI_1 or UHEI_2 car, but the result varies only minimally between 34% and 36%. However, the number of sites below detection limit varies significantly between the regions and also between oil and gas wells. The proportion of measurements below the detection limit is 35% for oil wells and 22% for gas wells. This result was surprising, as we would have expected a lower number of CH_4 leakages related to gas wells, and thus the proportion of measurements under detection limit should be higher. The differences in the regions reflects partly the share of the oil and gas wells in the regions investigated. Since we screened a much lower number of gas wells (6% of all screenings), it is unclear whether this distinction is robust. Therefore, we applied a mean factor of non-detects of 35% for all regions and all types of wells and facilities. To estimate emission rates from these non-detect sites, values between 0 gCH_4/s and our lowest determined value of 0.03 gCH_4/s were randomly assigned with equal probability similar to Robertson et al. (2020).

7.7 Comparison of estimated methane emission rates for regions and type of visited sites

As already shown in the studies of Brantley et al. (2014) and Robertson et al. (2017) the CH_4 emission rate distributions from oil and gas wells can be described best by a log-normal distribution. In Figure 56 and Figure 57 we show the determined CH_4 emission rates separately for each region as well as status of production. Using a non-parametric bootstrap method (with resampling $R=10000$), the mean and the 95% confidence interval for the logarithmic data were calculated and then calculated on the primary scale. The use of bootstrapping was chosen to take into account that the estimated emission rates may not represent for a given region, status or type of a given well. All data are summarized in the Table 25. The mean methane emission rates with 95% confidence intervals (CIs) are shown with red points and red error bars in Figure 56.

Table 25: Mean methane emission rates per site with 95% confidence intervals (CIs) for the different regions.

Region	Mean methane emission rate [gCH_4/s]	95% confidence intervals [gCH_4/s]
2	0.09	0.04 ; 0.20
4	0.17	0.07 ; 0.40
5	0.19	0.10 ; 0.35
6	0.11	0.04 ; 0.27
7	0.1	0.03 ; 0.32
8	0.15	0.03 ; 0.83

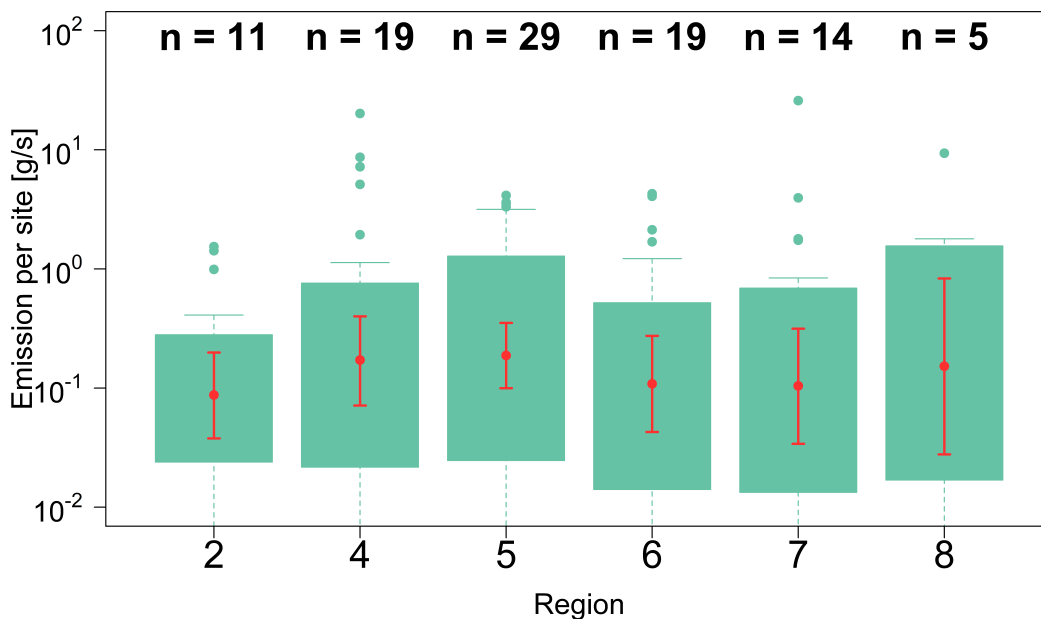


Figure 56: Comparison of derived methane emission rates by region. Boxes represents the first and third quartile of the data, while whiskers extend to the largest value that is within 1.5 times the interquartile range (IQR). Means and 95% CIs are shown in red and were calculated using a non-parametric bootstrap. Data are presented on a logarithmic y-axis. The number of accepted quantifications per region are written in the top line. This graph include already the non-detect as described in chapter Emission rates below the detection limit

The lowest CH_4 emission rates with $0.09 \text{ gCH}_4/\text{s}$ were found in region 2, whereas the CH_4 emission rates range between 0.10 and $0.19 \text{ gCH}_4/\text{s}$ for the other visited regions. However, the number of sites measured per region varies significantly between 5 and 29, and thus the confidence intervals values also have a wider range for region 8. Regions 2 and 8 have a larger share of gas wells with 40% and 56% compared to other regions with only up to 10% of gas wells. The lower CH_4 emission rates in Region 2 are in line with expectations for gas wells, as methane is the produced product and not an associated gas as for the oil extraction.

Figure 57 presents distribution of methane emission rates separated by production status (top panel) and the gas or oil type (lower panel) of the emitter. It is visible that the highest emission rates are found at wells which are still producing compared to the not producing ones. However the number of not producing wells is very small. When comparing the well type (figure 8 bottom panel), higher average emission rates are indicated by the oil sources, however again a larger number of quantifications have been made for the oil sources. The average emission rates per site are estimated to be 0.10 ($0.05, 0.23$)

gCH_4/s and 0.15 (0.09, 0.23) gCH_4/s for gas and oil related facilities, respectively.

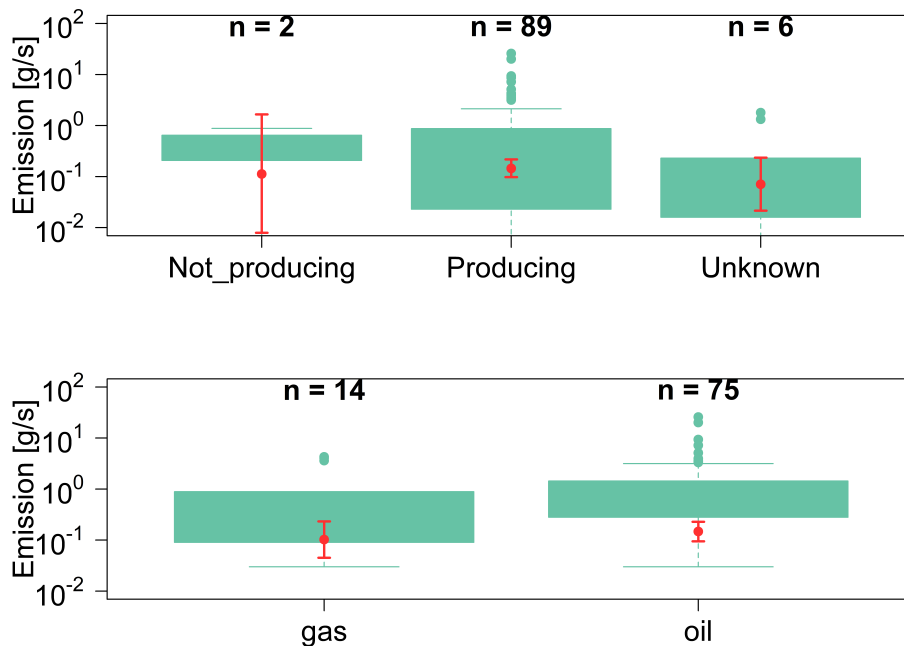


Figure 57: Estimated emission rates distributed by status (on the top) and type (on the bottom) of the quantified site. Means and 95% CIs are shown in red and were calculated using a non-parametric bootstrap. Note the logarithmic y-axis. The number of accepted quantifications per region are written in the top line. This graph include already the non-detect as described in chapter Emission rates below the detection limit.

7.8 Comparison to other studies

Emissions from the oil and gas industry have also been the subject of many studies in recent years - Robertson et al. (2017), Robertson et al. (2020), Brantley et al. (2014), Mitchell et al. (2015), Omara et al. (2018), Atherton et al. (2017), Zavala-Araiza et al. (2015).

In a study published by Robertson et al. (2017), methane emissions from four major U.S. basins were examined : Upper Green River (UPR), Denver-Julesburg (DJ), Uintah, and Fayetteville (FV). Measurements were made using the OTM-33A method and up scaled emissions for pads are presented. Estimated methane emission ranges of 95% confidence intervals per site are in the range of 0.38 to 3.1 kg/h (0.11 - 0.86 g/s) for UPR, DJ and FV. For Uintah it is 0.8 to 9.1 kg/h (0.22 - 2.52 g/s). A study by Brantley et al. (2014) found these values to be 0.11 to 0.74 g/s for samples from the Barnett, DJ and Pinedale basins respectively. A recent study from Permian Basin (U.S.) published by Robertson et al (2020) shows emission rates (95% CI) of 0.70 - 7.61 kg/h (0.19 - 2.11 g/s).

The values above are comparable to the methane emission rates obtained during the ROMEEO campaign. However, it should be taken into account that each of the basins in the United States is very large, even the size of Romania. Furthermore, the number of visited sites represents only 30% of the total sites reported by OMV Petrom. The share of sites for which emissions have been estimated is even smaller, but gives a first impression of methane emissions from the oil and gas industry in Romania. It should also be noted that ROMEEO campaign was focused on the southern part of the country, while oil and gas deposits also exist in the north, which has not been well explored so far. It would therefore be advisable to revisit the places where the estimated emissions exceeded the average emissions and to extend the measurements to other places in the southern regions, not forgetting to quantify the emissions from the north of the country.

8 Isotopic results

8.1 Heidelberg sources

In addition to the emission estimates for local sources, another part of this work was to continue the measurements of the isotopic composition from these sources initiated in previous years. For this purpose, mobile measurements were carried out using the CRDS analyser, the AirCore method, and also, when possible, samples were collected in bags and then analysed in the laboratory. The collected samples formed part of the isotopic database created from all isotopic measurements in the *MEMO*² project.

Measurements of isotopic composition ($\delta^{13}CH_4$) consisted of conducting mobile measurements and measuring the concentration of methane in the plume from the suspected source. When the measured CH_4 concentration exceeded 500 ppb above background, an AirCore was used to remeasure the just measured peak (3.3). In order to avoid additional vibrations during the measurement, the "Repeat mode" required the vehicle to stop in a safe place. Such a measurement typically lasted 10-20 minutes.

Table 26 shows the range in $\delta^{13}CH_4$ and the number of AirCore that were made. These values include the 5 main sources presented in this thesis and results for additional sites namely: the city of Heidelberg, the Waste Water Treatment Plant (WWTP) in Wieblingen, the Gas Compressor Station (GCS) in Scheidt and the Ruhr area. The value ranges shown below include all AirCore samples. Average daily values (values for an individual measurement campaign) are presented in Figure 58.

Table 26: $\delta^{13}CH_4$ value ranges obtained for main local methane sources and additional visited sources based on mobile measurements using AirCore.

Source	Min $\delta^{13}CH_4$ [‰]	Max $\delta^{13}CH_4$ [‰]	Nr of AirCores
Farm in Weinheim	-66.85	-45.31	75
Farm in Ladenburg	-72.06	-41.34	19
Biogas plant in Pfaffengrund	-72.24	-46.7	53
GCS in Gernsheim	-53.11	-33.07	21
Landfill in Sinsheim	-67.46	-43.46	27
Heidelberg City	-52.44	-40.62	5
WWTP in Wieblingen	-53.76	-49.98	5
GCS in Scheidt	-41.61	-40.74	3
Ruhr area - coal	-55.83	-24.64	13
Ruhr area - gas	-47.03	-36.6	4

The number of AirCore measurements depended on the concentration measured during the mobile measurements. The highest number of measurements was carried out at the Weinheim farm and at the Biogas plant in Pfaffengrund, where always peaks with a

concentration enhancement of 10 ppm were recorded. The small number of AirCore for additional sources correspond to campaigns, with single or limited measurement days. As shown in Figure 58, the collected samples include both methane of biogenic and thermogenic origin. This is consistent with expectations that sources such as farms and biogas plants will exhibit biogenic methane, while $\delta^{13}CH_4$ values for gas compressor stations and mines will converge in the range of thermogenic methane values.

For each campaign, the average $\delta^{13}CH_4$ value was calculated and the range of all average values is shown in Figure 58. In the case of the GCS in Scheidt, the GCS in Ruhr area and the WWTP in Wieblingen, there is one average value because there were single measurement campaign. Here, the range of $\delta^{13}CH_4$ shown for them is the variability of several measurements on one day. The shown $\delta^{13}CH_4$ ranges are ranked from biogenic to thermogenic, such that the farms, biogas plant, and landfill are in the left bottom, while the mines and GCSs are in the upper right. As shown in Figure 58, the $\delta^{13}CH_4$ values obtained from AirCore samples from the urban measurements are in the range of the values obtained for the GCS, indicating that the peaks observed during the urban campaigns come from subtle leaks from the urban natural gas network. The locations where the peaks were observed were reported to the city council, and repeat visits to the indicated locations did not show any peaks.

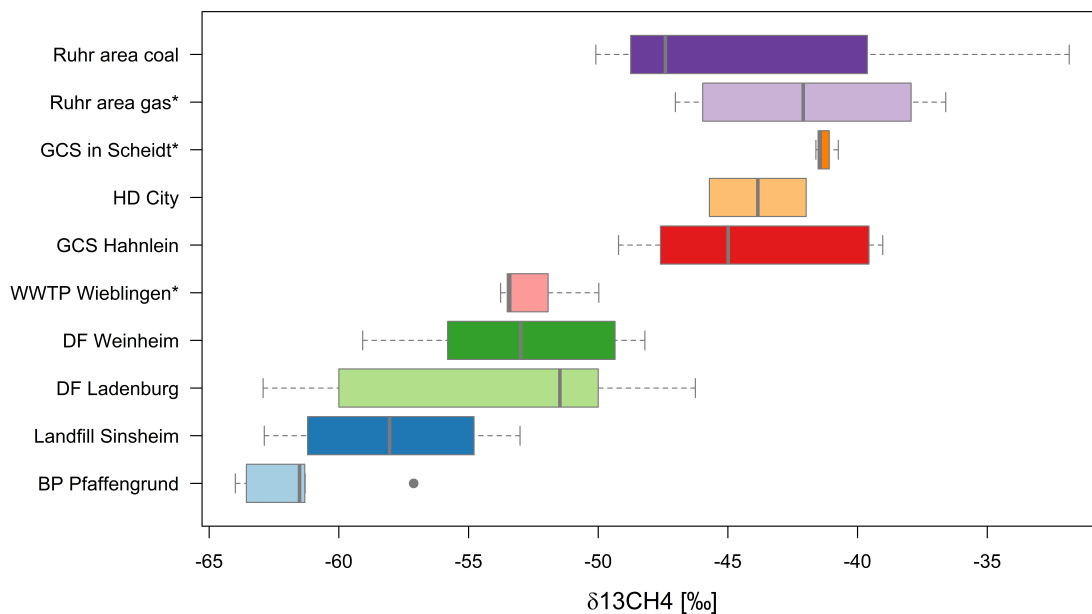


Figure 58: Isotope composition of CH_4 for 5 main Heidelberg sources and additionally visited sites obtained during this study.

Figure 59 to Figure 61 show the results of isotopic measurements for all five main

sources described in this study obtained for each measurement separately. The average time-series data were compared with data published by Hoheisel et al. (2019). The vertical black line in 2018 indicate data measured in the study of Hoheisel et al. (2019) bevor 2018 and data measured in the frame of this thesis, after 2018.

8.1.1 Isotopic analysis for farms in Weinheim and Ladenburg

Figure 59 shows the results of isotopic measurements for dairy farms with biogas plants in Weinheim and Ladenburg. The dark green color represents the measurements for the farm in Weinheim, while the light green color represents the measurements for the farm in Ladenburg. The isotopic methane source signature for the Weinheim farm is between -59 and -48 ‰ with an average measurement value in this work of -53.1 ± 4.1 ‰. For the Ladenburg farm it is slightly wider, between -62 and -46 ‰ with an average of -54.10 ± 7.0 ‰. The range of $\delta^{13}CH_4$ values is comparable for both farms (Table 26), and in comparison to previous measurements. Hoheisel et al. (2019) reported for Weinheim a $\delta^{13}CH_4$ range between -66 and -43.1 ‰ with averages of -64.9 ± 1.6 ‰ on the farm and -54.0 ± 8.0 ‰ for the plume including the biogas. For the Ladenburg farm it was a range between -64.0 and -40.3 ‰ with average values of -63.2 ± 1.4 ‰ and -44.4 ± 7.2 ‰ on the farm and for the biogas plume, respectively.

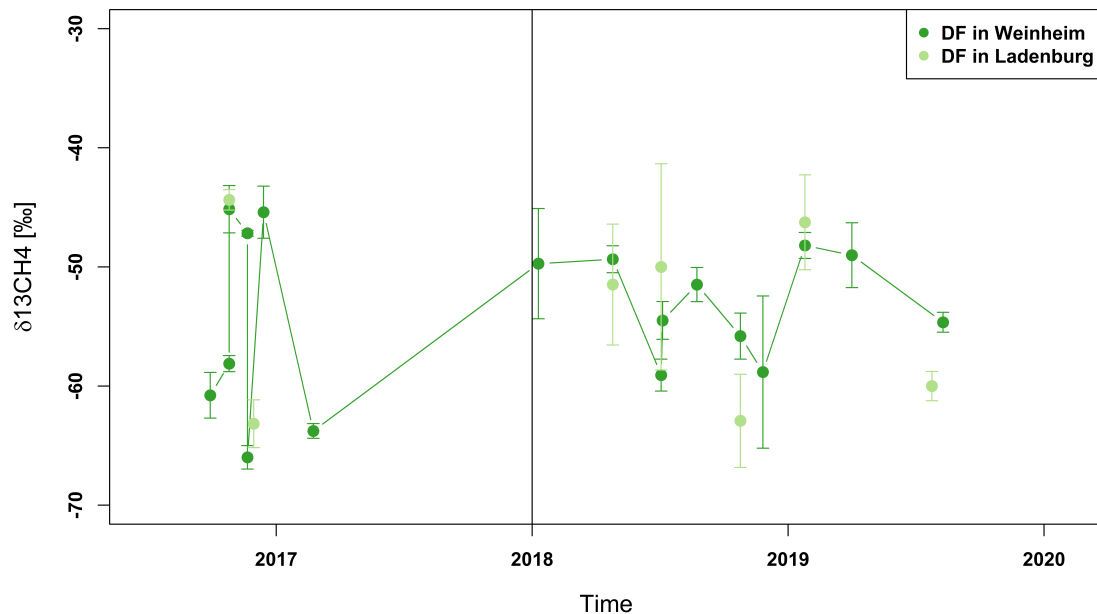


Figure 59: $\delta^{13}CH_4$ values for dairy farms in Weinheim and in Ladenburg together with previous collected data.

It has been observed that daily averages show seasonal variation (Hoheisel, 2017). During the winter months, the isotopic signature is more enriched compared to the summer months. As the measured plumes contain both sources it is difficult to uniquely determine the variation in isotopic signature. The correlation of isotopic signature with diet observed by Levin et al. (1993) states that a C3 diet has a depleted isotopic signature ($-65 \pm 1.7 \text{ ‰}$) compared to a C4 diet ($-55.6 \pm 1.4 \text{ ‰}$). Knowing that cows are fed the same diet all year round, seasonality due to diet can be excluded (Hoheisel et al., 2019). Probably this variation can be explained by the share of emissions from the biogas plant and from the cowshead. However, in order to test this assumption, it would be necessary to measure the AirCore plume from the mobile measurements each time, and to collect samples separately from the biogas plant and the cowshead for analysis in the laboratory, which would confirm the assumption or provide new information.

8.1.2 Isotopic analysis for biogas plant in Pfaffengrund and landfill in Sinsheim

The sources with the most biogenic isotopic signature that are described in this work (landfill, biogas plant) are presented in Figure 60. The light blue points indicate the daily average isotopic source signature values with uncertainties for the biogas plant at Pfaffengrund, while the dark blue points indicate the $\delta^{13}CH_4$ values for the landfill at Sinsheim. The biogas plant at Pfaffengrund shows the most constant isotopic source signature value over the year. The $\delta^{13}CH_4$ values obtained in this work are between -64 and 57 ‰. The average $\delta^{13}CH_4$ value from all measurements is $-61.8 \pm 2.4 \text{ ‰}$. The study by Hoheisel et al. (2019) showed a range of $\delta^{13}CH_4$ values between -67.4 and -59.0 ‰. The average isotopic signature for the measurements in this work was $-62.4 \pm 1.2 \text{ ‰}$. As can be seen, no seasonal variation is observable in either this work or previous studies. Furthermore, the values obtained in this work confirm previous findings described by Hoheisel et al. (2019). The results of the analysis of samples taken from two separate fermenter tanks showed values of $-61.5 \pm 0.1 \text{ ‰}$ and $-64.1 \pm 0.3 \text{ ‰}$, respectively. The former is fed with a substrate mainly consisting of maize silage, while the second is mainly of food waste. It was therefore expected to obtain an isotopic signature value from the plume measurements that would be between the two values, which has also been obtained in recent measurements.

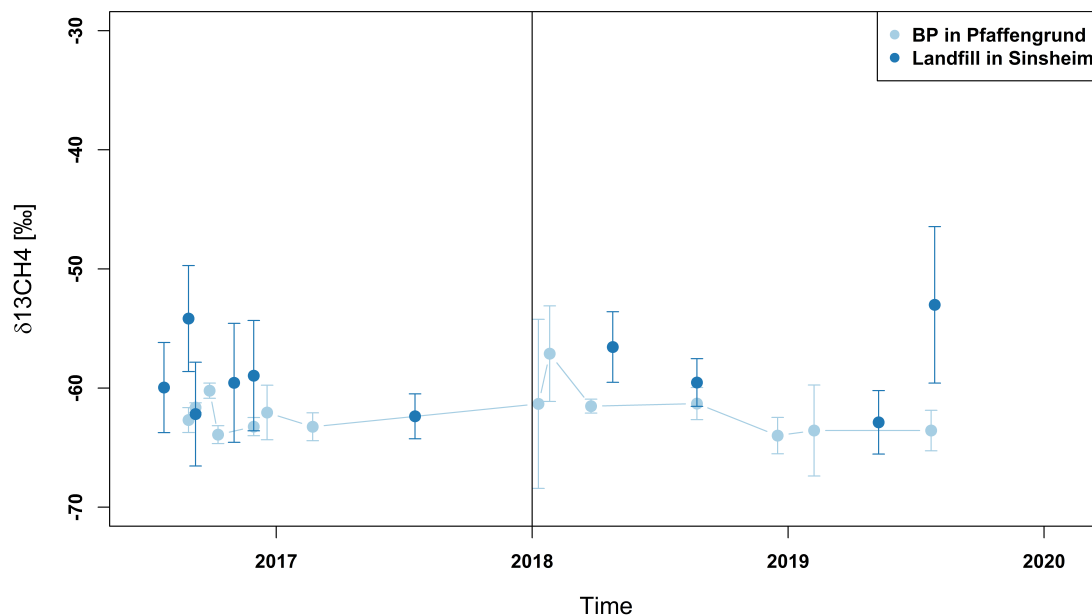


Figure 60: $\delta^{13}CH_4$ values for Biogas Plant in Pfaffengrund and for landfill in Sinsheim together with previous collected data.

At the landfill in Sinsheim a total of 27 AirCore samples were analysed which showed a range of isotopic source signature values between -62.9 and -53.0 ‰, with a mean value of -58.0 ± 4.2 ‰. The values above were obtained by measuring AirCore samples taken at the landfill area. The plumes measured outside the landfill did not have a sufficiently high concentration.

Previous studies of samples collected on the landfill showed an average isotopic signature of -59.5 ± 0.5 ‰ and -66.5 ± 2.5 ‰ for the two measurement campaigns (Hoheisel et al., 2019). Analysis of the isotopic signature from the plume resulted in a $\delta^{13}CH_4$ between -62.2 and -54.2 ‰ with an average value of -58.7 ± 3.3 ‰. These are values that characterize biogenic sources of methane (Zazzeri et al., 2015). Similar isotopic signature values have also been obtained in other studies on landfills in different countries. Xueref-Remy et al. (2020) reported isotopic signature values for 6 landfills in the IDF region (Paris) between -63.7 and -58.2 ‰ for CRDS measurements and between -65.9 and 53.0 ‰ for IRMS measurements. The values obtained by Defratyka (2021) also confirm the biogenic nature of methane from the landfills, giving values between -58.0 and -57.4 ‰ and between -63.3 and -60.0 ‰ for landfill D and E, respectively. Studies of several landfills in England showed an isotopic signature between -60.2 and -55.2 ‰, with an average value of -58.0 ± 3.0 ‰ (Zazzeri et al., 2015).

In estimating methane emission ratios from the landfill in Sinsheim, some seasonality

related to oxidation was noted. However, a similar relationship does not occur in the isotopic signature, as already reported by Hoheisel et al. (2019). A similar lack of seasonality was observed by Bakkaloglu (2021), where landfills in England were studied.

8.1.3 Isotopic analysis for gas sources

The GCS in Gernsheim is the connecting point for two large pipelines that carry natural gas from Russia and the North Sea respectively. Each of them is characterized by a different isotopic source signature in CH_4 . The gas from the North Sea is more enriched and has an isotopic signature value of -30‰ , while the gas from Russia is more depleted with a $\delta^{13}CH_4$ value of -50‰ (Levin et al., 1999). Therefore, we expected contributions from both gas pipeline in Gernsheim.

Figure 61 shows the isotopic signature values for the Gas Compressor Station (GCS) in Gernsheim relative to the time when the measurements were conducted. The results with uncertainties are shown in red. Additionally, the orange dots represent isotopic source signature values for natural gas samples that are collected regularly at the university and measured in the laboratory using a CRDS analyzer. As before, the presented values are daily averages calculated from AirCore samples collected during mobile measurements. All measurements carried out on the GCS in Gernsheim, show an average daily isotopic signatures between -50 and -40‰ . From 1960 to 2015, the Bundesamt für Wirtschaft und Ausfuhrkontrolle reported how much natural gas was imported into Germany by supplier, from Russia, the Netherlands and Norway. In 2015, each supplier accounted for 30% of the natural gas supply, and this percentage distribution remained constant throughout the year. This is different from the situation in the 1990s, when in the winter months less Russian gas (30%) and in the summer months more Russian gas (50%) was imported. This was observed in the isotopic signature, which was characterized by enriched $\delta^{13}CH_4$ values in winter (gas from the North Sea), and depleted in summer (gas from Russia) (Levin et al., 1999). Since currently the share of each supplier is similar, the isotopic signature is a mixture of both North Sea and Russian gas, as observed by Hoheisel et al. (2019), and confirmed in this study. Thus, the isotopic source signature values from the urban natural gas network do not show seasonal variation and the isotopic signature is between -47.4 and -39.5‰ , with an average $\delta^{13}CH_4$ value of $-43.2 \pm 0.3\text{‰}$. However, when looking at $\delta^{13}CH_4$ values from sites north of Heidelberg, slightly enriched values of the isotopic signature can be seen. Such sites are e.g. Scheidt (50.346450, 7.905812) and Lippe (Ruhr area, 52.058921, 8.699047), for which the measured values of the isotopic signature are $-41.3 \pm 0.5\text{‰}$ and $-42.0 \pm 3.1\text{‰}$, respectively.

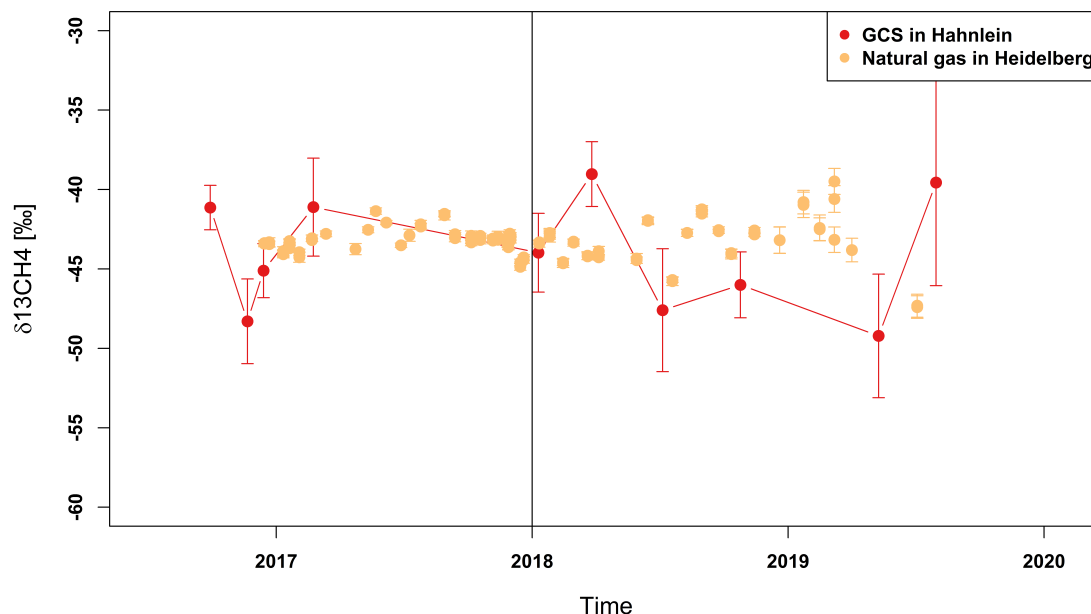


Figure 61: $\delta^{13}CH_4$ values for GCS in Gernsheim and natural gas network in Heidelberg together with previous collected data.

The isotopic signature for GCSs in the IDF region (Paris) is comparable to samples measured GCS in Gernsheim with values between -44.2 and 43.0 ‰, -44.1 and -40.1 ‰, and -49.6 and -40.8 ‰ for GCS A, B, and C, respectively (Defratyka, 2021). A similar gas mixture is transported through the MEGAL network via Germany to France. The values above were obtained by analyzing AirCore samples using a CRDS analyzer. They were also tested by IRMS (Isotope Ratio Mass Spectrometry) analyser in London and Utrecht. A study of the isotopic source signature of a urban natural gas network in Paris showed that they are slightly enriched (about 2 ‰) compared to the average isotopic signature of the network in Heidelberg and give a $\delta^{13}CH_4$ value between -41.8 and 39.1 ‰ (Xueref-Remy et al., 2020).

A study of the isotopic characterization of anthropogenic methane sources conducted in England by Zazzeri et al. (2015), shows that the isotopic signature of natural gas is more enriched and takes values of -36, which characterize the isotopic signature of southeast England. Even more enriched values were obtained for samples from the Netherlands, where the $\delta^{13}CH_4$ was -29.5 ± 0.1 ‰. As mentioned earlier, these values are characteristic of North Sea natural gas.

The isotopic signature studies allow to determine the origin of methane, in this case whether it is from Russia or the North Sea. The GCS in Gernsheim is an interconnection point for two large European natural gas pipelines, so it is difficult to determine its origin

at the moment because it is a mixture of both gases, especially since the current share of natural gas coming from Russia and the North Sea is similar. The measurement of the isotopic composition can help at the GCS to identify, whether the leakages belong more to the pipeline system coming from the East, or from the North.

8.2 Polish coal mines

The CoMet campaign took place in Silesia from May 20 to June 10, 2018. The main task was to conduct mobile measurements using CRDS analyzer and collect samples for isotopic composition analysis. In addition to mobile measurements for Gaussian plume modelling, the UHEI team provided support to the aircraft measurements, trying to follow the aircraft at ground level. The collected data were analysed by the UHEI team as well as by Fiehn et al. (2020) and Stanislavjevic et al. (2021), who analyzed the aircraft and ground data respectively to calculate emission rates.

A total of 75 AirCore samples were collected. This includes seven coal mines and one landfill. In addition, seven samples were taken directly from the wells into tedlar bags and analysed at the IUP laboratory for precise determination of isotopic composition. The data were analysed by Wietzel (2018) and are presented in Figure 62. The gray points represent each sample individually, while the black color indicates the average $\delta^{13}CH_4$ value of all samples for a given shaft. The samples taken directly from the wells are indicated in red.

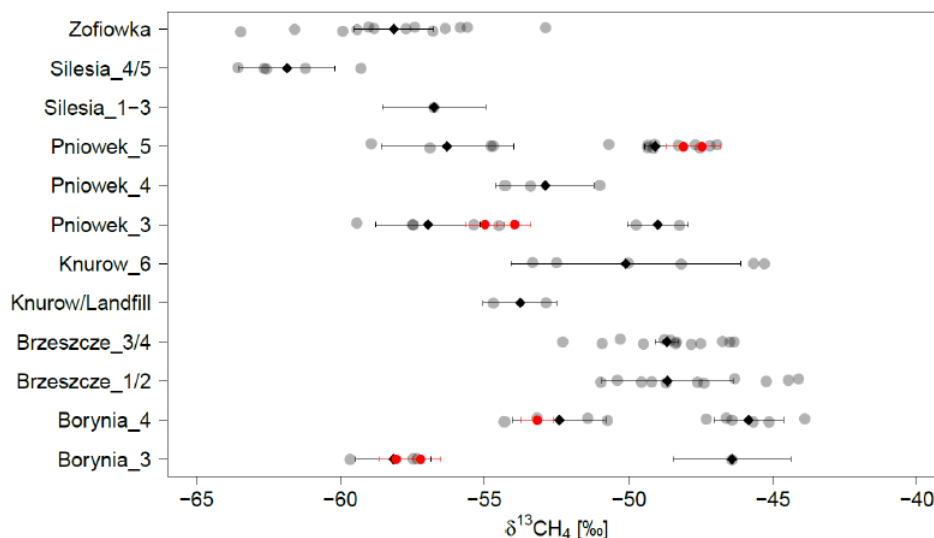


Figure 62: From Wietzel (2018). Isotopic signature results for visited coal mines. Grey points represent AirCore values, black points mean AirCore values and red points mean direct samples.

One of the mines we visited was Zofiowka. Mobile measurements allowed observation of 13 peaks on two different days, 27.05.2018 and 08.06.2018. The measured methane

concentrations ranged from 4.8 to 38.7 ppm. All of the peaks were analysed and gave a $\delta^{13}\text{CH}_4$ range of -63.5 to -52.9 ‰. This wide range can be explained by the presence of multiple mines in the vicinity, and by the fact that the Zoflowka mine has two shafts within the plant. The average $\delta^{13}\text{CH}_4$ value for the two measurement days is -59.12 ± 2.83 ‰ and -57.2 ± 2.5 ‰, respectively.

For the Silesia coal mine, 6 peaks were analysed. Five of these were taken as AirCore samples from Shafts 4 and 5, which were treated together because of their close proximity. For these mines, the $\delta^{13}\text{CH}_4$ range is -63.6 to -59.3 ‰, with an average value of -61.9 ± 1.7 ‰. For shafts 1-3, a total of 3 AirCores were collected, but 2 of them had too much uncertainty, so one was left with a $\delta^{13}\text{CH}_4$ value of -56.7 ± 1.8 ‰.

The largest number of measurements were taken for 3 shafts belonging to the Pniowek coal mine. These are shaft III (8 samples), IV (3 samples) and V (17 samples), respectively. As can be seen in Figure 62, the isotopic analysis for these shafts shows a range of $\delta^{13}\text{CH}_4$ values of -46.9 to -59.4 ‰. The analysed peaks generally did not exceed 15 ppm, with the exception of two peaks which had concentrations of 21 and 68 ppm. For the shafts III and V we can observe two ranges of $\delta^{13}\text{CH}_4$ values. As both shafts are relatively close to each other, we can not exclude that an incorrect shaft was possible. The average $\delta^{13}\text{CH}_4$ values for the three shafts of the Pniowek coal mine are -56.8 ± 2.0 ‰, -52.9 ± 1.7 ‰ and -49.1 ± 2.2 ‰ for Shaft III, IV and V, respectively.

Another site visited was Knurów, for which samples were taken from one shaft (VI) and from the landfill, which 6 and 4 AirCore samples were taken respectively. Peaks coming from the well were collected during two days of measurements, with methane concentrations reaching 40 ppm. The $\delta^{13}\text{CH}_4$ range was -55 to -45 ‰, with an average of -49.2 ± 3.4 ‰. In the case of the landfill, an isotopic composition analysis showed an average value of -53.8 ± 1.3 ‰.

The case of Brzeszcze coal mine is similar to Silesia coal mine. Also here the ventilation shafts are located in close distances so the peaks measured for them were treated as coming from both, because of the impossibility of separating them. In this way samples for shafts 1/2 and 3/4 were analysed, however the $\delta^{13}\text{CH}_4$ range in both cases is very similar, as shown in the Figure 62. The average $\delta^{13}\text{CH}_4$ values are -47.6 ± 2.4 ‰ and -48.7 ± 1.8 ‰, respectively.

The last visited mine was the Borynia coal mine, specifically two shafts, 3 and 4. With a total of 16 AirCore, 3 were rejected due to high uncertainty. The remaining values show two value ranges for both shafts. As revealed by Witzel (2018), it is difficult to explain such a situation. From the meteorological data we could not reconstruct any influence of shafts from other mines. The higher $\delta^{13}\text{CH}_4$ values were obtained from measurements almost 2 weeks later than the first ones. One explanation may be that the first measure-

ments (26 and 27.05.2018) were taken over the weekend, when the mine was closed, but the ventilation shafts were still working, in comparison with the second measurements (6 and 7.06.2018), conducted during working days.

Stanisavljević et al. (2021) showed analysis of isotopic composition from 23 coal mines with comparison to earlier studies. The obtained range of $\delta^{13}CH_4$ values was -58.7 ± 2.5 to -41.6 ± 0.9 ‰. These are the comparable values to our study with values of -61.9 to -45.7 ‰. The collected data were compared to the results obtained by Kotarba (2001). The $\delta^{13}CH_4$ values published by Kotarba (2001) range from -79.9 to -44.5 ‰. This is even larger than the range measured by the UHEI team or published by Stanisavljević et al. (2021). Only 5 samples can be directly compared between Kotarba (2001) and the results of the analysis presented by Wietzel (2018). Among them, only the measurement for Brzeszcze III/IV is in the close range of about -50 ‰. The other shafts, in comparison to Kotarba (2001), show $\delta^{13}CH_4$ with higher values. Stanisavljević et al. (2021) explained the shift in isotopic composition as result of changes in mining operations, as well as the depth at which samples were taken.

According to the isotopic CoMet database, the average value of the isotope signature for the USCB was -49.03 ± 5.28 ‰ (Stanisavljević et al., 2021), which is similar to the previous measurement results where -50.9 ± 0.6 ‰ was obtained by Zazzeri et al. (2016). Furthermore, the measurements for the direct samples taken from the shafts are in good agreement with the mobile measurements (Wietzel, 2018). However, these values are slightly more depleted in isotopic signature than the value for deep bituminous coal mines in England (Zazzeri et al., 2016). In comparison, the carbon isotopic signature values for coal mines in Australia are between -66.4 and -55.5 ‰. Both the emissions and isotopic signatures of coal mine methane depend on the type of mine, its status and the depth at which mining takes place (Zazzeri et al., 2015). For open coal mines the values are more depleted compared to deep mines where the isotopic signature is more enriched (Zazzeri et al., 2016). However, the range of isotopic signature for coal mine methane is relatively wide, and coal mines in China may exhibit an even more enriched isotopic signature (-40 ‰). All this requires regular studies of the isotopic signature in order to establish appropriate values for the global modelling of the isotopic signature (Zazzeri et al., 2016). This is all the more important as coal mines are being closed and the coal-based power industry is being phased out. This has happened in Germany and there is now a discussion in Poland about the environmental, economic and social consequences of mine closures, which in Upper Silesia are an important economic factor.

8.3 Isotopic database of *MEMO*²

The samples collected during these surveys are part of an isotopic database created by the *MEMO*² project members. It contains both, samples measured by the AirCore method and samples collected in tedlar bags and analysed in the laboratory. The isotopic signature of methane has been studied for various sources in Europe and includes both natural and anthropogenic sources of methane. The isotopic signature of methane has been studied for various sources in Europe and includes both natural and anthropogenic sources of methane. Samples in the *MEMO*² isotopic database were collected by all project participants and during large measurement campaigns such as CoMet and ROME0. In this way, samples were collected for the following sectors: wetlands, agriculture and waste management (farms and landfills), biogas plants, natural gas network (gas compressor stations and urban natural gas networks), fossil fuels (coal mines, oil and gas). Figure 63 (prepared by M. Menoud, Utrecht University) shows ranges of methane isotopic signature values for carbon (¹³C) and hydrogen (D) isotopes. Delta values for carbon were obtained by CRDS and IRMS, and hydrogen isotopic sub-analysis was performed on IRMS by laboratories at RHUL (Royal Holloway University of London, UK) and UU (Utrecht University, the Netherlands).

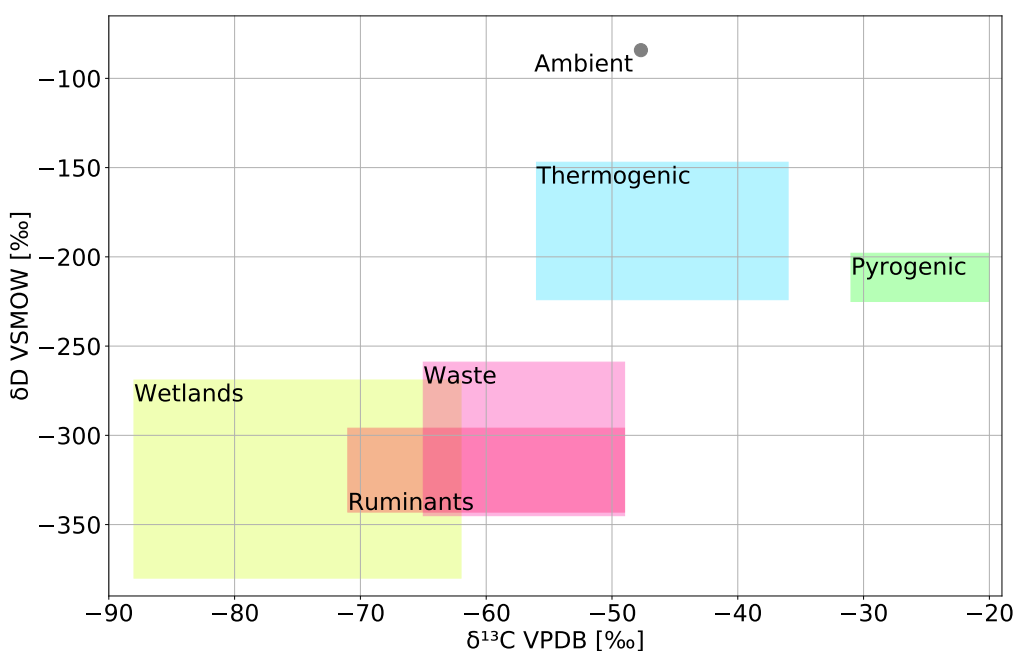


Figure 63: Based on *MEMO*² isotopic database, prepared by M. Menoud. Distribution of the isotopic signature for various methane sources in Europe, with respect to carbon and hydrogen isotopes.

The methane isotopic signature ranges shown above demonstrate the agreement of the samples and analysis performed at Heidelberg in the overall cross-section of sam-

ples in the *MEMO*² isotopic database. The average isotope signature values for the gas compressor station in Gernsheim ($-44.23 \pm 4.2 \text{ ‰}$) and samples collected during CoMet campaign ($-49.03 \pm 5.28 \text{ ‰}$) are in the middle part of the range for thermogenic sources. A high degree of agreement is also found in the case of biogas plant in Pfaffengrund ($-61.77 \pm 2.36 \text{ ‰}$) and the landfill in Sinsheim ($-58.0 \pm 4.2 \text{ ‰}$) which belong to waste sector. The average values of the isotope signatures for the farm in Weinheim ($-53.06 \pm 4.07 \text{ ‰}$) and farm in Ladenburg ($-54.13 \pm 7.03 \text{ ‰}$) are shifted towards enriched values compared to the other samples from the ruminants.

9 Conclusions and Outlook

The aim of this thesis was to estimate methane emission rates and to study the isotopic composition of methane from different sources on local and regional scale. For this purpose, regular measurement campaigns were carried out at sites such as dairy farms, biogas plants, gas compressor stations and landfills. In addition, measurement campaigns in larger regions were carried out: Upper Silesian Coal Basin and Romania. These were focused on the coal mine industry and the oil and gas sector respectively.

The controlled release tests of methods for the estimation of emission rates showed new elements of the data analysis which should be taken into account. The Gaussian Plume Model (GPM) method and Other Test Method 33A (OTM-33A) were tested, depending on the chosen parameters. The definition of the background level of the GPM method does not play a significant role, since the estimated emission level varies up to 8%. More important are the atmospheric conditions under which the measurements are performed. It is important that the wind direction fluctuates in a small spectrum (up to 45 degrees) with wind speeds exceeding 2 m/s. Then, using the GPM method and a stability class calculated from wind speed and insolation, methane emissions can be obtained with an accuracy of up to 30% of the true emissions. It is confirmed that the minimum number of transects to be performed during mobile measurements is 10, with an indication to perform 20 transects for more accurate emission estimates. Furthermore, the final result should be presented as the median of the emission levels for each transect together with its uncertainty, which is due to the possibility of the occurrence of some individual high peaks and thus the estimated emission level. The most important parameter that was analysed was how to determine the wind speed used in the model. The performed experiments show that the best estimation of the emission rate occurs at the wind speed selected for each transect and individually. More important for mobile measurements are the atmospheric conditions under which the measurements are performed. It is important that the wind direction fluctuates in a small spectrum (up to 45 degrees) with wind speeds exceeding 2 m/s. Then, using the GPM method and a stability class calculated from wind speed and sunshine level, methane emissions can be obtained with an uncertainty of up to 30% of the true emissions.

Again for the OTM-33A method, atmospheric conditions and the way in which the measurement is done are crucial for the obtained methane emission rates. All parameters in the model are important because they determine the uncertainty of the obtained result. It is recommended to precisely determine all variables, especially the measurement distance, in order to minimize the uncertainty of the obtained emission levels. The validation of OTM-33A effectively emphasized the importance of repeatability of measurements. Many quantifications should be made in order to determine the variability of methane emissions.

Both methods (GPM and OTM-33A) give reliable values of methane emission rates and are useful tools for monitoring methane sources. However, it would be recommended to perform more controlled release experiment in different weather conditions.

Studies on methane emissions from local sources have shown the importance of regular measurement campaigns. It is difficult to estimate methane emission rates for facilities with several emission sources (farms with biogas plants). Dairy farms are a relatively well identified source of methane, however, the problem is how to determine the impact of nearby biogas plants from such farms. In the Rhein-Neckar region, farms with biogas plants are typical sources and it is therefore necessary to estimate the levels of methane emissions from such sources that count into the local methane budget. Measurements for sources such as gas compressor stations and landfills introduce new insights into methane emissions inventories. Although such emitters are regulated under methane mitigation projects, they may have emission rates that are not reportable. The likely occurrence of many such sources contributes to global estimates of methane emissions, and thus to uncertainty in the global methane budget. An additional element is the seasonality of emissions for sources such as landfills, which increases in winter and decreases in summer. Knowing about this phenomenon, we can better plan measurement campaigns and more accurately determine the periodic rates of methane emissions.

The methane sources described above, as well as coal mines and oil and gas, can also be monitored by isotopic signature to better determine the origin of the emissions. In addition, large emitters on a European scale, such as coal mines in Poland and oil and gas in Romania, need to be better quantified as, despite the studies carried out, there is still a large percentage of uncertainty in the estimated emission rates, especially considering the amount of methane emitted into the atmosphere (coal mines) and the number of potential sources (oil and gas wells).

The conducted research was part of research projects that brought together many scientists into one network. This allowed the creation of a larger database with information on many sources throughout Europe. By collaborating with other research groups, I was able to gain additional knowledge about other measurement methods and their properties. I was also able to support the research of others, which was later summarized in scientific publications (CoMet campaign). As one of the scientists, I was charged with carrying out the data analysis for the mobile measurements during the ROMEO campaign, which leads to a joint publication draft on methane emissions from the oil and gas industry. This publication is the first approach to methane emission rates from this sector in Romania.

In conclusion, the results of the research work presented in this dissertation show the necessity of conducting regular and well-planned measurement campaigns. They also emphasize the monitoring of methane emission levels from various sources on a local,

regional and national scale. Improvement of the measurement network and increase of the research intensity will allow for more accurate estimation of the global methane emission and reduction of its uncertainty, and having a better knowledge of the methane emission rates it is possible to introduce new actions which will allow to mitigate it.

10 List of publications of the author

Publications Included in This Thesis

1. **Korbeń P.**, Jagoda P., Maazallahi H., Kammerer J., Necki J.M., Bartyzel J, Radovici A., J.Wietzel, Schmidt M, Röckmann T. and other ROMEO team members, *Quantification of methane emission from oil and gas wells using Other Test Method 33A and Gaussian Plume Model during ROMEO campaign, Romania*, [in review]
2. **Korbeń P.**, Wietzel J., Kammerer J., Schmidt M., *Quantification of methane emission from different sources in the region of Heidelberg, Germany*, [in prep]

Additional Publications

1. Defratyka S.M., Paris J-P, Yver-Kwok C., Fernandez J.M., **Korbeń P.**, Bousquet P., *Mapping urban methane sources in Paris, France*, Environ. Sci. Technol., 2021
2. Fiehn A., Kostinek J., Eckl M., Klausner T., Gałkowski M., Chen J., Gerbig C., Röckmann T., Maazallahi H., Schmidt M., **Korbeń P.**, Necki J.M., Jagoda P., Wildmann N., Mallaun C., Bun R., Nickl A-L., Jöckel P., Fix A., Roiger A., *Estimating CH₄, CO₂ and CO emissions from coal mining and industrial activities in the Upper Silesian Coal Basin using an aircraft-based mass balance approach*, Atmos. Chem. Phys., 20, 12675–12695, 2020
3. Morales R., Ravelid J., Vinkovic K., **Korbeń P.**, Tuzson B., Emmenegger L., Chen H., Schmidt M., Humbel S., and Brunner D., *Estimating local methane sources from drone-based measurements using mass-balance method*, [in prep]
4. Stanisavljević M., Necki J.M., Swolkień J., Gałkowski M., Maazallahi H., **Korbeń P.**, Menoud M., van der Veen C., Röckmann T., Schmidt M., Wietzel J., Vinković K., Defratyka S., Zieba D., Chmura Ł., Wołkowicz W., *Determination of methane emission rates and isotopic signatures from coal mine ventilation shafts in the Upper Silesia, Poland*, [in prep]
5. Menoud M., van der Veen C., Maazallahi H., Hensen A., Velzeboer I., van den Buk P., Delre A., **Korbeń P.**, Schwietzke S., Ardelean M., Calcan A., Baciu C., Scheutz C., Schmidt M., Röckmann T., *CH₄ isotopic signatures of emissions from oil and gas extraction sites in Romania*, [in prep]

Appendices

A List of figures

List of Figures

1	From NOAA. Increase of global monthly CH_4 concentration over last 40 years.	15
2	Methane sources divided by origin into natural and anthropogenic. Based on Sauniois et al. (2020).	16
3	From Sauniois et al. (2020). Global methane budget in years 2008 - 2017 in environment including different kind of fluxes (anthropogenic and natural). The numbers on the left represent bottom-down estimates and the numbers on the right represent top-down estimates, while the numbers in parentheses indicate the emission range (performed).	20
4	Characterization of methane based on its isotopic composition ($\delta^{13}C$, δ^2H), from Sherwood et al. (2017). M: microbial, T: thermogenic, A: abiotic, MCR: microbial CO_2 reduction, MAF: microbial acetate fermentation, ME: microbial in evaporitic environment, T_O : thermogenic with oil, T_C : thermogenic with condensate, T_D : dry termogenic, T_H : thermogenic with high-temperature $CO_2 - CH_4$ equilibration: T_{LM} : thermogenic low maturity, GV: geothermal-volcanic systems, S: serpentized ultramafic rocks, PC: Precambrian crystalline shields.	22
5	From Hoheisel (2017). Isotope signatures of different methane emitters based on several publications (1988 - 2016). Dots with/without errorbars represents averaged isotopic signature values, while color lines represent ranges of $\delta^{13}CH_4$ reported by authors.	24
6	Coordinate system with Gaussian plume of a tracer gas released from point source and transported in the horizontal (y) and vertical (z) direction (Turner, 1970).	26
7	Coordinate system with Gaussian plume of a tracer gas released from point source and transported in the horizontal (σ_y) and vertical (σ_z) direction (Turner, 1970).	27
8	Illustration of stationary field measurements with marked position of the source of the emission and the observation point (Thoma et al., 2014).	31
9	Distribution of gas concentration in relation to the measured wind direction (Thoma et al., 2014).	31

10	Top-down view. Example illustrating a representative (top) and unrepresentative (bottom) gas concentration profile in terms of wind direction (Thoma et al., 2014; Omara, 2018).	33
11	Side view. Example illustrating a representative (top) and unrepresentative (bottom) gas concentration profile in terms of wind speed (Thoma et al., 2014; Omara, 2018).	33
12	Top-down view. Example illustrating a representative (top) and unrepresentative (bottom) gas concentration profile due to possible obstacles between the source and the receiver (Thoma et al., 2014; Omara, 2018).	34
13	Side view. Example illustrating a representative (top) and unrepresentative (bottom) gas concentration profile due to possible obstacles between the source and the receiver (Thoma et al., 2014; Omara, 2018).	34
14	Top-down view. An example illustrating a representative (top) and unrepresentative (bottom) gas concentration profile due to the vehicle's orientation with respect to the plume transport (Thoma et al., 2014; Omara, 2018).	35
15	An example of an acceptable topography (A, top) and an unacceptable topography (B, bottom) for OTM-33A application (Thoma et al., 2014; Omara, 2018).	35
16	Diagram and principle of analyzer using Cavity Ring-Down Spectroscopy. (a) Schematic of CRDS Analyzer (Saad et al., 2009; Wahl et al., 2008), (b) The scheme of comparison of the cavity with and without sample (Picarro manual).	41
17	Cavity Ring-Down Spectrometer (CRDS) - Picarro G2201-i. Instrument to measure a mole fraction and isotopes of CO_2 and CH_4 and concentration of H_2O (G2201-i Analyzer Datasheet)	42
18	Optical Feedback - Cavity - Enhanced Absorption Spectroscopy, scheme of work (Licor manual).	43
19	LICOR LI-7810, the Optical Feedback - Cavity - Enhanced Absorption Spectrometer used for mobile measurement to monitor concentration of CH_4 , CO_2 and H_2O (Licor manual).	44
20	Scheme of AirCore used for mobile measurements (Hoheisel, 2017). The blue arrows indicate the flow of air in the "monitoring mode", while green arrows show the flow of air in "replay mode".	45

21	An example of a methane plume measured by Hoheisel et al. (2019). The plots on the left side show the methane concentration and the $\delta^{13}CH_4$, respectively. The vertical black line shows the point at which the measurement was switched from "monitoring mode" to "replay mode". The blue color represents the monitoring mode and the black and red (15 s mean) ones the replay mode. The Keeling plot and Miller-Tans plot for the peak are shown on the right.	46
22	Dependency between peak height above background and the fit error of $\delta^{13}CH_4$ signature from the corresponding measured peak (Hoheisel et al., 2019).	46
23	Scheme of MaxiMet GMX500 Compact Weather Station (MaxiMet GMX500 manual), own gallery.	48
24	Scheme of 3D Ultrasonic Anemometer weather station, manufactured by METEK (METEK manual), own gallery.	49
25	Facility in Weinheim. Note that for this location a double source exists, green pin is biogas tank and yellow pin is cowshed.	52
26	Facility in Ladenburg. Note that for this location a double source exists, the green pin is the biogas tank and the yellow pin is the cowshed.	54
27	Biogas plant in Pfaffengrund. Green pin means the middle of the facility.	55
28	The Gas Compressor Station in Gernsheim. The red pin means indicates the probable source of the methane leak.	57
29	Landfill on the north of Sinsheim. Red pin means the middle of landfill area.	58
30	From UNFCCC. Percentage shares of greenhouse gases in the total national emissions in 2017 (excluding category 4. LULUCF)	59
31	CoMet campaign logo (on the left) and map of target region on the campaign (on the right) (DLR website).	60
32	Methane emissions from oil and gas industry for few European countries, in order Germany, the United Kingdom, Italy, the Netherlands, Norway, Poland and Romania (<i>MEMO</i> ² website).	61
33	Map of target regions in Romania during ROMEO campaign	62
34	On the left, time series data of mobile measurements during one of the release. Black lines represent methane concentration over time, while blue line indicate background concentration. On the right, comparison of measured (green) and modelled peak (blue).	64
35	Map for controlled release experiments in Mannheim on Maimarktgelände parking. The pins mark the location where the controlled CH_4 releases were performed. Source: Google Earth.	65

36	Test of determination statistical description of obtained results. Boxplots represent min, max, first and third quartile values for the data set. Red points corresponds to median \pm u(median), while blue dots corresponds to mean \pm SEM.	71
37	Test of determination wind speed method, transect wind speed (TWS, blue dots and line) and mean wind speed (MWS, green dots and line). Red line corresponds to the real emission rate.	72
38	Example of OTM-33A measurement. Background-substracted methane concentration versus binned wind direction, where 0 degrees corresponds to the main wind direction. Black dots are data points, blue dots are averaged methane concentration values in each bin, red dots represent fitted values from Gaussian fit.	73
39	Location of release points (RP, in red) and OTM measurement locations (in yellow).	75
40	Difference in wind direction bin with maximal mean methane concentration and maximal number of data points in bin. 3a) Ideal case when both curves overlap. 3b) Problematic case with 3 possible reasons.	76
41	Estimated emission based on different stability classes. Orange dots represent values of emission for stability class based on variability of wind direction, while green dots represent values of emission of turbulent stability class.	77
42	Uncertainty analysis of the estimated emissions after taking into account all component uncertainties. Green points (Partial uncertainty) show the uncertainty range of the emission estimate considering only the uncertainty of the peak, whereas blue dots (Full uncertainty) show the uncertainty of the emission estimate considering all contributions.	78
43	Dependency of estimated emissions on the duration of the measurement. Blue dots represent the estimated emissions for the measurement duration as indicated on the OX axis. Green dots represent emission values for the first, second and third hour of measurement respectively.	80
44	Barplot presenting frequency of visited sites around Heidelberg between 2016 and 2020. The black dashed line divides the period into measurements carried out by Hoheisel (2017) and during this study.	84
45	Estimated emission rates for the Weinheim farm. The light green and dark green points indicate 8 and 12 peaks for measurements on 02.04.2029 respectively.	86

46	Estimated emissions for the Ladenburg farm. The red point indicates the estimate made using the OTM-33A method.	88
47	Estimated emissions for the biogas plant in Pfaffengrund. The red point indicates the estimate made using the OTM-33A method.	90
48	Time series of CH_4 and CO_2 measurements in Weinheim, 02.04.2019 (Kammerer, 2019).	93
49	Estimated methane emission rates for the Gas Compressor Station in Gernsheim.	97
50	Estimated methane emission rates for the landfill in Sinsheim.	100
51	Different installations visited during mobile measurements (source: Own gallery). Normal view when driving a car in Romania, in the regions visited by the ROMEO team.	109
52	Comparison of two visited regions, 5a (left) and 6 (right).	110
53	Distribution of visited sites based on information given by OMV: differentiates according to the given production status (left panel) and to gas or oil (right panel).	111
54	Calculated CH_4 emission rates for 20 sites using a Gaussian Plume Model. Green dots show emission rates for oil well, orange for gas well and blue are for unknown type of the source. The shaded area marks a comparison measurements with parallel measurements by 3 teams (ROM4080). . . .	112
55	Calculated emission rates by Other Test Method 33A. Green, orange and blue dots represent CH_4 emission rates for oil, gas and unknown type of the source site respectively. The shaded areas mark sites with several application of OTM-33A.	113
56	Comparison of derived methane emission rates by region. Boxes represents the first and third quartile of the data, while whiskers extend to the largest value that is within 1.5 times the interquartile range (IQR). Means and 95% CIs are shown in red and were calculated using a non-parametric bootstrap. Data are presented on a logarithmic y-axis. The number of accepted quantifications per region are written in the top line. This graph include already the non-detect as described in chapter Emission rates below the detection limit	116

57	Estimated emission rates distributed by status (on the top) and type (on the bottom) of the quantified site. Means and 95% CIs are shown in red and were calculated using a non-parametric bootstrap. Note the logarithmic y-axis. The number of accepted quantifications per region are written in the top line. This graph include already the non-detect as described in chapter Emission rates below the detection limit.	117
58	Isotope composition of CH_4 for 5 main Heidelberg sources and additionally visited sites obtained during this study.	120
59	$\delta^{13}CH_4$ values for dairy farms in Weinheim and in Ladenburg together with previous collected data.	121
60	$\delta^{13}CH_4$ values for Biogas Plant in Pfaffengrund and for landfill in Sinsheim together with previous collected data.	123
61	$\delta^{13}CH_4$ values for GCS in Gernsheim and natural gas network in Heidelberg together with previous collected data.	125
62	From Wietzel (2018). Isotopic signature results for visited coal mines. Grey points represent AirCore values, black points mean AirCore values and red points mean direct samples.	126
63	Based on <i>MEMO</i> ² isotopic database, prepared by M. Menoud. Distribution of the isotopic signature for various methane sources in Europe, with respect to carbon and hydrogen isotopes.	129

B List of tables

List of Tables

1	Stable isotopes of hydrogen and carbon (Hitchman et al., 1989).	20
2	Briggs parametrisation for stability classes (x is a distance in m). $\sigma_y[m]$ and $\sigma_z[m]$ mean horizontal and vertical dispersion coefficients	27
3	Atmospheric stability classes by Pasquill for daytime insolation (Turner, 1970; NOAA).	28
4	Atmospheric stability classes by Pasquill for nighttime conditions (Turner, 1970; NOAA).	28
5	Local atmospheric stability class during stationary measurements based on wind direction and wind speed, (Thoma et al., 2014; Omara, 2018). . .	37
6	Controlled release test performed performed to verify the quality of quantifications performed using the GPM and OTM-33A.	50
7	Measurement campaigns performed on the dairy farm in Weinheim with the recorded number of observed peaks and Aircore samples.	53
8	Measurement campaigns performed on the dairy farm in Ladenburg with the recorded number of observed peaks and Aircore samples.	54
9	Measurement campaigns performed on the biogas plant in Pfaffengrund with the recorded number of observed peaks and Aircore samples.	56
10	Measurement campaigns performed on the Gas Compressor Station in Gernsheim with the recorded number of observed peaks and Aircore samples.	57
11	Measurement campaigns performed on landfill in Sinsheim with the recorded number of observed peaks and Aircore samples.	58
12	Different scenarios for release test M4.	68
13	Estimated emission for scenarios during release experiment Mannheim 4.	68
14	Different scenarios for release test M5.	69
15	Collected OTM-33A data during DüREX campaign with necessary information.	74
16	Emission (Q) estimated for all OTM-33A applications during DuREX campaign listed in Table 15. Test with * does not fulfil the quality criteria.	80
17	Emission (Q) estimated for all OTM-33A applications during M5 test. The method was tested in different distances.	81
18	Description of the values used in the tables summarizing the measurements for a given source.	85

19	Results of GPM for Dairy Farm in Weinheim.	87
20	Results of GPM for Dairy Farm in Ladenburg. Date with "*" means measurements made using OTM-33A.	89
21	Results of GPM for Biogas plant in Pfaffengrund. Date with "*" means measurements made using OTM-33A.	91
22	Results of GPM for Gas Compressor Station in Gernsheim.	98
23	Results of GPM for landfill in Sinsheim.	101
24	Specification of in-situ analysers used for quantifications and screening including methane and meteorology measurements.	107
25	Mean methane emission rates per site with 95% confidence intervals (CIs) for the different regions.	115
26	$\delta^{13}CH_4$ value ranges obtained for main local methane sources and additional visited sources based on mobile measurements using AirCore. . . .	119
27	List of flasks to calibrate all instruments for the ROMEO campaign. . . .	142

C Calibration gases for ROMEO campaign

Table 27: List of flasks to calibrate all instruments for the ROMEO campaign.

Name of flask	Pic 6_2 / Pic 7	5 ppm tank	25 ppm tank	Arizona	Jezowe	Montana	UU ambient	UU 6.3 ppm	UU 27 ppm	UU 130 ppm
CH_4 [ppm]	2	$5.05 \pm 5\%$	$24.98 \pm 5\%$	2	9.5	51	2	6.3	27	130

D Coal mines in Poland - description

Zofiówka (source: JSW)

The hard coal mine (Polish: Kopalnia Węgla Kamiennego, KWK) Żofiowka was built in the years 1962-1969. From January 2020, the "Zofiówka" mine has operated as part of the combined mine KWK Borynia-Zofiówka. The "Zofiówka" field is located on an area of 16.4 km² and has an operational resource of 50.9 million tons. The daily net coal production is 8,000 tons / day. The bed has 5 shafts, 1 of which is a mining shaft, 3 shafts are downhill - material and 1 is a ventilation shaft. There are 3 levels, mining at 900 m, and ventilation at 705 m and 580 m. The mine was visited during three days and the estimated emissions for the visited shafts based on the data is 13 500 tCH₄/yr.

Pniówek (source: JSW)

The "Pniówek" coal mine deposit is located in the Pawłowice commune (87.1%) as well as in the city of Jastrzębie-Zdrój (12.9%), and the mine belongs to JSW. The "Pniówek" deposit has a mining area of 28.6 km² with operable resources of 101.9 million tons. The net daily production is about 12,200 tons / day. The mine has 5 shafts: 1 mining, 2 material and 2 ventilation shafts. The ventilation levels are respectively at the depth of 580 m and 705 m, and the extraction levels at the depth of 830 m and 1000 m. Shafts Pniówek III, IV and V have been visited several times. Based on CoMet v2 inventory, each shaft emits 17 500 tons of methane per year.

Borynia (source: JSW)

The deposit of KWK "Borynia" is located in the commune of Mszana, Świerklany, Pawłowice and the city of Jastrzębie. The mining area of the mine is 17.4 km². It has operational resources of 30.9 million tons, and the net daily production is 7,300 tons / day. Currently, the mine's staff consists of 3,083 employees. The mine has 5 shafts: 2 for downhill ones, and 1 for mining, material and ventilation. The extraction levels are at a depth of 838 m and 950 m, respectively, while the extraction level is at a depth of 713 m. For Borynia Mine, Shafts III and IV were visited a total of 3 times and sample bags were collected. Referring to the CoMet inventory, each of the above shafts emits 9550 tons of methane per year.

Brzeszcze (source: TAURON)

The Brzeszcze hard coal deposit has been documented to the depth of seam at 510 m, i.e. to a depth of approximately 1,150 m. The Brzeszcze coal mine has 56.5 million tons of operable coal resources, of which almost 42% is located at the most productive level at 510 m. The mineral accompanying the hard coal deposit is methane. Methane is obtained by means of drainage holes, methane galleries and is captured there from behind the insulation. Through a network of pipelines and methane drainage stations, methane is brought to the surface and economically used. Its balance resources amount to 3 494.9 million m^3 . The Brzeszcze hard coal deposit is accessible through eight shafts. The plant's spatial structure is supplemented by the main trenches at the levels of 512 m, 640 m, 740 m and 900 m, as well as by departmental trenches. The main mining level of the mine is 640 m, while the level at 900 m is under construction. In the case of the Brzeszcze mine, Shafts 1-4 were visited, but Shafts 1/2 and 3/4 are located next to each other so they cannot be distinguished (Wietzel, 2018). Each of them emits about 9000 tCH_4/yr .

Silesia (source: SILESIA)

The hard coal mine "Silesia" is located in the following cities: Czechowice-Dziedzice and Pszczyzna and the communes of Goczałkowice-Zdrój, Bestwina and Miedźna, about 30 km from the Polish-Czech border. Its balance resources exceed 500 million tons of low-sulfur coal, and its balance resources of methane exceed the value of 1.1 billion m^3 . The underground part of the mining plant includes 2 mining levels and 2 ventilation levels with a network of 39.7 kilometers of mine workings. The surface part includes the coal mechanical processing plant, the salt water retention and dosing reservoir in Kaniów, as well as the mechanical, electrical and shaft infrastructure. The underground part is connected with the surface part by 5 shafts: 3 mining and service shafts and 2 ventilation shafts with a maximum depth of 556 meters. The shafts assigned to this mine emit up to 12 300 tCH_4/yr .

Knurów (source: JSW)

The KWK "Knurów-Szczygłowice" coal mine was established on February 1, 2010 as a result of the merger of two mines "Knurów" and "Szczygłowice" and became a two-cycle plant with independent production lines. Knurów VI shaft was visited which according to CoMet inventory emits 16 600 tCH_4/yr .

References

- [1] A. Abdel-Rahman. On the atmospheric dispersion and gaussian plume model. 10 2008.
- [2] C. Arndt, A. Leytem, A.N. Hristov, D. Zavala-Araiza, J.P Cativiela, S. Conley, C. Daube, I. Faloon, and S.C. Herndon. Short-term methane emissions from 2 dairy farms in california estimated by different measurement techniques and us environmental protection agency inventory methodology: A case study. *Journal of Dairy Science*, 101, 10 2018.
- [3] S. Ars, G. Broquet, C. Yver Kwok, Y. Roustan, L. Wu, E. Arzoumanian, and P. Bousquet. Statistical atmospheric inversion of local gas emissions by coupling the tracer release technique and local-scale transport modelling: a test case with controlled methane emissions. *Atmospheric Measurement Techniques*, 10(12):5017–5037, 2017.
- [4] E. Atherton, D. Risk, C. Fougere, M. Lavoie, A. Marshall, J. Werring, J. P. Williams, and C. Minions. Mobile measurement of methane emissions from natural gas developments in northeastern british columbia, canada. *Atmospheric Chemistry and Physics*, 17(20):12405–12420, 2017.
- [5] AVR. Deponien Sinsheim und Wiesloch. 2016. <http://www.gillinstruments.com/data/datasheets/1957-008%20Maximet-gmx500%20Iss%207.pdf>.
- [6] S. Bakkaloglu. *Isotopic Characterisation and Quantification of Methane Emissions from Waste Sources in Europe*. PhD thesis, Royal Holloway University of London, 2021.
- [7] S. Bakkaloglu, D. Lowry, R.E. Fisher, J.L. France, D. Brunner, H. Chen, and E.G. Nisbet. Quantification of methane emissions from uk biogas plants. *Waste Management*, 124:82–93, 2021.
- [8] Pfistererhof Biogasanlage. <https://www.pfistererhof.de/>.
- [9] H. L. Brantley, E. D. Thoma, W. C. Squier, B. B. Guven, and D. Lyon. Assessment of methane emissions from oil and gas production pads using mobile measurements. *Environmental Science & Technology*, 48(24):14508–14515, 2014. PMID: 25375308.
- [10] M. Brass and T. Roeckmann. Continuous-flow isotope ratio mass spectrometry method for carbon and hydrogen isotope measurements on atmospheric methane. *Atmospheric Measurement Techniques*, 3(6):1707–1721, 2010.

- [11] G.A. Briggs. Diffusion estimation for small emissions. (ATDL Contribution File No.79), 1973. Atmospheric Turbulence and Diffusion Laboratory.
- [12] N. Büttner. Aircore systems for mobile CH₄ and $\delta^{13}\text{CH}_4$ measurements by car and UAV. Master's thesis, Heidelberg University, 2019.
- [13] D. R. Caulton, Q. Li, E. Bou-Zeid, J. P. Fitts, L. M. Golston, D. Pan, J. Lu, H. M. Lane, B. Buchholz, X. Guo, J. McSperritt, L. Wendt, and M. A. Zondlo. Quantifying uncertainties from mobile-laboratory-derived emissions of well pads using inverse gaussian methods. *Atmospheric Chemistry and Physics*, 18(20):15145–15168, 2018.
- [14] J. Chanton, Ch. Rutkowski, C. Schwartz, D. Ward, and L. Boring. Factors influencing the stable carbon isotopic signature of methane from combustion and biomass burning. *Journal of Geophysical Research*, 2000.
- [15] J. Craig, F. Gherali, F. MacAulay, and R. Sorkhabi. *The history of the European oil and gas industry - Introduction*, volume 465, page SP465.23. 06 2018.
- [16] S.M. Defratyka. *Characterization of CH₄ emissions in urban environments (Paris)*. PhD thesis, LSCE, 2021.
- [17] Deloitte. The contribution of Black Sea Oil & Gas projects to the development of the Romanian economy. 2018. https://www2.deloitte.com/content/dam/Deloitte/ro/Documents/ImpRepOffshoreProjects_ENG.PDF.
- [18] F. Dinger. Characterization of a cavity ring-down spectrometer for measuring CO₂, CH₄, $\delta^{13}\text{CO}_2$ and $\delta^{13}\text{CH}_4$ in ambient air. Master's thesis, Heidelberg University, 2014.
- [19] DLR. https://www.dlr.de/DE/Home/home_node.html. Deutsches Zentrum für Luft- und Raumfahrt website.
- [20] DWGV. Methane emissions from natural gas infrastructure. facts, figures and initiatives by the gas industry. *Deutscher Verein des Gas- und Wasserfaches*, 2020.
- [21] R. Edie, A. M. Robertson, R. A. Field, J. Soltis, D. A. Snare, D. Zimmerle, C. S. Bell, T. L. Vaughn, and S. M. Murphy. Constraining the accuracy of flux estimates using otm-33a. *Atmospheric Measurement Techniques*, 13(1):341–353, 2020.
- [22] EIA. <https://www.eia.gov/>.

- [23] A. Fiehn, J. Kostinek, M. Eckl, T. Klausner, M. Galkowski, J. Chen, C. Gerbig, T. Roeckmann, H. Maazallahi, M. Schmidt, P. Korben, J. Necki, P. Jagoda, N. Wildmann, C. Mallaun, R. Bun, A.-L. Nickl, P. Jockel, A. Fix, and A. Roiger. Estimating CH₄, CO₂ and CO emissions from coal mining and industrial activities in the Upper Silesian Coal Basin using an aircraft-based mass balance approach. *Atmospheric Chemistry and Physics*, 20(21):12675–12695, 2020.
- [24] F.I. Frank. *Atmospheric methane and its isotopic composition in a changing climate: A modeling study*. PhD thesis, Ludwig-Maximilians-Universität München, 2018.
- [25] F. A. Gifford Jr. Use of routine meteorological observations for estimating atmospheric dispersion. *Nuclear Safety*, 2:47–51, 1961.
- [26] F. A. Gifford Jr. An outline of theories of diffusion in the lower layers of the atmosphere. Technical report, Environmental Science Services Administration, (Oak Ridge, Tenn.), 1968.
- [27] Open Grid Europe GmbH. <https://oge.net/>.
- [28] S.R. Hanna, G.A. Briggs, and R.P. Hosker Jr. Handbook on atmospheric diffusion. *Technical Information Center U.S. Department of Energy*, 1982.
- [29] M. Harrison, L. Campbell, T. Shires, and R. Cowgill. Methane emissions from the natural gas industry. 1993.
- [30] S.P. Hitchman, W.G. Darling, and G.M. Williams. Stable isotopes ratios in methane containing gases in the united kingdom. *British Geological Survey*, 1989. Technical report.
- [31] A. Hoheisel. Characterization of a CRDS Analyzer and Determination of Isotopic Signatures of Anthropogenic CH₄ Sources Using Mobile Measurements. Master's thesis, Heidelberg University, 2017.
- [32] A. Hoheisel, C. Yeman, F. Dinger, H. Eckhardt, and M. Schmidt. An improved method for mobile characterisation of delta 13CH₄ source signatures and its application in Germany. *Atmospheric Measurement Techniques*, 12(2):1123–1139, 2019.
- [33] INGAA. <https://www.ingaa.org/>. Interstate Natural Gas Association of America.

- [34] GILL instruments. MaxiMet GMX500 Compact Weather Station. <http://www.gillinstruments.com/data/datasheets/1957-008%20Maximet-gmx500%20Iss%207.pdf>.
- [35] E-PRTR inventory. <https://prtr.eea.europa.eu/#/home>.
- [36] S. Jayasundara, J.A.D. Ranga Niroshan Appuhamy, E. Kebreab, and C. Wagner-Riddle. Methane and nitrous oxide emissions from canadian dairy farms and mitigation options: An updated review. *Canadian Journal of Animal Science*, 96(3):306–331, 2016.
- [37] JSW. <https://www.jsw.pl/o-nas/zaklady/>. Jastrzebska Spolka Weglowa website.
- [38] J. Kammerer. A study of controlled methane release experiments for emmissions quantification with an application to a dairy farm. Master’s thesis, Heidelberg University, 2019.
- [39] A. Karion, C. Sweeney, P. Tans, and T. Newberger. Aircore: An innovative atmospheric sampling system. *Journal of Atmospheric and Oceanic Technology*, 27(11):1839 – 1853, 2010.
- [40] C.D. Keeling. The concentration and isotopic abundances of atmospheric carbon dioxide in rural areas. *Geochimica et Cosmochimica Acta*, 13:322–334, 1958. Pergamon Press Ltd., London.
- [41] S. Kirschke, P. Bousquet, P. Ciais, M. Saunois, J. G. Canadell, E. J. Dlugokencky, P. Bergamaschi, D. Bergmann, D. R. Blake, L. Bruhwiler, P. Cameron-Smith, S. Castaldi, F. Chevallier, L. Feng, A. Fraser, M. Heimann, E. L. Hodson, S. Houweling, B. Josse, P. J. Fraser, P. B. Krummel, J.-F. Lamarque, R. L. Langenfelds, C. Le Quéré, V. Naik, S. O’Doherty, P. I. Palmer, I. Pison, D. Plummer, B. Poulter, R. G. Prinn, M. Rigby, B. Ringeval, M. Santini, M. Schmidt, D. T. Shindell, I. J. Simpson, R. Spahni, L. P. Steele, S. A. Strode, K. Sudo, S. Szopa, G. R. van der Werf, A. Voulgarakis, M. van Weele, R. F. Weiss, J. E. Williams, and G. Zeng. Three decades of global methane sources and sinks. *Nat. Geosci.*, 6:813–823, 2013.
- [42] M. Kotarba. Composition and origin of coalbed gases in the upper silesian and lublin basins, poland. *Organic Geochemistry*, 32:163–180, 01 2001.
- [43] H. Krümpelmann. CH_4 Emissionsbestimmungen mit der OTM 33A Methodeim Raum Heidelberg, 2019. bachelor thesis.

- [44] P. Kumar, G. Broquet, C. Yver-Kwok, O. Laurent, S. Gichuki, C. Caldw, F. Crop-ley, T. Lauvaux, M. Ramonet, G. Berthe, F. Martin, O. Duclaux, C. Juery, C. Bouchet, and P. Ciais. Mobile atmospheric measurements and local-scale inverse estimation of the location and rates of brief CH₄ and CO₂ releases from point sources. *Atmospheric Measurement Techniques Discussions*, 2020:1–27, 2020.
- [45] Y-Y. Lee, H. Jung, H-W. Ryu, K-C. Oh, J-M. Jeon, and K-S. Cho. Seasonal characteristics of odor and methane mitigation and the bacterial community dynamics in an on-site biocover at a sanitary landfill. *Waste Management*, 71:277–286, 2018.
- [46] I. Levin, H. Glatzel-Mattheier, T. Marik, M. Cuntz, M. Schmidt, and D. Worthy. Verification of german methane emissions inventories and their recent changes based on atmospheric observations. *Journal of Geophysical Research - Atmospheres*, 104, 02 1999.
- [47] L. Levin, P. Bergamaschi, H. Dörr, and D. Trapp. Stable isotopic signature of methane from major sources in germany. *Chemosphere*, 26(1):161–177, 1993. Proceedings of the NATO advanced research workshop.
- [48] LICOR. Li-7810 ch₄/co₂/h₂o trace gas analyzer instruction manual. <https://www.licor.com/documents/zsce2z88fgkfpbiguqi0k3g537jllsl7>.
- [49] J. Liebetrau, T. Reinelt, A. Agostini, and B. Linke. Methane emission from biogas plants. methods for measurement, results and effect on greenhouse gas balance of electricity produced. *IEA Bioenergy*, 2017.
- [50] W. Lizik, J. Im, J.D. Semrau, and M.J. Barcelona. A field trial of nutrient stimulation of methanotrophs to reduce greenhouse gas emissions from landfill cover soils. *Journal of the Air & Waste Management Association*, 63(3):300–309, 2013.
- [51] F. Lucernoni, M. Rizzotto, L. Capelli, V. Busini, R. Del Rosso, and S. Sironi. Sampling method for the determination of methane emissions from landfill surfaces. *Waste Management & Research*, 35(10):1034–1044, 2017. PMID: 28784047.
- [52] P. Mandal. Locate fugitive methane emission from compressor station of natural gas transmission and distribution system for reducing environmental risk. *International Journal Of Petrochemical Science & Engineering*, 2, 05 2017.
- [53] K. Manfred, L. Ciaffoni, and G. Ritchie. Optical-feedback cavity-enhanced absorption spectroscopy in a linear cavity: model and experiments. *Applied Physics B*, 120, 07 2015.

- [54] V. Masson-Delmotte, P. Zhai, H. O. Pörtner, D. Roberts, J. Skea, P.R. Shukla, A. Pirani, W. Moufouma-Okia, C. Péan, R. Pidcock, S. Connors, J. B. R. Matthews, Y. Chen, X. Zhou, E. Gomis, M. I. and Lonnoy, T. Maycock, M. Tignor, and T. Waterfield. Global warming of 1.5 C. An IPCC Special Report on the impacts of global warming of 1.5 C above pre-industrial levels and related global greenhouse gas emission pathways, in the context of strengthening the global response to the threat of climate change, sustainable development, and efforts to eradicate poverty. *IPCC, 2018*, 2018. In Press.
- [55] *MEMO²*. <https://h2020-memo2.eu/>.
- [56] METEK. USA-1, user manual, Sonic Anemometer.
- [57] J.B. Miller and P.P. Tans. Calculating isotopic fractionation from atmospheric measurements at various scales. *Tellus*, pages 207–214, 2003.
- [58] A. L. Mitchell, D. S. Tkacik, J. R. Roscioli, S. C. Herndon, T.I. Yacovitch, D. M. Martinez, T. L. Vaughn, L. L. Williams, M. R. Sullivan, C. Floerchinger, M. Omara, R. Subramanian, D. Zimmerle, A. J. Marchese, and A. L. Robinson. Measurements of methane emissions from natural gas gathering facilities and processing plants: Measurement results. *Environmental Science & Technology*, 49(5):3219–3227, 2015. PMID: 25668106.
- [59] W.G. Mook. Environmental isotopes in the hydrological cycles, principles and applications. *International Atomic Energy Agency and United Nations Educational, Scientific and Cultural Organization*, 2000.
- [60] R. Morales, J. Ravelid, K. Vinkovic, P. Korbeń, B. Tuzson, L. Emmenegger, H. Chen, M. Schmidt, S. Humbel, , and D. Brunner. Estimating local methane sources from drone-based measurements using mass-balance method. 2021. in prep.
- [61] J. Morville, S. Kassi, M. Chenevier, and D. Romanini. Fast, low-noise, mode-by-mode, cavity-enhanced absorption spectroscopy by diode-laser self-locking. *Applied Physics B*, 80:1027–1038, 06 2005.
- [62] V. Motto-Ros, M. Durand, and J. Morville. Extensive characterization of the optical feedback cavity enhanced absorption spectroscopy (of-ceas) technique: ringdown-time calibration of the absorption scale. *Applied Physics B*, 91:203–211, 2008.
- [63] E. G. Nisbet, E. J. Dlugokencky, M. R. Manning, D. Lowry, R. E. Fisher, J. L. France, S. E. Michel, J. B. Miller, J. W. C. White, B. Vaughn, P. Bousquet, J. A.

- Pyle, N. J. Warwick, M. Cain, R. Brownlow, G. Zazzeri, M. Lanoisellé, A. C. Manning, E. Gloor, D. E. J. Worthy, E.-G. Brunke, C. Labuschagne, E. W. Wolff, and A. L. Ganesan. Rising atmospheric methane: 2007–2014 growth and isotopic shift. *Global Biogeochemical Cycles*, 30(9):1356–1370, 2016.
- [64] E. G. Nisbet, R. E. Fisher, D. Lowry, J. L. France, G. Allen, S. Bakkaloglu, T. J. Broderick, M. Cain, M. Coleman, J. Fernandez, G. Forster, P. T. Griffiths, C. P. Iverach, B. F. J. Kelly, M. R. Manning, P. B. R. Nisbet-Jones, J. A. Pyle, A. Townsend-Small, A. al Shalaan, N. Warwick, and G. Zazzeri. Methane mitigation: Methods to reduce emissions, on the path to the paris agreement. *Reviews of Geophysics*, 58(1):e2019RG000675, 2020. e2019RG000675 2019RG000675.
- [65] NOAA. <https://www.ready.noaa.gov/READYpgclass.php>.
- [66] A. O’Keefe and D. A. G. Deacon. Cavity ring-down optical spectrometer for absorption measurements using pulsed laser sources. *Review of Scientific Instruments*, 59(12):2544–2551, 1988.
- [67] M. Omara, N. Zimmerman, M. R. Sullivan, X. Li, A. Ellis, R. Cesa, R. Subramanian, A. A. Presto, and A. L. Robinson. Methane Emissions from Natural Gas Production Sites in the United States: Data Synthesis and National Estimate. *Environmental Science & Technology*, 52(21):12915–12925, 2018. PMID: 30256618.
- [68] F. Pasquill. The estimation of the dispersion of windborne material. *Met. Mag.*, 90:33, 1961.
- [69] F. Pasquill. Atmospheric diffusion. *John Wiley & Sons*, 1974.
- [70] S. Petersen. Greenhouse gas emissions from liquid dairy manure: Prediction and mitigation. *Journal of Dairy Science*, 101:6642–6654, 06 2018.
- [71] Picarro. Document library g2201-i analyzer datasheet. https://www.picarro.com/support/library/documents/g2201i_analyzer_datasheet.
- [72] I. M. Rachor, J. Gebert, A. Gröngröft, and E.-M. Pfeiffer. Variability of methane emissions from an old landfill over different time-scales. *European Journal of Soil Science*, 64(1):16–26, 2013.
- [73] T. Reinelt and J. Liebetrau. Monitoring and mitigation of methane emissions from pressure relief valves of a biogas plant. *Chemical Engineering & Technology*, 43, 10 2019.

- [74] C. W. Rella, H. Chen, A. E. Andrews, A. Filges, C. Gerbig, J. Hatakka, A. Karion, N. L. Miles, S. J. Richardson, M. Steinbacher, C. Sweeney, B. Wastine, and C. Zellweger. High accuracy measurements of dry mole fractions of carbon dioxide and methane in humid air. *Atmospheric Measurement Techniques*, 6(3):837–860, 2013.
- [75] C. W. Rella, J. Hoffnagle, Y. He, and S. Tajima. Local- and regional-scale measurements of CH₄, delta 13CH₄, and C₂H₆ in the Uintah Basin using a mobile stable isotope analyzer. *Atmospheric Measurement Techniques*, 8(10):4539–4559, 2015.
- [76] A. M. Robertson, R. Edie, R. A. Field, D. Lyon, R. McVay, M. Omara, D. Zavala-Araiza, and S. M. Murphy. New Mexico Permian Basin Measured Well Pad Methane Emissions Are a Factor of 5–9 Times Higher Than U.S. EPA Estimates. *Environmental Science & Technology*, 54(21):13926–13934, 2020. PMID: 33058723.
- [77] A. M. Robertson, R. Edie, D. Snare, J. Soltis, R. A. Field, M. D. Burkhart, C. S. Bell, D. Zimmerle, and S. M. Murphy. Variation in methane emission rates from well pads in four oil and gas basins with contrasting production volumes and compositions. *Environmental Science & Technology*, 51(15):8832–8840, 2017. PMID: 28628305.
- [78] M. Saunio, A. R. Stavert, B. Poulter, P. Bousquet, J. G. Canadell, R. B. Jackson, P. A. Raymond, E. J. Dlugokencky, S. Houweling, P. K. Patra, P. Ciais, V. K. Arora, D. Bastviken, P. Bergamaschi, D. R. Blake, G. Brailsford, L. Bruhwiler, K. M. Carlson, M. Carrol, S. Castaldi, N. Chandra, C. Crevoisier, P. M. Crill, K. Covey, C. L. Curry, G. Etiope, C. Frankenberg, N. Gedney, M. I. Hegglin, L. Hoglund-Isaksson, G. Hugelius, M. Ishizawa, A. Ito, G. Janssens-Maenhout, K. M. Jensen, F. Joos, T. Kleinen, P. B. Krummel, R. L. Langenfelds, G. G. Laruelle, L. Liu, T. Machida, S. Maksyutov, K. C. McDonald, J. McNorton, P. A. Miller, J. R. Melton, I. Morino, J. Muller, F. Murguia-Flores, V. Naik, Y. Niwa, S. Noce, S. O’Doherty, R. J. Parker, C. Peng, S. Peng, G. P. Peters, C. Prigent, R. Prinn, M. Ramonet, P. Regnier, W. J. Riley, J. A. Rosentreter, A. Segers, I. J. Simpson, H. Shi, S. J. Smith, L. P. Steele, B. F. Thornton, H. Tian, Y. Tohjima, F. N. Tubiello, A. Tsuruta, N. Viovy, A. Voulgarakis, T. S. Weber, M. van Weele, G. R. van der Werf, R. F. Weiss, D. Worthy, D. Wunch, Y. Yin, Y. Yoshida, W. Zhang, Z. Zhang, Y. Zhao, B. Zheng, Q. Zhu, Q. Zhu, and Q. Zhuang. The global methane budget 2000–2017. *Earth System Science Data*, 12(3):1561–1623, 2020.
- [79] C. Scheutz and A.M. Fredenslund. Total methane emission rates and losses from 23 biogas plants. *Waste Management*, 97:38–46, 2019.

- [80] M. Seyfarth. Quantifying of methane emissions from biogas plants, cattle and peatland with mobile measurements in germany, 2021. bachelor thesis.
- [81] O. A. Sherwood, S. Schwietzke, V. A. Arling, and G. Etiope. Global inventory of gas geochemistry data from fossil fuel, microbial and burning sources, version 2017. *Earth System Science Data*, 9(2):639–656, 2017.
- [82] SILESIA. <https://www.pgsilesia.pl/pl/o-firmie/informacje-ogolne>. Przedsiębiorstwo Górnicze "SILESIA" sp. z o.o.
- [83] M. Stanisavljevic, J.M. Necki, J. Swolkień, M. Gałkowski, H. Maazallahi, P. Korbęń, M. Menoud, C. van der Veen, T. Röckmann, M. Schmidt, J. Wietzel, K. Vinkovic, S. Defratyka, D. Zieba, Ł. Chmura, and W. Wołkowicz. Determination of methane emission rates and isotopic signatures from coal mine ventilation shafts in the Upper Silesia, Poland. 2021. in prep.
- [84] T.F. Stocker, D. Qin, G.-K. Plattner, M. Tignor, J. Allen, S.K. and Boschung, A. Nauels, Y. Xia, V. Bex, and P.M. Midgley. Climate Change 2013: The Physical Science Basis. Contribution of Working Group I to the Fifth Assessment Report of the Intergovernmental Panel on Climate Change. *IPCC, 2013*, 2013. Cambridge University Press, Cambridge, United Kingdom and New York, NY, USA, 1535 pp.
- [85] R. Subramanian, L. L. Williams, T. L. Vaughn, D. Zimmerle, J. R. Roscioli, S. C. Herndon, T. I. Yacovitch, C. Floerchinger, D. S. Tkacik, A. L. Mitchell, M. R. Sullivan, T. R. Dallmann, and A. L. Robinson. Methane Emissions from Natural Gas Compressor Stations in the Transmission and Storage Sector: Measurements and Comparisons with the EPA Greenhouse Gas Reporting Program Protocol. *Environmental Science & Technology*, 49(5):3252–3261, 2015. PMID: 25668051.
- [86] O. G. Sutton. A theory of eddy diffusion in the atmosphere. *Proceedings of the royal society of London. Series A, Containing papers of a mathematical and physical character*, 135(826):143–165, 1932.
- [87] TAURON. <https://www.tauron-wydobycie.pl/spolka/zg-brzeszcze/charakterystyka-zakladu>. TAURON Wydobycie S.A.
- [88] E. Thoma and B. Squier. OTM 33 Geospatial Measurement of Air Pollution, Remote Emissions Quantification (GMAP-REQ) and OTM33A Geospatial Measurement of Air Pollution-Remote Emissions Quantification-Direct Assessment (GMAP-REQ-DA). *US Environmental Protection Agency, Cincinnati, OH*, 2014.

- [89] D.B. Turner. Workbook of atmospheric dispersion estimates, office of air programs pub. No. AP-26, *Environmental Protection Agency*, 1970.
- [90] UBA. Submission under the united nations framework convention on climate change and the kyoto protocol 2018. 2018. <https://www.umweltbundesamt.de/publikationen/submission-under-the-united-nations-framework-3>.
- [91] UNFCCC. <https://unfccc.int/>.
- [92] A. van Pelt. Real-time atmospheric monitoring of stable isotopes and trace greenhouse gas. *Picarro*, 2008.
- [93] I. Ventrillard-Courtillot, T. Gonthiez, C. Clerici, and D. Romanini. Multispecies breath analysis faster than a single respiratory cycle by optical-feedback cavity-enhanced absorption spectroscopy. *Journal of Biomedical Optics*, 14(6):1–5, 2009.
- [94] J. C. von Fischer, D. Cooley, S. Chamberlain, A. Gaylord, C. J. Griebenow, S. P. Hamburg, J. Salo, R. Schumacher, and J. Theobald, D. and Ham. Rapid, vehicle-based identification of location and magnitude of urban natural gas pipeline leaks. *Environmental Science & Technology*, 51(7):4091–4099, 2017. PMID: 28326761.
- [95] E.H. Wahl, B. Fidric, C.W. Rella, S. Koulikov, B. Kharlamov, S. Tan, A.A. Kachanov, B.A. Richman, E.R. Crosson, B.A. Paldus, S. Kalaskar, and D.R. Bowling. Applications of cavity ring-down spectroscopy to high precision isotope ratio measurement of $^{13}\text{C}/^{12}\text{C}$ in carbon dioxide. *Isotopes in Environmental and Health Studies*, 42(1):21–35, 2006. PMID: 16500752.
- [96] J. Wietzel. Carbon isotopic source signature of CH_4 -emissions of mines in the upper silesian basin, 2018. bachelor thesis.
- [97] J. Wietzel. Estimation of methane emissions in the urban area of heidelberg by mobile measurements. Master’s thesis, Heidelberg University, 2021.
- [98] J. Wilczak, S. Oncley, and S. Stage. Sonic anemometer tilt correction algorithms. *Boundary-Layer Meteorology*, 99, 04 2001.
- [99] I. Xueref-Remy, G. Zazzeri, F.M. Bréon, F. Vogel, P. Ciais, D. Lowry, and E.G. Nisbet. Anthropogenic methane plume detection from point sources in the Paris megacity area and characterization of their delta ^{13}C signature. *Atmospheric Environment*, 222:117055, 2020.
- [100] C. Yeman. Quantifying emission rates and isotopis signatures of methane source-using a mobile crds analyzer. Master’s thesis, Heidelberg University, 2015.

- [101] D. Zavala-Araiza, D. Lyon, R. A. Alvarez, V. Palacios, R. Harriss, X. Lan, R. Talbot, and S. P. Hamburg. Toward a functional definition of methane super-emitters: Application to natural gas production sites. *Environmental Science & Technology*, 49(13):8167–8174, 2015. PMID: 26148555.
- [102] G. Zazzeri, D. Lowry, R. E. Fisher, J. L. France, M. Lanoiselle, B. F. J. Kelly, J. M. Necki, C. P. Iverach, E. Ginty, M. Zimnoch, A. Jasek, and E. G. Nisbet. Carbon isotopic signature of coal-derived methane emissions to the atmosphere: from coalification to alteration. *Atmospheric Chemistry and Physics*, 16(21):13669–13680, 2016.
- [103] G. Zazzeri, D. Lowry, R.E. Fisher, J.L. France, M. Lanoisell , and E.G. Nisbet. Plume mapping and isotopic characterisation of anthropogenic methane sources. *Atmospheric Environment*, 110:151–162, 2015.
- [104] L.-T. Zhan, T. Wu, S. Feng, G.-Y. Li, H.-J. He, J.-W. Lan, and Y.-M. Chen. Full-scale experimental study of methane emission in a loess-gravel capillary barrier cover under different seasons. *Waste Management*, 107:54–65, 2020.
- [105] A. Zieba. Analiza danych w naukach scislych i technice. *PWN*, 2014.
- [106] D. J. Zimmerle, L. L. Williams, T. L. Vaughn, C. Quinn, R. Subramanian, G. P. Duggan, B. Willson, J. D. Opsomer, A. J. Marchese, D. M. Martinez, and A. L. Robinson. Methane emissions from the natural gas transmission and storage system in the united states. *Environmental Science & Technology*, 49(15):9374–9383, 2015. PMID: 26195284.

Acknowledgements - Danksagung - Podziękowania

Writing this paper was not easy. It took a lot of work, additional skills, and a lot of patience. This dissertation would not have been possible without many people who have contributed to where I am and what I have accomplished.

First of all, I would like to thank the members of my PhD committee: Prof. Norbert Frank, Prof. Andre Butz, Prof. Tilman Plehn and Prof. Frank Keppler, who agreed to review my work. Special thanks to Prof. Norbert and Prof. Andre who additionally decided to read carefully my dissertation. It is an honor that such respected scientists have agreed to review this dissertation.

Throughout my 3 years of research, I have had the pleasure of being a part of a larger group of scientists who have created the *MEMO*² project. I would like to thank all its members for their participation and always great willingness to cooperate. It was a pleasure to meet you all. Even though there are 13 of us and we did our PhDs in 7 European countries, we are all part of the same *MEMO*² family. At this point I would like to express my gratitude to Dr. Martina Schmidt who, as my mentor, was always supporting me. She did not hesitate to criticize as well as to encourage. You gave me free hand to conduct my research and to gather my own experience. Thank you, Martina, for choosing me as your PhD student. I hope that the research I have done has at least compensated a little for all the difficulties. The *MEMO*² project would not have happened without my next two supervisors, Prof. Thomas Röckmann and Bill Hirst. I enjoyed every opportunity to talk with them and to learn something new. Thank you, Bill, for every motivating word. But the *MEMO*² project is all about the students, so thanks to each of you for the great work and the new relationships, let's hope we can see each other again, 3 out of 13 people were from Poland. Thanks to Sara and Patryk that we could share the next years of our bumpy academic careers together, it cost us a lot but it was definitely worth it.

Thank you also to my GGWI group, where I enjoyed working and meeting many people. Special thanks go to Julia Wietzel, with whom the measurements were always fun and never boring. I wish everybody to have more such friends at work.

Doing a doctorate first requires completing previous degrees. Another person I am grateful to is Dr inż. Jarosław M. Nęcki. Thanks Jarek for getting me interested in environmental physics and for encouraging me to go in this direction. The project in Spain was the beginning of our collaboration and I hope that it will continue.

I would also like to thank Anna Zarzecka, because without her my studies would have been an insurmountable obstacle and I would not be here. She has always supported and motivated me to work hard.

The help and support I received from the LifeChurch Heidelberg community is also invaluable. You guys are amazing and one of the best things during this PhD was the friendship with you. Especially thanks to Kyle Garner, who is always available to talk about everything, especially about language issues, Polish is fantastic.

Irreplaceable at any stage of life is the help of loved ones. That is why I would like to express my deepest gratitude to my parents, Krzysztof and Anna, and my brother Adam. They have always supported me, motivated me, did not let me give up and this doctorate is also thanks to them.

Last but not least, I would like to thank God for being there and for never leaving me. Especially in moments of doubt and resignation, His Word has always been a help. As the Bible says, with God nothing is impossible, even to get a PhD degree.

THANK YOU ALL
VIELEN DANK AN EUCH ALLE
DZIĘKUJE WAM WSZYSTKIM